SENS4ICE

SENSORS AND CERTIFIABLE HYBRID ARCHITECTURES
FOR SAFER AVIATION IN ICING ENVIRONMENT

Sensor evaluation results and final roadmaps for future technology development and exploitation

SENS4ICE Deliverable D4.1

Lead beneficiary (organisation):	Collins Aerospace
Document manager	El Hassan Ridouane
Actual submission date:	06/02/2024
Dissemination level	Public

Grant Agreement number:	824253
Project acronym:	SENS4ICE
Project title:	SENSors and certifiable hybrid architectures FOR safer aviation in ICing Environment
Funding scheme:	Research and Innovation Action
Project coordinator:	DLR (German Aerospace Center)
Project website:	www.sens4ice-project.eu

This project has received funding from the European Union's Horizon 2020 research and innovation programme under grant agreement No 824253.

File name	SENS4ICE_D4.1_Sensor_Evalation_and_Final_Technology_Roadmaps_Collins_20240209.docx

APPROVALS

Role	Name	Organisation	Date
Coordinator	Schwarz	DLR	2024.01.12
WP leader	Deiler	DLR	2023.12.13
Task leader	Ridouane	Collins Aerospace	2023.12.12
Other (quality)	Behrendt	L-UP	2023.12.18

DOCUMENT HISTORY

Version	Date	Modification	Author
1.0	2023.09.11	Updated version with partner input	Ridouane
1.1	2023.09.13	Refined version with addition of introduction section	Ridouane
1.2	2023.09.10	Revised with input from partners following review comments	Ridouane
1.3	2023.11.19	Revised with input from partners/coordinator	Ridouane
1.4	2023.12.12	Minor modifications	Schwarz
1.5	2023.12.18	Quality review	Behrendt

LIST OF AUTHORS

Name	Organisation
Document manager/editor: El Hassan Ridouane	Collins Aerospace
Contributors:	AeroTex, Collins Aerospace, DLR, Honeywell, INTA, ONERA, SAFRAN

DISTRIBUTION LIST

This deliverable report is public.

TABLE OF CONTENTS

GLOSSARY

Acronym	Signification
AHDEL	Atmospheric Hydrometeor Detector based on Electrostatics
AIP	Atmospheric Icing Patch
AIWT	Atmospheric Icing Wind Tunnel
AMPERA	Atmospheric Measurement of Potential and ElectRic field on Aircraft
AOD	Appendix O Discriminator
APP. C	Appendix C
APP. O	Appendix O
BCPD	Backscatter Cloud Probe with Polarization Detection
BIWT	Braunschweig Icing Wind Tunnel
CCP	Cloud Combination Probe
CM2D	Cloud Multi-Detection Device
CU	Control Unit
DAL	Design Assurance Level
DMAX	Maximum Diameter
DWT	Discrete Wavelet Transforms
FOD	Fiber Optic Detector

FPGA	Field Programmable Gate Array
FT	Flight Test
FZDZ	Freezing Drizzle
HAIC	High Altitude Ice Cristal (UE project)
HIDS	Hybrid Ice Detection System
IDS	Ice Differentiator System
IKP2	Isokinetic Probe
IWT	Icing Wind Tunnel
IWTT	Icing Wind Tunnel Test
LILD	Local Ice Layer Detector
LW	Liquid Water Icing Conditions
LWC	Liquid Water Content
MTBF	Mean Time Between Failures
MVD	Median Volume Diameter
NRC	National Research Council of Canada
PFIDS	Primary in-Flight Icing Detection System
PICU	Power Interface Control Unit
PIU	Power Interface Unit
SAFIRE	Service des avions français instrumentés pour la recherche en environnement (French facility for airborne research)
SIPS	Smart Ice Protection System
SLD	Supercooled Large Drops
SOF	Safety Of Flight
SRP	Short Range Particulate
TRL	Technology readiness level
TWC	Total Water Content
TUBS	Technische Universität Braunschweig

LIST OF FIGURES

LIST OF TABLES

If not acknowledged otherwise, images courtesy of the SENS4ICE consortium partners.

This document reflects only the consortium's view. The European Commission and the European Climate, Infrastructure and Environment Executive Agency (CINEA) are not responsible for any use that may be made of the information it contains.

This document is one of the four final public deliverables for the EU-funded project SENS4ICE (Grant Agreement No 824253, 2019-2023):

D4.1 Sensor evaluation results and final roadmaps for future technology development and exploitation

D4.2 Final report on hybrid ice detection development

D4.3 Final report on airborne demonstration and atmospheric characterisation

D4.4 Final report on evaluation of technologies developed in SENS4ICE and technical project results

1. Executive summary

The EU-funded Horizon 2020 project SENS4ICE addresses reliable detection and discrimination of supercooled large droplets (SLD) icing conditions. These conditions are considered as particularly safety-relevant and have been included in airplane certification specifications. The SENS4ICE project comprises technology development, icing wind tunnel upgrading/testing and flight testing. The first part of the project was devoted to the development and maturation of icing detection technologies, with a focus on Appendix O (of 14 CFR Part 25 and CS-25) icing conditions. Ice wind tunnel testing (including App. O) of the developed sensing technologies concluded the first part of the project. The second part of the project is dedicated to flight testing of icing technologies in natural icing conditions including App. O.

Ten different direct ice detection sensors with diverse physical principles (atmospheric sensors and accretion sensors) have been developed and matured in SENS4ICE project. The following is the list of sensors by acronym and developer: AIP by AeroTex, IDS by Collins Aerospace, LILD by DLR, SRP by Honeywell, FOD by INTA, AHDEL by ONERA, AMPERA by ONERA, CM2D by DLR, AOD by Safran, and PFIDS by Safran. SENS4ICE core approach is the development of a novel hybrid system for icing detection that combines direct sensing (atmospheric conditions / ice accretion) with an indirect technique based on changing aircraft flight performance characteristics.

Three icing wind tunnel (IWT) test facilities were available for testing including Collins Aerospace Icing Wind Tunnel, TU Braunschweig Icing Wind Tunnel and National Research Council (NRC) Altitude Icing Wind Tunnel. Sensors performed well in IWT test campaigns with several sensors having correctly detected 100% of the test points for App. C and also for App. O, also within the required maximum response time as per EUROCAE inflight icing systems standard ED-103. Only two sensor technologies were not considered for flight testing at the evaluation gate (at the end of the first part of the project) due to less promising performance results. These are the AHDEL by ONERA and AOD by SAFRAN. The rest of sensor technologies were approved to continue to the second part of the project and flight test.

Two flight campaigns with a total flight time of about 75 hours have been conducted in 2023 to test and demonstrate eight of the direct ice detection technologies under development in particular in App. O/ SLD icing conditions. The North America flight test operated by Embraer on Embraer Phenom 300 during February/March 2023 and the European flight test operated by Safire on the French ATR 42 environmental research aircraft during April 2023. Both flight tests campaigns encountered numerous App. O/SLD conditions and gathered valuable data sets for sensor validation for both App. C and O. Assessment of flight test data for ice detection technologies shows that successful detections have been achieved with a good sensor performance and good progress was made in general regarding technology readiness level.

The project also identified gaps and areas for further technology development to bring the sensors closer to production ready technologies. Such gaps are translated into roadmaps for further development and exploitation by the technology owners in future collaboration opportunities targeting additional testing in IWT and flight tests. This is very important despite the very good progress made, as the relevant icing conditions particularly for App. O/ SLD are very complex and the envelopes for the relevant parameters are large, multi-dimensional and have not been fully covered with the test data obtained in this project. However, it is very clear based on the flight test results that the matured and demonstrated technologies allow for a broad and promising application for various different purposes and types of vehicles, as many of the novel technologies are of low size/ low weight/ low power. This is considered to be particularly beneficial also beyond usual aircraft configurations, namely for future novel air vehicle concepts like greener aviation, more/all electric aircraft and UAV/UAM.

2. Introduction

SENS4ICE addressed development, test (icing wind tunnel and in flight, in both cases with a focus on freezing drizzle and without addressing freezing rain conditions), validation, and maturation of different detection principles, as well as the final airborne demonstration of technology capabilities in relevant natural icing conditions [1, 2].

Ten different technologies with diverse physical principles for directly detecting icing conditions have been developed and/or advanced with the EU funding. At the project beginning, the sensor technologies had different levels of technology readiness, some at very low levels and others having had already passed steps of technology testing. In the first phase of the project, all sensors reached the status to be ready for icing wind

tunnel testing. One particular technology (Cloud Multi-Detection Device - CM2D, combining the Nevzorov Probe and the Backscatter Cloud Probe with Polarization Detection (BCPD)) aims to improve airborne scientific and reference measurements. The other nine target applications for operational air transport. The sensor technologies can be clustered into two categories, atmospheric sensors, that are measuring the atmospheric conditions, and accretion sensors, that measure ice accretion on the aircraft. Table 1 gives an overview of the icing sensor technologies under development in the SENS4ICE project.

Table 1: SENS4ICE sensor technologies overview, sensor types and principles.

Sensor / Developer	Sensor Type	Sensor Principle
AIP / AeroTex	Atmospheric	Isothermal with inertial separation at different sensors along aircraft
IDS / Collins	Atmospheric	Thermal response to heat impulse
LILD / DLR	Accretion	Ultrasonic wave attenuation / phase change
SRP / Honeywell	Atmospheric	Collecting backscattered light from particles
FOD / INTA	Accretion	Latent heat measured with fiber optic
AHDEL / ONERA	Atmospheric	Particle charging and subsequent measurement of the charge
AMPERA / ONERA	Atmospheric	Measurement of aircraft electric potential
AOD / Safran	Atmospheric	Shadowgraphy
PFIDS / Safran	Accretion	Optical reflection from accretion
CM2D [BCPD] / DLR	Atmospheric	Single particle optical backscatter
CM2D [Nevzorov] /DLR	Atmospheric	Isothermal measurement of water content

2.1 Ice Wind Tunnel Campaigns

In order to test the direct sensors three icing wind tunnel (IWT) test facilities were involved:

- Collins Aerospace Icing Wind Tunnel
- TUBS BIWT (Braunschweig Icing Wind Tunnel) [3]
- National Research Council of Canada (NRC): Altitude Icing Wind Tunnel (AIWT) [4].

While the NRC AIWT already provided the capability to achieve SLD in full bimodal freezing drizzle conditions, the other two icing wind tunnel facilities improved their capabilities to represent App. O conditions in the scope of the SENS4ICE project. These improvements mainly included adapting the spray nozzle setup and were aiming at freezing drizzle conditions, while testing freezing rain conditions was out of the scope for the SENS4ICE project.

A standardised testing procedure and partly common test points between the different icing wind tunnels served for adequate comparability of the results. Significant emphasis was put on the development of test matrices for each involved IWT facility following the EUROCAE inflight icing systems guidelines of ED-103 [5]. As the setup and capabilities of each IWT facility vary, icing envelopes differ from one IWT facility to another with very limited overlap. This effect was leveraged by establishing a common test procedure and by selecting common test points between all or some of the facilities (Table 2). For a selected subset of the test points, 3 cycles of icing have been completed (to test repeatability to the extent possible with the available IWT time). In order to test sensor ability to maintain its functionality over an extended period, one Appendix C test point was selected for endurance. This test point was tested with the icing cloud turned on for a duration of 45 minutes.

Table 2 Common test points between IWT facilities TUBS, Collins and NRC.

IWT	App C						App O					
	Total Test Points	Common with 3 IWT	Common with 2 IWT	Only at 1 IWT	CM Test Points	IM Test Points	Total Test Points	Common with 3 IWT	Common with 2 IWT	Only at 1 IWT	Total Points [unimodal]	Total Points [bimodal]
TUBS	19	4	1	14	10	9	18	0	1	17	0	18
Collins	18	4	4	10	9	9	6	0	1	5	6	0
NRC	19	4	4	11	9	10	17	0	2	15	4	13

Apart from the reference instruments, eight technologies have provided testing results in different icing wind tunnels in App. C and O conditions. Due to the fact that the sensor technology AMPERA (ONERA) uses the aircraft as a sensor (measurement of aircraft electric potential), IWT testing is not feasible. Instead, flight test data from previous projects were assessed to investigate the correlation between the electrostatic field and the total water content [6]. IWT results were used towards sensor technology evaluation and down-selection supported by the project advisory board. Table 3 gives a summary of the different technologies with respect to which IWT facility used and result of the SENS4ICE evaluation.

Table 3: Grouping between sensors and IWT facilities and summary result of SENS4ICE evaluation.

Sensor / Developer	**Sensor Type**	**IWT Facility Used**	**Outcome of Evaluation supported by Advisory Board**
AIP / AeroTex	Atmospheric	NRC	Pass
IDS / Collins	Atmospheric	Collins and NRC	Pass
LILD / DLR	Accretion	TUBS	Pass
SRP / Honeywell	Atmospheric	Collins and NRC	Pass
FOD / INTA	Accretion	NRC	Pass
AHDEL / ONERA	Atmospheric	TUBS	Stop developments with SENS4ICE
AMPERA / ONERA	Atmospheric	N/A	Pass
AOD / Safran	Atmospheric	withdrawn	Stop developments with SENS4ICE
PFIDS / Safran	Accretion	TUBS	Pass
CM2D [BCPD] / DLR	Atmospheric	TUBS	Pass
CM2D [Nevzorov] /DLR	Atmospheric	TUBS	Pass

Sensor technologies performed generally very well in IWT tests and several sensors have correctly detected 100% of the test points for App. C and also for App. O, also within the required maximum response time as per ED-103. An overview of the detection rates (test cases successfully detected related to the total number of test cases) is shown in Figure 1, excluding DLR's CM2D scientific/ reference sensor and one other sensor (AOD) that was withdrawn from IWT testing in the context of Covid-19 related delays.

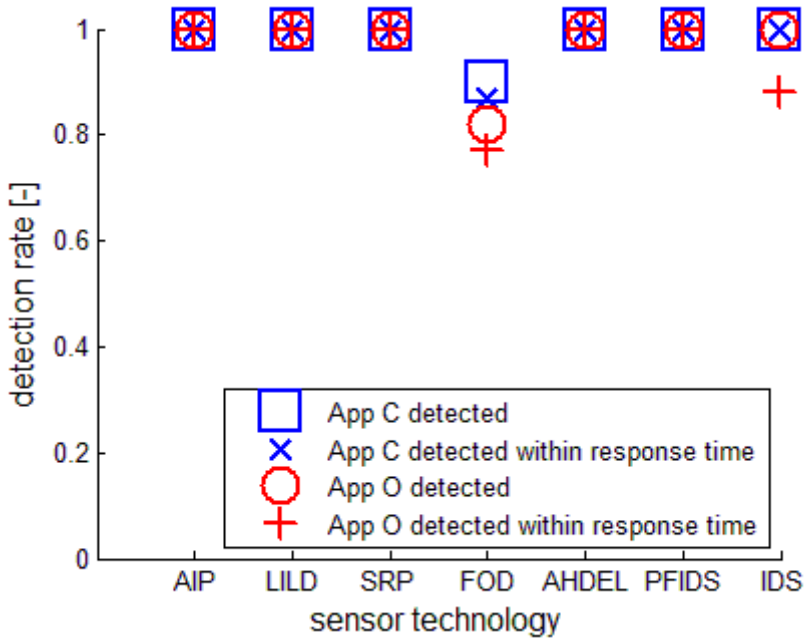

Figure 1: SENS4ICE sensor detection rates overview for App. C and O icing condition IWT test points for seven detection technologies.

A qualitative overview (anonymised) of measured sensor response times compared to required response times as per ED-103 is shown in Figure 2 (top) for App. C icing condition test points. In almost all cases the response times for the detection technologies are within the requirements, i.e. below the black reference line which is representing a measured response time equal to the required response time. Measured sensor response times compared to required response times for detecting liquid water icing conditions for App. O IWT test points are shown in Figure 2 (bottom).

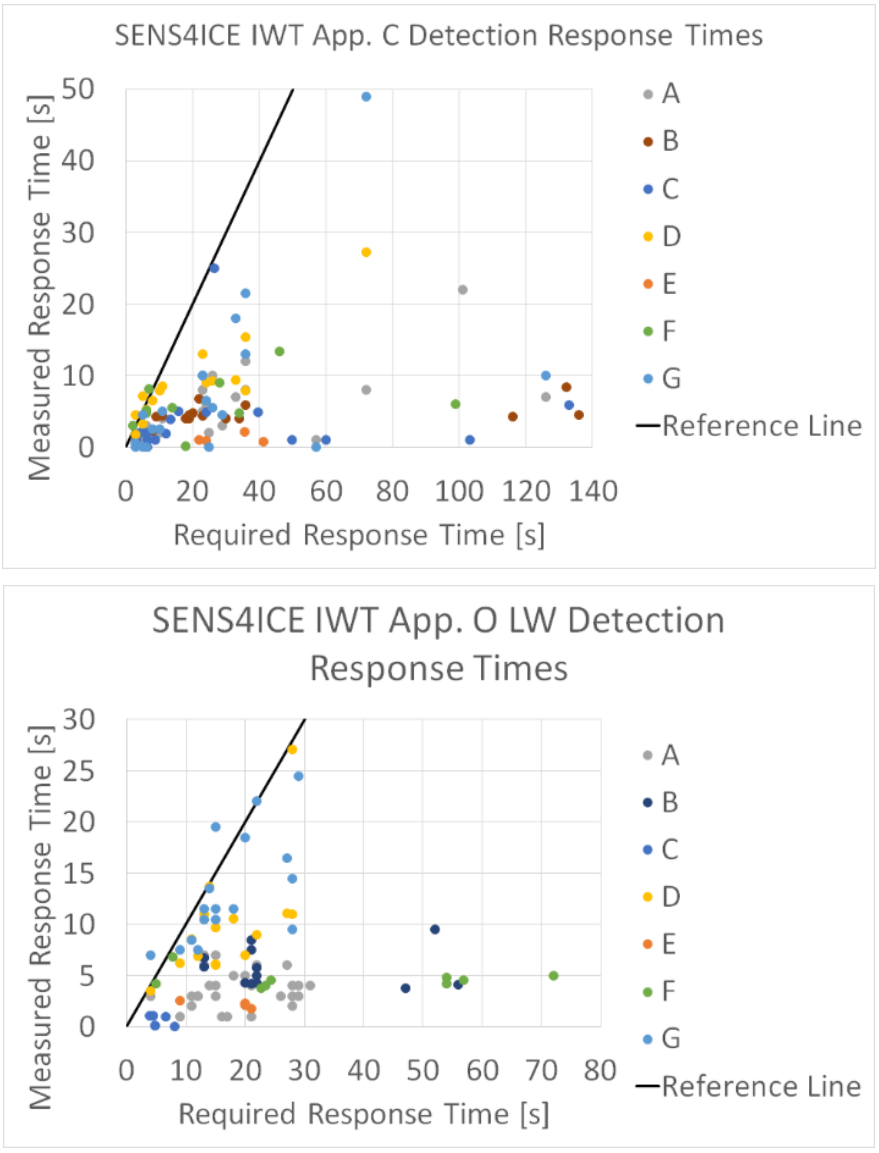

Figure 2: Measured sensor response times compared to required response times for App. C IWT test points (top) Measured sensor response times compared to required response times for detecting liquid water (LW) icing conditions for App. O IWT test points (bottom).

Measured sensor response times compared to required response times for differentiating App. C conditions from App. O condition are shown in Figure 3. Note that not all sensor technologies have provided differentiation information for the IWT tests.

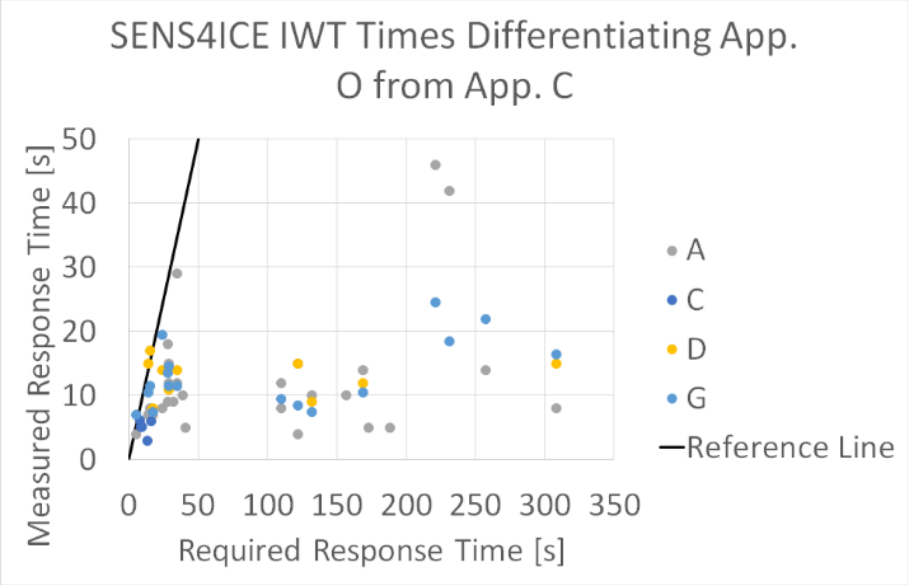

Figure 3: Measured sensor response times compared to required response times for differentiating App. C conditions from App. O conditions in IWT (for sensors providing differentiation information).

2.2 Natural Icing Flights Campaigns

Technology testing in natural in-flight icing conditions allows to increase the Technology Readiness Level (TRL) for the technologies under development and to pave the way towards industrialization and operational application and also to support future aircraft certification activities. Two flight campaigns with a total flight test time of about 75 hours have been conducted in 2023 to test and demonstrate eight of the direct ice detection technologies under development in particular in App. O/ SLD icing conditions:

- February/March 2023, North America, Embraer Phenom 300 operated by Embraer
- April 2023, France, French ATR 42 environmental research aircraft of Safire

Apart from aircraft interface definitions for direct, indirect and hybrid detection technologies, particular focus was put on selecting suitable aircraft locations for mounting external sensors in order to allow for good icing detection. Further emphasis was put on ensuring adequate reference measurements. These reference measurements serve as a profound basis for analysis of flight test data and technology evaluation (see SENS4ICE public deliverable D4.3). Aircraft specific safety requirements and flight procedures have been developed, including minimum altitudes for natural icing flight tests. This is reducing the likelihood to encounter relevant icing conditions, as only icing conditions above a certain altitude can be encountered during measurement flights. Hence, extensive meteorological and climatological analysis was undertaken in order to select suitable regions to encounter icing conditions including App. O conditions, as described in more detail in the next section.

2.2.1 Flight Campaign North America

An Embraer Phenom 300 prototype was equipped with flight test instrumentation including various reference sensors and several cameras for icing monitoring for a flight campaign in natural icing conditions in North America in late February/ early March 2023. In this campaign, four of the icing detection technologies under development in the SENS4CE project have been tested: AIP/ AeroTex, IDS/ Collins, SRP/ Honeywell and PFIDS/ Safran.

Figure 4: Embraer Phenom 300 prototype with test sensors and reference instruments [image Embraer/ SENS4ICE project].

15 flights with a total of 25 flight hours (including ferry and check flights) have been successfully conducted allowing to target natural liquid water icing conditions and in particular SLD conditions. Ice was visible on the windshield during the ice encounters and this is serving as a good indicator for estimating icing conditions and ice accretion on the airframe. Appendix O conditions solely comprised FZDZ and tended to be bimodal and had mostly MVDs < 40 µm with average around 23 µm. The altitude of icing conditions. Higher LWCs in the range up to 1 g/m³ were observed. In total, 4 hours and 23 minutes were spent in icing conditions, 42 minutes in Appendix O conditions was achieved. For more details refer to SENS4ICE deliverable D4.3 “Final report on airborne demonstration and atmospheric characterisation”.

The regions of sampling flights were mainly southeast, south and west of Lake Michigan in Northern America. Figure 5 shows a detailed overview of individual flights conducted as part of the campaign between 22 February and 10 March 2023 (not including all check flights). Flights were conducted from Alton/ St. Louis Regional Airport (KALN) and in several cases included refuelling stops.

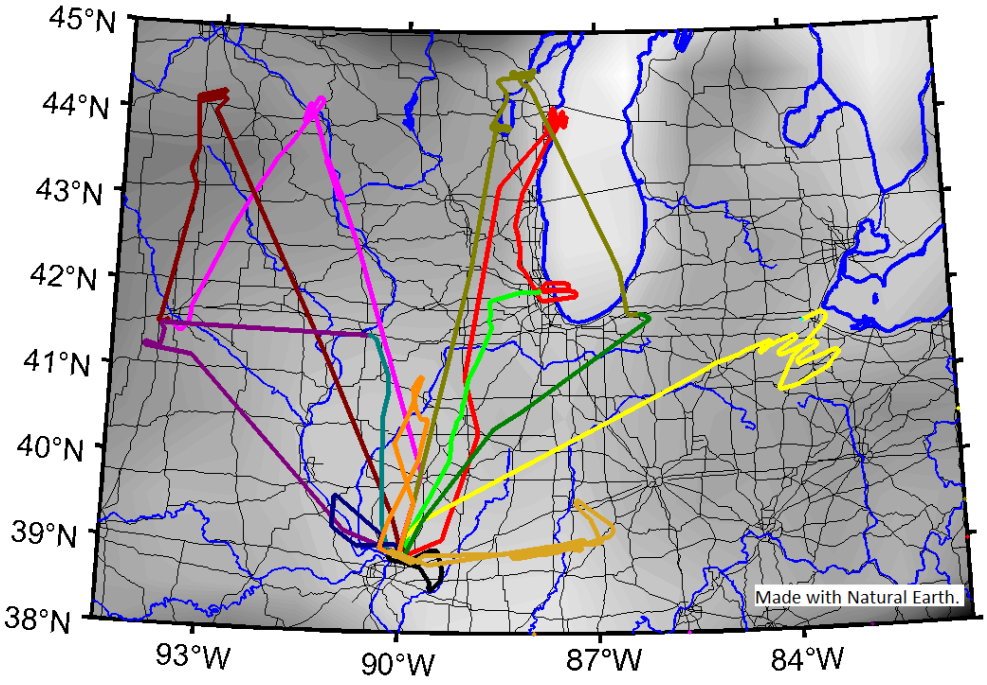

Figure 5: Flight Campaign North America February/ March 2023 overview of flight tracks for flights in natural icing conditions [image DLR/ SENS4ICE project].

Based on flight test micro physics data analysis, the SENS4ICE North America flight campaign provides a very good amount of measurements of liquid water icing conditions and SLD conditions in particular. Flight test results generally show that the different icing detection technologies have been able to successfully detect relevant conditions [7, 8, 9] and further assessment of ice detection technologies detection capabilities is detailed in section 3.

2.2.2 Flight Campaign Europe

The French ATR 42 environmental research aircraft of Safire was equipped with flight test instrumentation including various reference sensors and several cameras for icing monitoring for a flight campaign in natural icing conditions in Europe in April 2023 (Figure 6). In this campaign, the following four of the icing detection technologies under development in the SENS4CE project have been tested: FOD/ INTA, LILD/ DLR, AMPERA/ ONERA and CM2D/ DLR.

Figure 6: SAFIRE ATR 42 with test sensors and reference instruments [image DLR/ SENS4ICE project].

15 flights with a total of about 50 flight hours have been successfully conducted targeting natural liquid water icing conditions and in particular SLD conditions. Figure 7 shows an example of the SAFIRE ATR 42 horizontal tail with ice accretion. Appendix O conditions solely comprised FZDZ and were often unimodal and had MVDs which mostly ranged between 25 and 60 µm with average of 45 µm. LWCs higher than 1 g/m³, contained in the SLD mode, were observed. A total of more than 10 hours were spent in icing conditions, and more than 2 hours in Appendix O conditions were achieved.

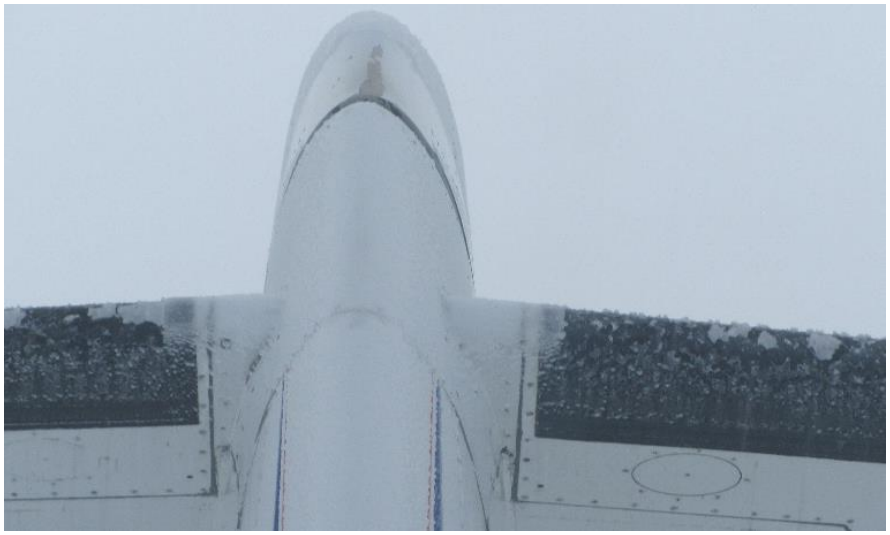

Figure 7: SAFIRE ATR 42 horizontal tail with ice accretion [image DLR/ SENS4ICE project].

Ground tracks of the European flight test campaign are shown in Figure 8.

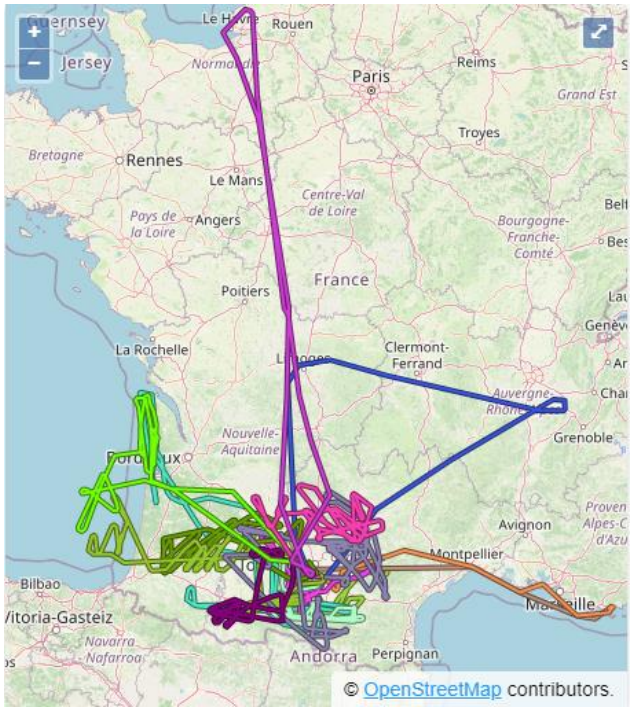

Figure 8: Flight campaign Europe ground tracks [image credit SAFIRE, Map data from OpenStreetMap/ SENS4ICE project].

Based on flight test data analysis the SENS4ICE Europe flight campaign provides extensive measurements of liquid water icing conditions including SLD conditions. The assessment of ice detection technologies shows that promising detection results have been achieved as detailed in section 3.

This report documents the evaluation of the developed sensing technologies with respect to icing wind tunnel tests and flight test. The evaluation is presented in section 3, for each sensor technology, along with a technology description and any lab testing done during the early-stage developments of SENS4ICE. Section 4 is devoted to the technology roadmaps highlighting any major gaps for further development beyond SENS4ICE as well as opportunities for technology exploitation.

For more details on flight campaigns please refer to the SENS4ICE deliverables D4.3 “Final report on airborne demonstration and atmospheric characterisation”. Similarly, details on the hybrid and indirect flight test results are available in the SENS4ICE deliverable D4.2 “Final report on hybrid ice detection development”.

3. Individual Sensor Evaluation

3.1 AeroTex – AIP

3.1.1 Technology Description

The AeroTex-AIP comprises of two key components; the isothermal heater unit and a data processing and control unit. The heater is a custom designed 20mm square patch that is installed on an insulated mount that prevents excess heat being drawn into the aircraft structure. An erosion shield is bonded on top of the heater and mount to provide protection for the heater. Two temperature sensors are integrated in the development unit to monitor and control any over-temperature of the system. The individual heater patches operate at high temperature (~120°C) but their small size means that they draw little power (<30W).

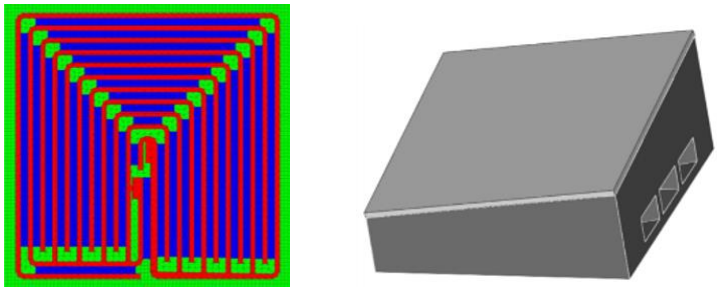

Figure 9: AIP heater (left) and an insulated mount (right).

The second unit part of the system is the data processor. The primary role of the data processor is to process atmospheric and operating condition data from the flight computer (speed, temperature, angle-of-attack etc.) and combine it with a measurement of the power drawn by the heater units to determine whether icing conditions exist. The data processor unit also provides a safety role as it monitors for weight-on-wheels, sensors overtemperatures and sensor open or closed circuits.

A key aspect of the AIP system is the use of a network of sensors distributed over the forward fuselage which allows differentiation between small and large droplet icing to be differentiated. Figure 10 shows an example installation when the forward two sensor are only subject to impingement under large droplet icing conditions, as indicated by the blue/grey curves with the small droplet icing conditions indicated by green curves indicating zero impingement. The figure also shows that AIP_3 and AIP_4 sensors are subject to icing in both large droplet and small droplet icing conditions. Therefore, by monitoring the system response in these different positions, icing can be identified. Figure 11 shows an example response for a two-sensor system under two different icing conditions, small droplet and large droplet, with the large droplet sensor only responding when the larger droplets are present.

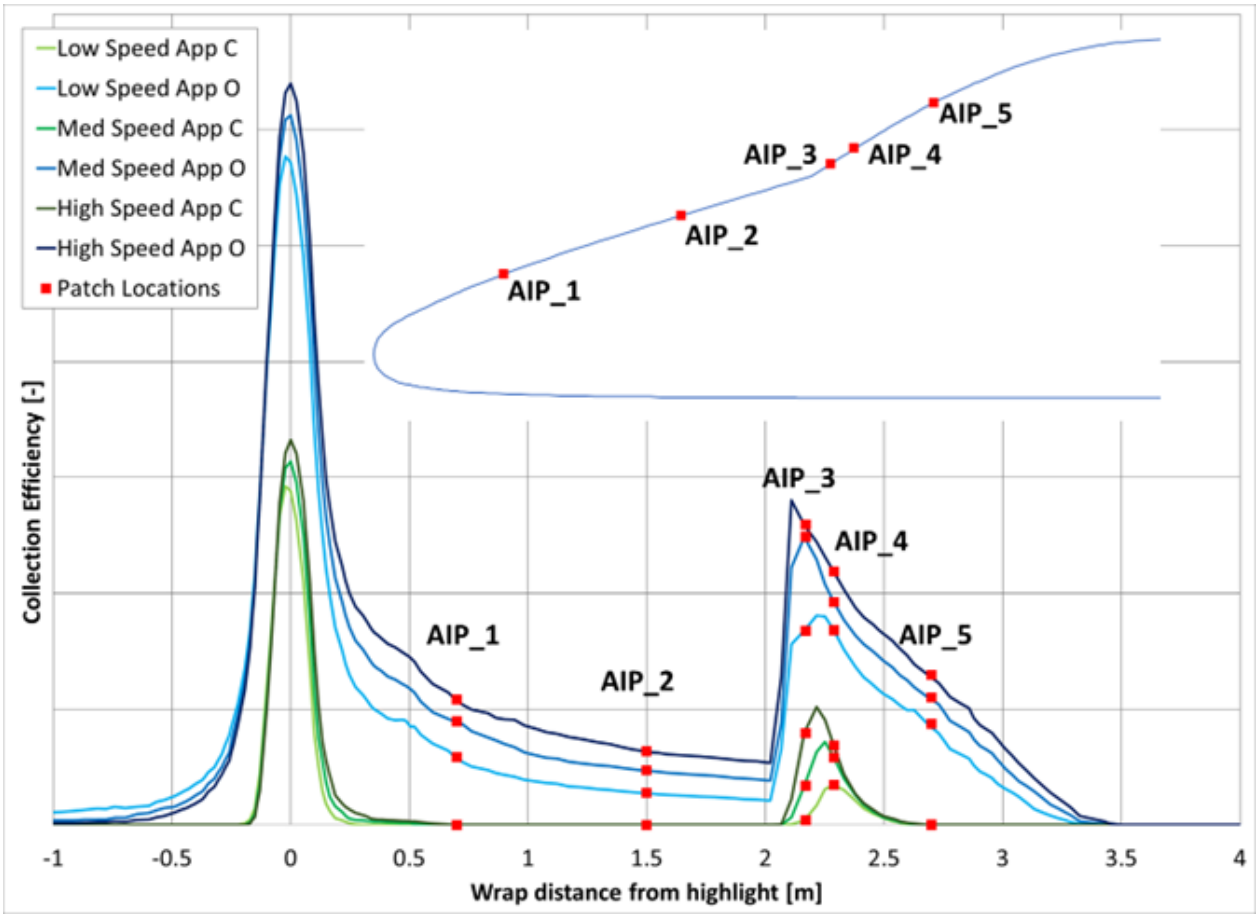

Figure 10: Example showing sensor locations on the forward fuselage.

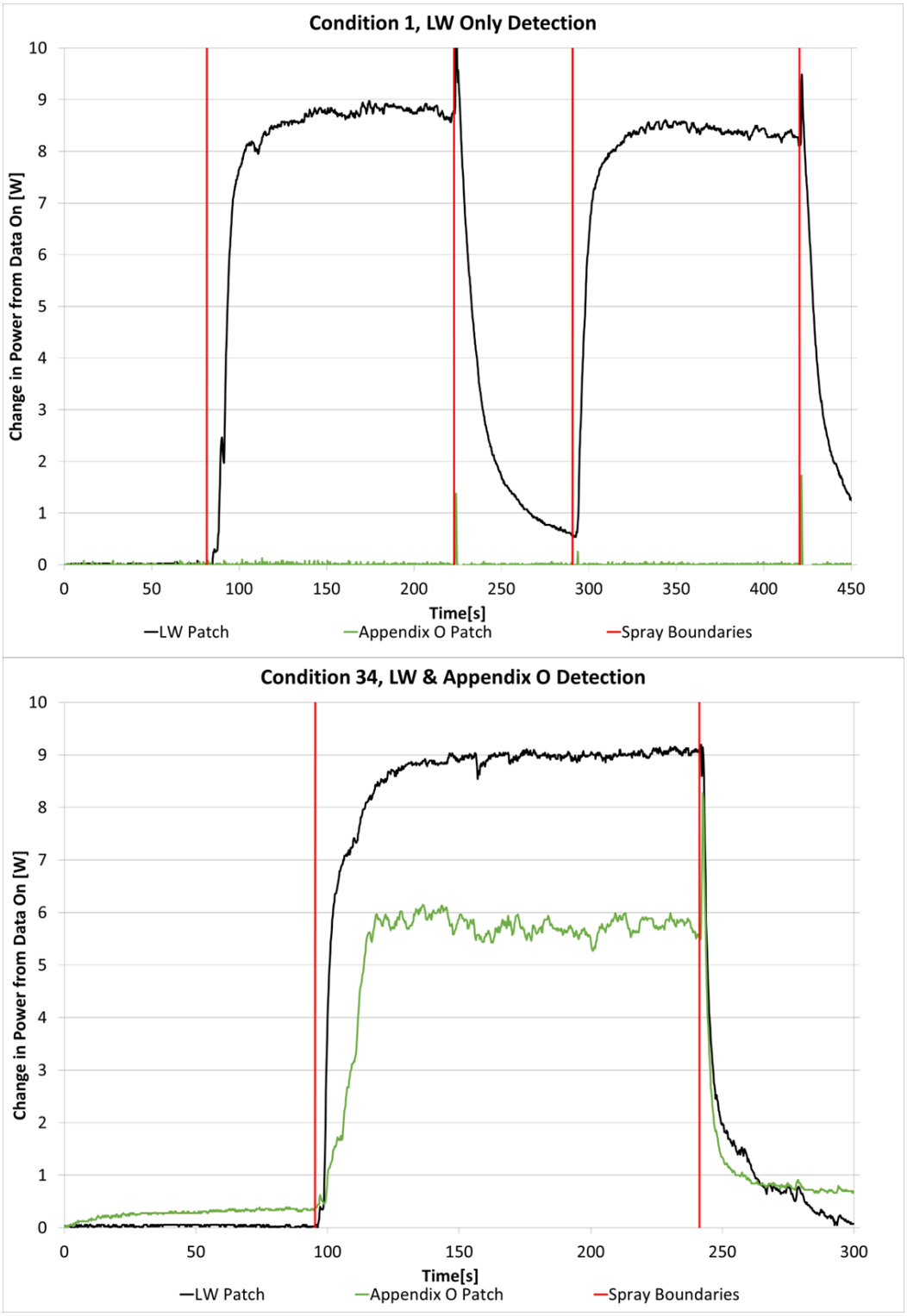

Figure 11: Example of sensor response for small droplet icing conditions (upper) and large droplet icing conditions (lower).

3.1.2 Laboratory Tests

Much of the laboratory scale testing was focused on the development of the software for the AIP system. Using the complete system, we were able to simulate the system response and to test thermal control to assess overshoot so safety levels could be set appropriately.

Prior to conducting the icing wind tunnel test, the system was also demonstrated whilst mounted on a car. Whilst not representative of flight conditions, the response of the various sensor technologies to changes in speed and precipitation could be assessed. This allowed relative performance of different technologies and builds to be directly compared. This proved to be crucial in defining the build for the heaters' insulated mounts.

AeroTex also benefitted from a close working relationship with the RTA icing wind tunnel in Vienna who allowed the technology to be tested as "ride-along" tests. This was outside of the SENS4ICE project but contributed to the development. For these tests the sensors were not mounted in optimal positions in the tunnel but provided invaluable data for the down selection of technologies for use in the AIP.

3.1.3 Ice Wind Tunnel Tests

Two icing wind tunnel campaigns were performed under SENS4ICE:

- The first test was conducted in the NRC Atmospheric Icing Wind Tunnel (AIWT) in Ottawa in April 2021. This test provided the data to support the Gate two assessment as well as assessing a secondary technology type.
- The second test was conducted in the TUBS Braunschweig Icing Wind Tunnel (BIWT) in May 2022. This test confirmed the performance of the redesigned AIP incorporating the insulated mount

The pre-evaluation two testing performed at NRC utilised a custom designed aerofoil that allowed inertial separation of droplet similar to that on an aircraft but a smaller scale (Figure 12). The testing showed that the sensors could accurately and quickly detect icing conditions down to low LWC conditions (Figure 13).

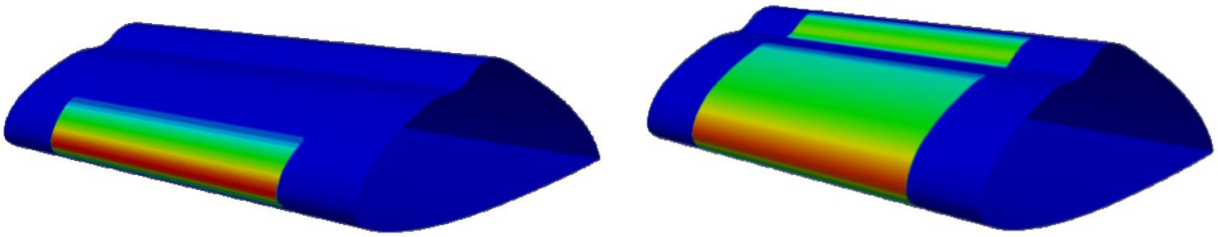

Figure 12: NRC IWT model configuration showing impingement for small droplets (left) and large droplets (right).

In addition, the NRC testing demonstrated that the concept of a network of sensors located in different positions could discriminate between icing conditions (Figure 11). Furthermore, an experimental approach to assessing the icing severity was also demonstrated based on a Nusselt-Reynolds correlation in dry conditions.

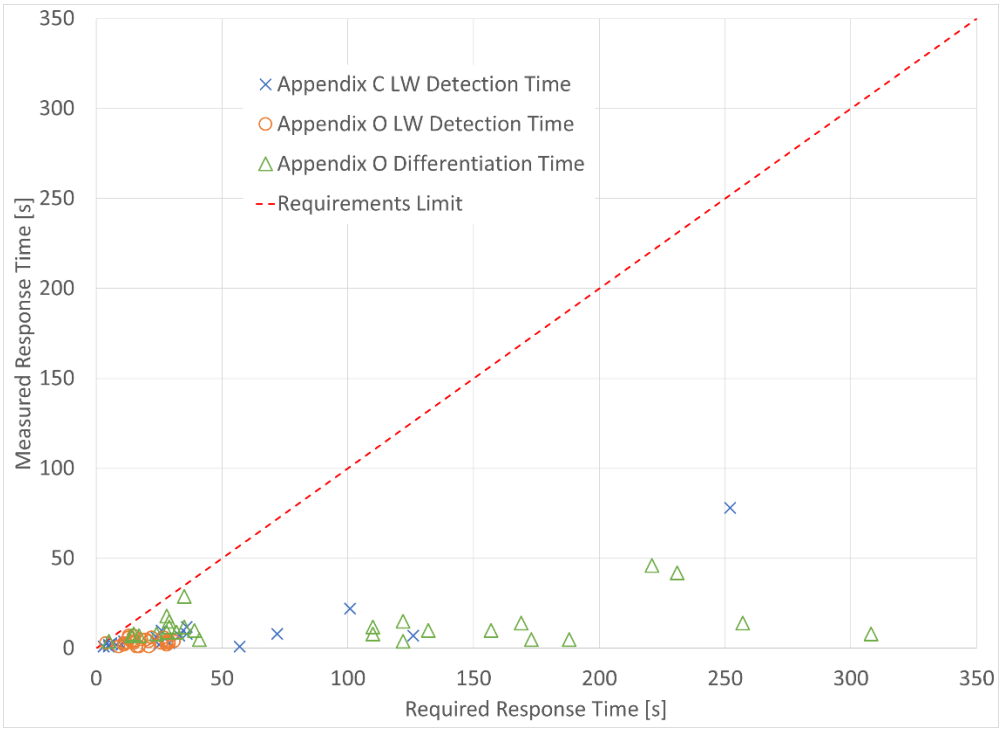

Figure 13: Graph showing measured vs required response time for all test points at the NRC AIWT test.

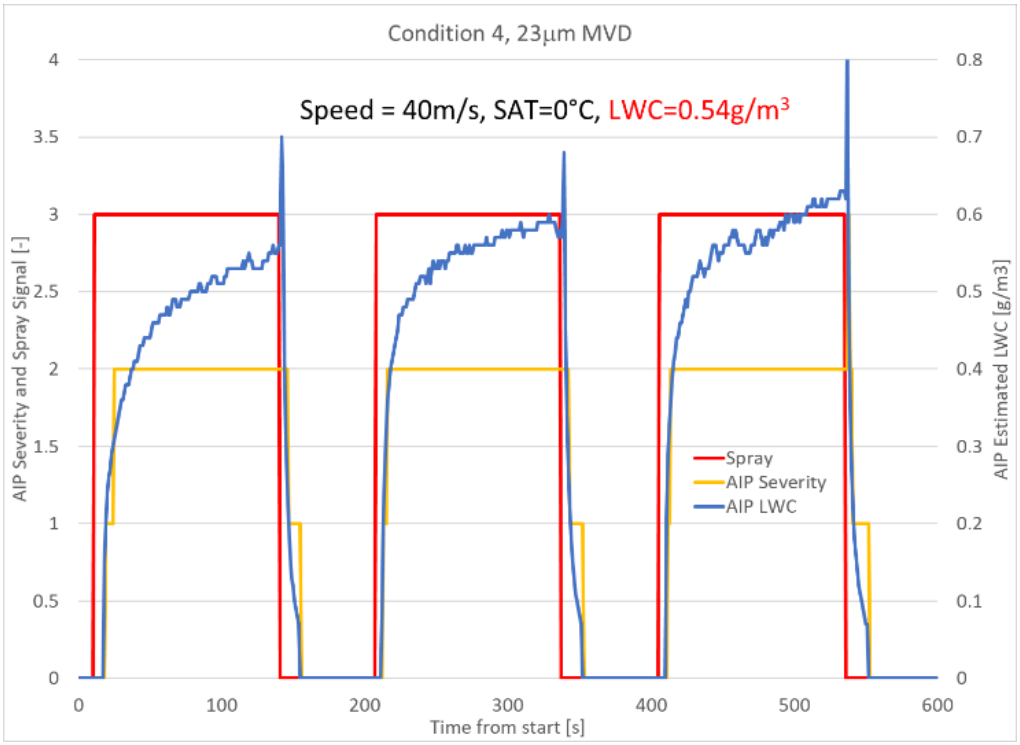

Figure 14: Example of LWC severity detection showing the raw LWC estimate and the associated AIP severity level.

After the AIP was down selected for flight test a design update phase was initiated to address potential issues with the system that were highlighted during the NRC test. This consisted of three main aspects: increasing operating temperature, reducing the sensor patch size to reduce power consumption and designing the thermal mount. These configurations were iterated as part of laboratory tests until two concepts were down selected

for test in the TUBS BIWT (Figure 15). This testing successfully allowed the best solution to be defined and taken forward to flight test.

Figure 15: Final icing AIP sensor design being tested in the TUBS BIWT.

3.1.4 Flight Test

For the flight test an array of 5 AIP were located along the centreline of the Embraer Phenom 300 flight test platform. The locations for the installation were based on the locations shown in Figure 10 and are shown mounted on the aircraft inFigure 16. For this installation wire bundles were run along the outside of the aircraft and routed in through a ventilation pot into the forward luggage bay.

Figure 16: AIP sensors mounted along the centreline of the aircraft [image AeroTex/ SENS4ICE project].

The AIP control and logging system that was installed on an equipment rack inside the aircraft is shown in Figure 17. The system consists of the main processor, logging and communication unit shown (orange box in

the figure), a power regulator unit (dark grey) and two in-house manufactured electronics units used for power monitoring and controlling power to the patches and the control unit.

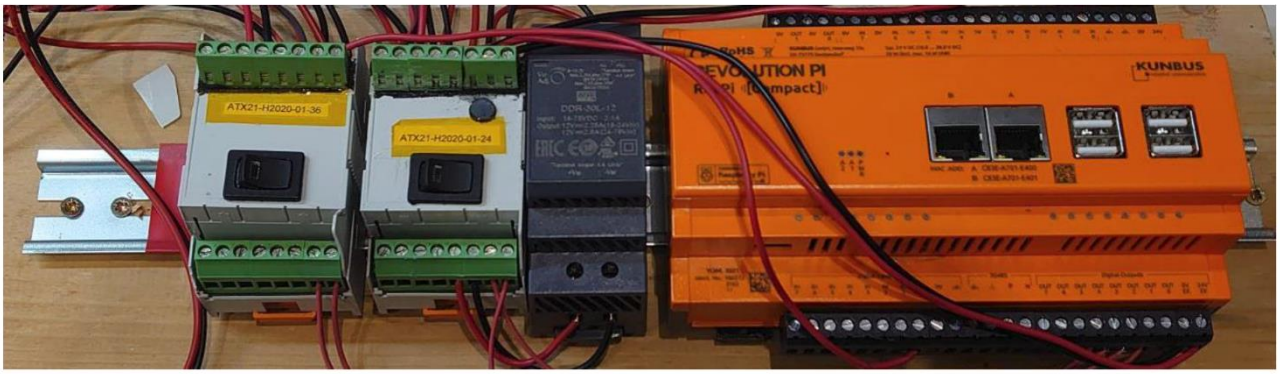

Figure 17: AIP control and logging system [image AeroTex/ SENS4ICE project].

The flight tests were based in East Alton, Illinois and were performed between the 22nd February 2023 and the 10th March 2023.

The system showed good response during the initial flight tests and some initial results are shown in Figure 18. The black dots represent when the reference ice detector detected any form of icing and the green dots show the MVD measured by the reference ice detector. The yellow dots show when any form of icing was detected by the AIP system and the yellow dots show when SLD conditions were detected. The figure shows that the system performed well in detecting all icing conditions and differentiating between small droplet and large droplet icing conditions.

Figure 18: AIP system response for flight 1475, shown alongside data from the reference sensors.

Initial attempts at assessing the severity of the icing conditions were also made and the results are presented in Figure 19. This approach shows some promise but requires further maturation.

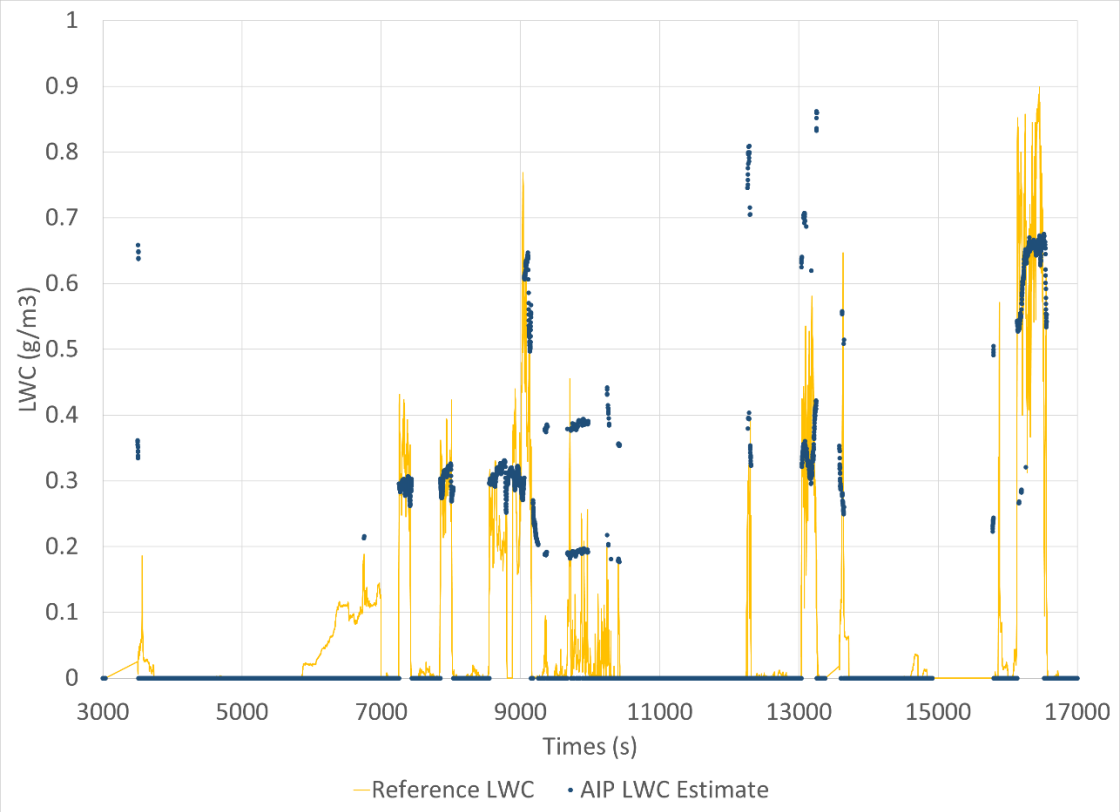

Figure 19: AIP icing severity estimation compared to reference instrumentation data.

During the tests the response of the AIP sensors degraded and the reason for this is currently under investigation.

3.2 Collins – IDS

3.2.1 Technology Description

Collins-IDS is made of two components: (1) Sensing Element that uses a proven and certified construction made of high temperature composite, temperature sensors and metallic heater that measure heat flux distribution and communicate this to the power interface control unit. (2) Power Interface Control Unit (PICU) that provides the necessary power to the sensing element, analyses the measurements, and makes recommendation on icing conditions Dry or App. C or App. O. Detection and differentiation is done with a built-in detection algorithm within the PICU. The system is scalable to include one or multiple sensing elements positioned on sensitive areas of the airplane, powered individually, and controlled together by a master controller.

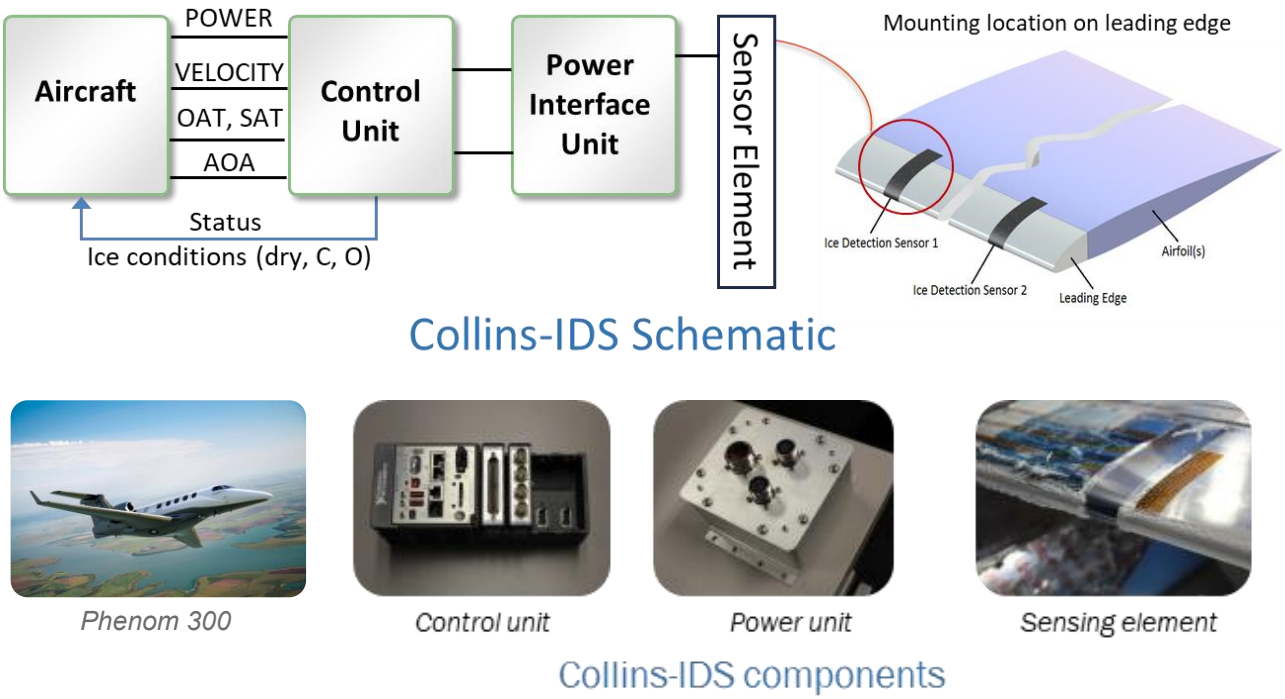

Figure 20: Overview of Collins-IDS structure, possible mounting location, and communication with the aircraft [Phenom 300 aircraft image copyright Embraer].

Installation of Collins-IDS on the aircraft is flexible. It can be integrated on the leading edge by being installed inside of the leading edge and/or areas of the leading edge where no ice protection is installed, for example wing and/or tail tips, vertical fin and other. IWT and flight test results in sections 3.2.3 and 3.2.4 show very good performance for detection and differentiation within the required response time for installation on the leading edge. Further improvements can be achieved by installing the sensor in other more sensitive areas than the wing leading edge to ensure ice detection before wing or other aerodynamic surfaces. For easy maintenance and replacement, the sensor can be installed in a dedicated strip over the leading edge, under the leading edge or integrated in a recessed composite leading edge. This way Collins-IDS is replaceable without replacing the whole leading edge.

IWT and flight test results also showed the potentiality of the sensor to different icing conditions by using one single sensing element. If necessary, further improvements can be done tailoring the heater strips with different power density along the sensor chord to improve performance.

Prior to flight test, further refinements of the power interface control unit was carried out reducing the sensor power requirement by over 62% from 800W to less than 300W and improving the accuracy of the detection algorithm. The sensor completed 220 hours of icing wind tunnels tests at Collins Aerospace and NRC test facilities as well as 25 hours of flight test in natural icing conditions.

The system achieved TRL 6 in 2023 following a successful flight test with Embraer during the SENS4ICE North America flight test campaign.

3.2.2 Laboratory Tests

Laboratory tests were performed on Collins-IDS components at early stage of the project to fine tune the design parameters and to prove the concept. The first set of tests were conducted on the Control Unit (CU) with the primary objective to evaluate the functionality of the detection algorithm and the communication interfaces. The second tests were conducted on the Power Interface Unit (PIU) to verify the functionality and ability of the unit to provide necessary power the sensing element and to prepare the unit for Safety of Flight (SOF) tests. SOF tests were then performed to confirm that the component can function efficiently and safely under flight operational conditions. Lastly, third tests were carried out on the sensing elements prior to its integration in the Ice Wind Tunnel. In this final stage, operational tests were performed on the sensing element (sensors and heater), aiming to ensure that the readings obtained from the sensors were accurate and aligned with the estimates.

3.2.3 Ice Wind Tunnel Tests

Table 4: IWT tests completed by Collins-IDS as part of SENS4ICE technology development and maturation.

IWT test	Test Facility	Duration	Description
Round 1, May 2020	Collins, Ohio	40 Hours	Feasibility tests to validate CFD models over Dry, App C and App O conditions and to verify App C/O discrimination.
Round 2, Oct. 2020	Collins, Ohio	40 Hours	Tested operation of integrated system over a wide range of icing conditions. Data used to validate the detection algorithm and its ability to detect and discriminate App C/O conditions.
Round 3, Jan. 2021	Collins, Ohio	40 Hours	Demonstrate (1) reduction in power requirements and improved sensor performance (2) the online ice detection and differentiation between App C and App O icing conditions taking the sensor to the next level towards flight test.
Round 4, Mar. 2021	NRC, Canada	20 Hours	NRC facility provided more capabilities within the App. O icing envelope. The data was used to expand the detection envelope beyond the capabilities in the Collins facility and to demonstrate the efficacy of the sensor in differentiating the App. C and App. O as well as extend the points for our simulation verification & validation.
Round 5, Apr. 2022	Collins, Ohio	40 Hours	Validate results for installation on vertical fin instead of horizontal stabiliser.
Round 6, Sep. 2022	Collins, Ohio	40 Hours	Validate the integrated system as per the flight test configuration and verify that all system components are performing as expected.

Collins-IDS sensor was tested at Collins Aerospace and NRC icing wind tunnel facilities. Collins-IDS completed 220 hours of IWT tests over the course of its development to date. This was done over six phases/rounds as presented in Table 4, providing a good data set for incremental improvement of the technology.

From the IWT tests, the sensor is capable of detecting and differentiating icing conditions presented in the NRC test matrix with no false alarms. The results show the sensor ability to detect entry and exit of icing clouds with the required response time. For most App. C conditions, the LW entry and exit response times are similar. For those conditions where there is a significant difference between the two, both the response times are still significantly less than the required response time. All but two of App. O conditions have entry and exit detection times within the required values. For all App. O conditions, the discrimination entry and exit times are well within the required values. Furthermore, the total time from entry to discrimination is always within the required discrimination times.

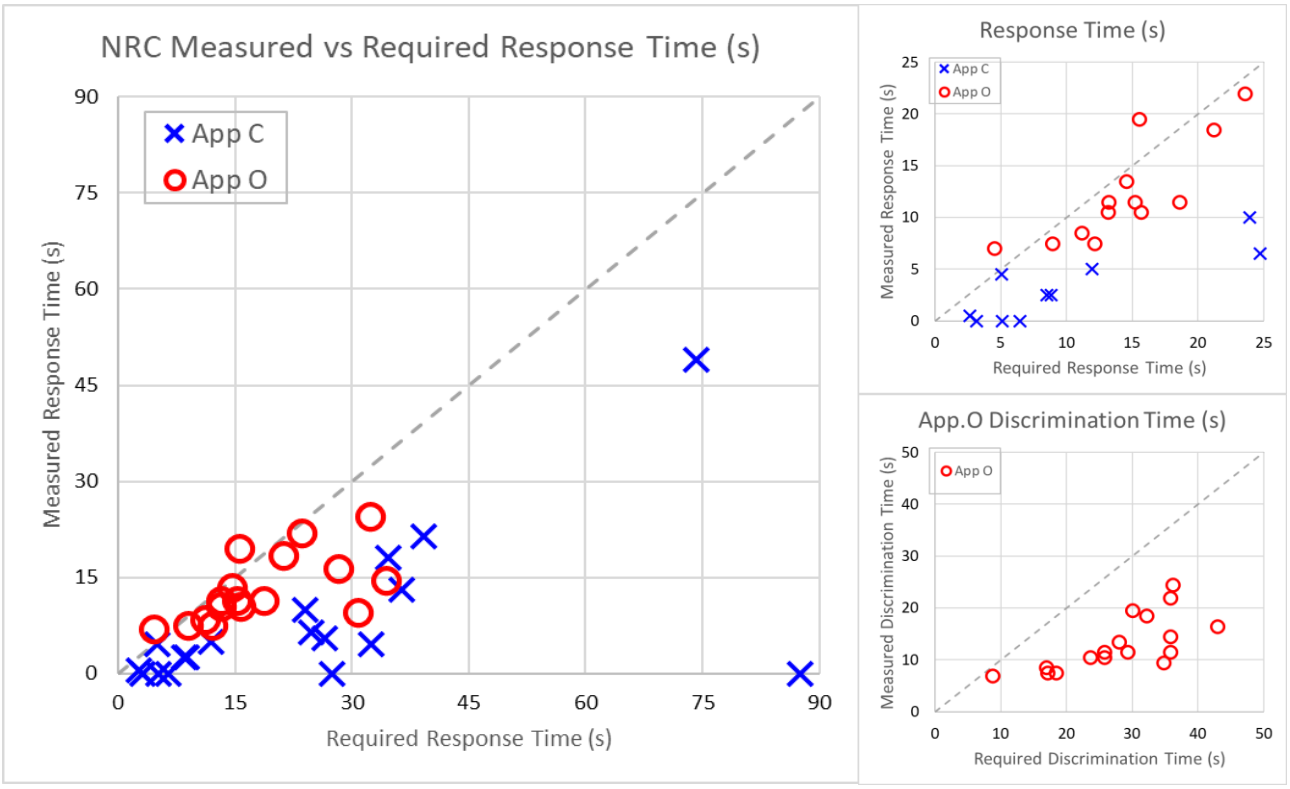

Figure 21: Graphs showing measured vs required response time for all test points (left) and test points with low response times (top right), and measured vs required discrimination time for all App. O test points (bottom right). All the points below the grey dashed line indicate a discrimination time that met the requirements.

From Figure 21, it can be seen that the Collins-IDS has response times almost always lower than the required values. While the lower response times are significantly lower, the ones that are higher than the required values are higher by a small amount, which could be put down to experimental error. In all App. O. conditions, the discrimination times are lower than the required values.

Table 5 shows the summary of results of the testing. While the percentage of test points within required response times uses the hard limit of the required response times (although these are more guidelines), a better evaluation of the system can be seen by the average time and percentage deviations, which are calculated as the averages of $t - t_{required}$ and $\frac{t - t_{required}}{t_{required}} \times 100$ respectively (t indicates the sensor response time). The values suggest that for most of the cases, the values are overwhelmingly lower, and for those cases where they are higher, they are higher by only a small amount, which could be attributed to experimental error.

Table 5: Results summary table, including the standard and repeat test points. For all columns indicating the percentage of test points meeting some criteria (e.g., Test Points Detected), the denominator is the total number of test points.

	Test	Test Points Detected [%]	Test Points Detected within Response Time [%]	Test Points Detected within 1.5X Response Time [%]	Average Time Deviation [s]	Average Percentage Deviation [%]
NRC	**App. C Test Points**	100.00%	100.00%	100.00%	-23.08	-72.31%
	App. C Repeat Points	100.00%	100.00%	100.00%	-51.21	-82.55%
	App. O Test Points	100.00%	88.24%	94.12%	-14.85	-51.63%
	App. O Repeat Points	100.00%	100.00%	100.00%	-2.10	-23.53%

3.2.4 Flight Test

The Collins-IDS sensor was flight tested in the SENS4ICE North America Flight Test campaign in February/March 2023. Figure 22 shows a view of Collins-IDS installed on Embraer Phenom 300.

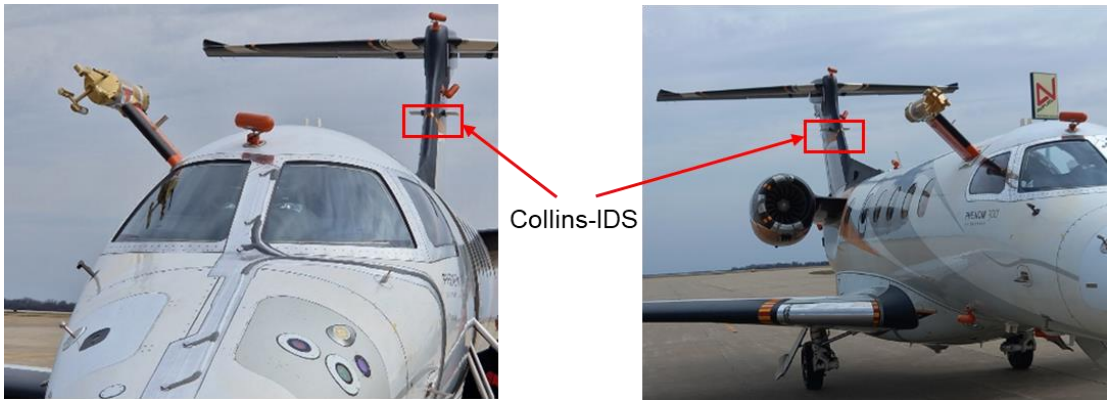

Figure 22: Collins-IDS sensors mounted on the vertical fin of the aircraft [image copyright Embraer/ SENS4ICE project].

While during the IWT, the conditions were controlled both in terms of LWC and MVD, the conditions during the flight tests were more fluid; both the LWC and MVD were temporally variable. Both the control algorithm as well as the detectors were updated to perform better under non-experimental (uncontrolled) conditions. The class boundaries for the new combined differentiator are shown in Figure 23.

For the flight tests, the sensor can detect and differentiate icing conditions encountered by the aircraft, to a great degree of accuracy, and within a short time of conditions being encountered. The performance of the detector is shown in Table 6.

The confusion matrix was generated using class boundaries calculated using observed prior probabilities of conditions – this results in the best possible confusion matrix where every classification error has the same weight. The priors could instead be weighted according to the impact of misclassification, moving the boundaries slightly and resulting in a more practical classifier.

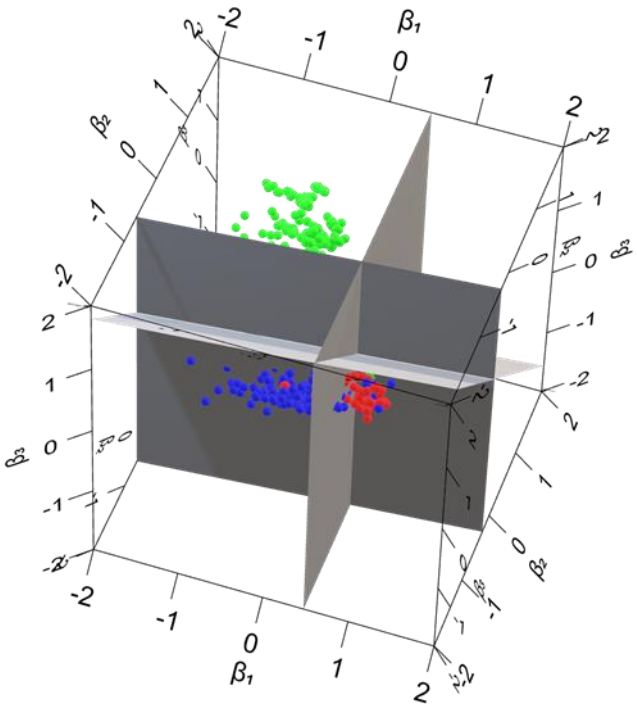

Figure 23: Classification boundaries for all three conditions. Dry conditions (green), App C conditions (blue), and App O (red).

Table 6: Confusion Matrix for Collins-IDS detection and differentiation algorithm

		Predicted Class		
		Dry	App C	App O
True Class	Dry	97.17%	2.83%	0%
	App C	1.69%	91.53%	6.78%
	App O	2.44%	18.29%	79.27%

An example flight test campaign is shown in Figure 24. The raw outputs of the Collins-IDS are shown on the top graph, along with the areas denoting detected conditions: dry (green), App. C (blue), and App. O (red). For comparison, the graph on the bottom shows the reference measurements “ground truth” LWC and MVD, and the “ground truth” conditions are again depicted with areas of the same colours.

Flight test 1476 - 25 February 2023

During the North America flight test campaign, the flight 1476 encountered multiple significant icing events. Specifically, there were five instances where the aircraft experienced App. O icing conditions, which were denoted in red. Concurrently, App. C conditions were observed and marked in blue.

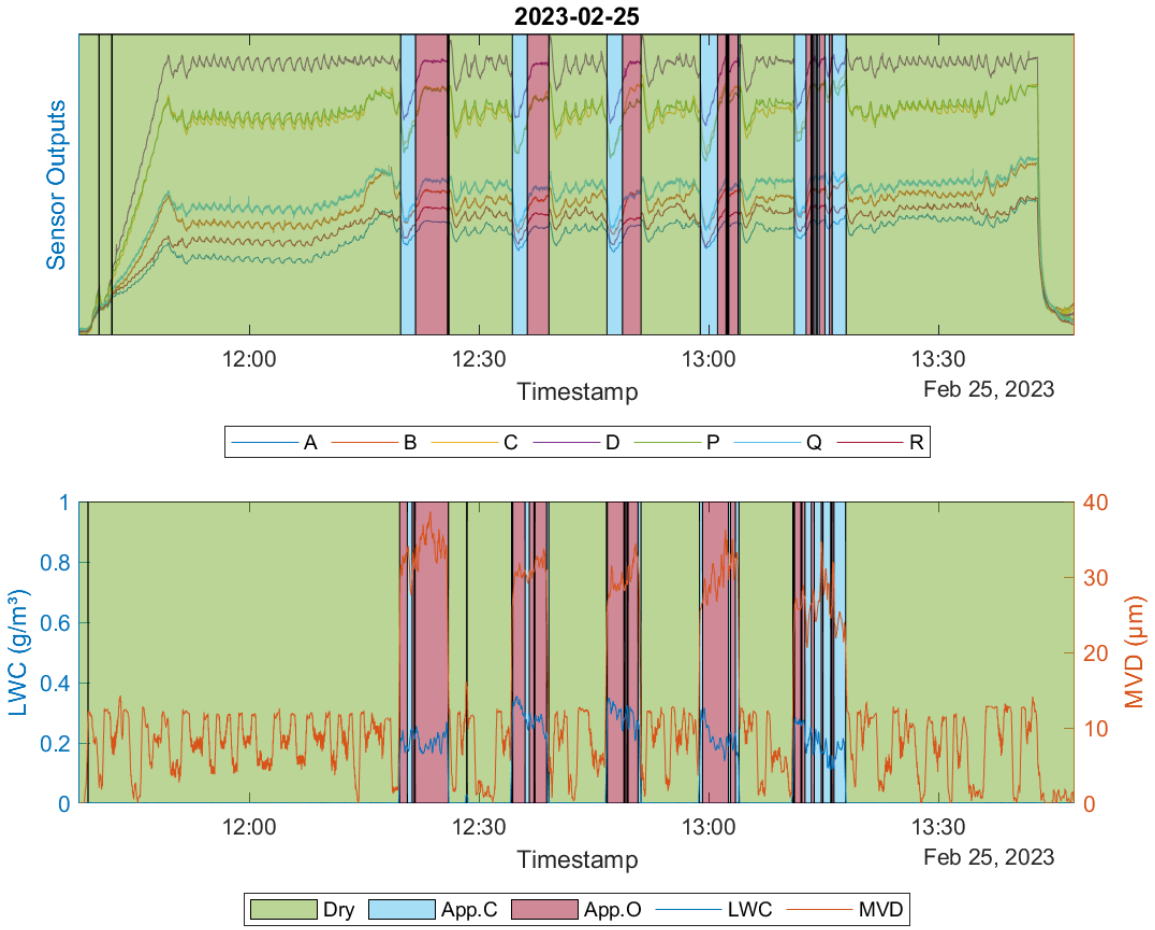

Figure 24: App. C and App. O encounters during Flight Test. Bottom figure is ground truth, top graph is Collins-IDS sensors and detector outputs.

3.3 DLR – LILD

3.3.1 Technology Description

The basic working principle of the LILD sensor consists in detecting ultrasonic lamb wave packets, which are transmitted through an icing prone aircraft structure as e.g. wing or tail leading edges. Therefore, a transmitter and a receiver are placed on this structure in order to obtain the wave propagation behavior, see Figure 25 left. An ice accretion can be detected in a variation of the received signal amplitude and propagation time, since a layer of ice changes the mechanical parameters (stiffness, damping and mass) of the skin material. The sensor itself consists of an electronics box within the fuselage, which is used to generate the transmitter signals and to analyse and process the obtained receiver signals, and at least one transmitter and one receiver piezoelectric transducer, which have to be applied on the aircraft surface, where ice accretion has to be detected, see Figure 25 on the right.

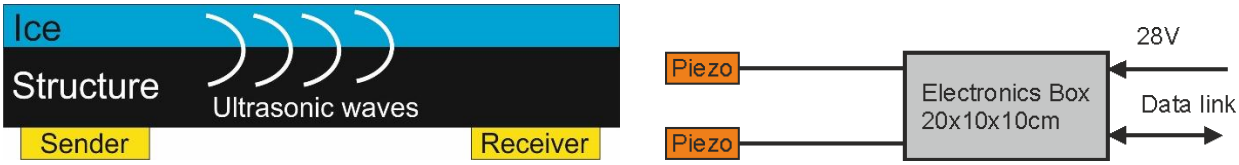

Figure 25: Sensor principle (left) and sensor setup (right).

Aircraft use and mounting

As already mentioned, the mounting location on aircraft is where an ice accretion needs to be detected, as e.g. leading edges as shown in Figure 26. An ice accretion can be sensed and the ice protection system can be activated instantly to remove the ice and prevent further accretion. In addition, the LILD sensor allows a success check of the ice protection system or in the case of electric ice protection systems a modulation of the heating power to prevent ice accretion without using too much excess power thus saving energy.

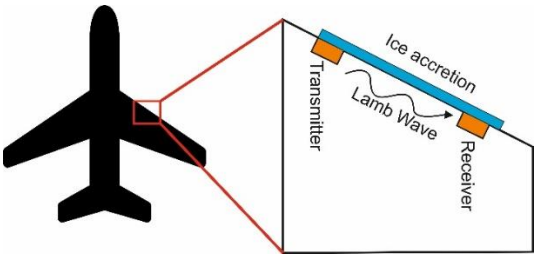

Figure 26: Mounting principle on aircraft.

3.3.2 Laboratory Tests

In the SENS4ICE test campaign, ice thicknesses of more than approx. 5mm led to a loss of the sensor signal due to the damping of the ice layer and insufficient amplitude at the receiver. In pretests in a different icing wind tunnel, signals could still be obtained up to ice thicknesses of 15mm. In this case, bigger transducers have been used, which are able to provide more signal amplitude and therefore allow measuring higher ice thicknesses. An example measurement and a photo of the ice layer after separating from the airfoil is given in Figure 27. Every data point corresponds to 30s of icing time.

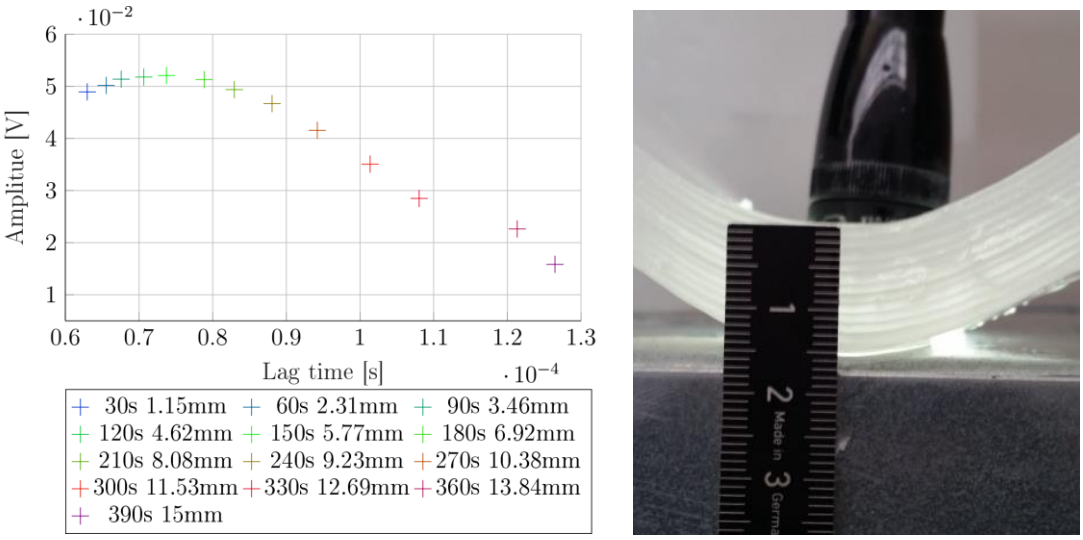

Figure 27: Detection of ice layer of up to 15mm.

3.3.3 Ice Wind Tunnel Tests

After analysing all performed measurements, the following trends are visible for the LILD sensor in the tested configuration

- The beginning of the ice accretion from the clean airfoil without ice is detected at very thin ice coverages with a very low delay time in the range of few seconds well below the maximum times, see Figure 28.
- The delay for detecting the end of the icing period is significantly greater ranging up to more than a minute;
- A detection of ice present on the structure is possible without actual icing (in contrast to e.g. heat flux sensors, which only detect icing in progress due to latent heat release) so ice remaining on the aircraft after exiting the icing cloud can be detected;
- Ice thicknesses above a certain threshold lead to signal loss due to damping of the waves. This was only relevant for one repeat test point and the endurance test;
- A discrimination between App. O and App. C was not possible with the setup since the spatial ice accretion patterns were too similar.
- An ice thickness measurement and by this an accretion rate measurement is possible but by the time quite noisy;

Since the SENS4ICE IWT was the first test in a calibrated IWT, only the weeks between finishing the test at 12.03.2021 and the project-internal deadline of the IWT report could be used to analyse the data and develop detection algorithms for the beginning of the icing, the end of icing and the detection of the ice thickness and accretion rate. Future development of the LILD sensor should therefore include more IWT testing to increase the data basis and obtain improved algorithms to derive the sensor output signals from the measured wave paths.

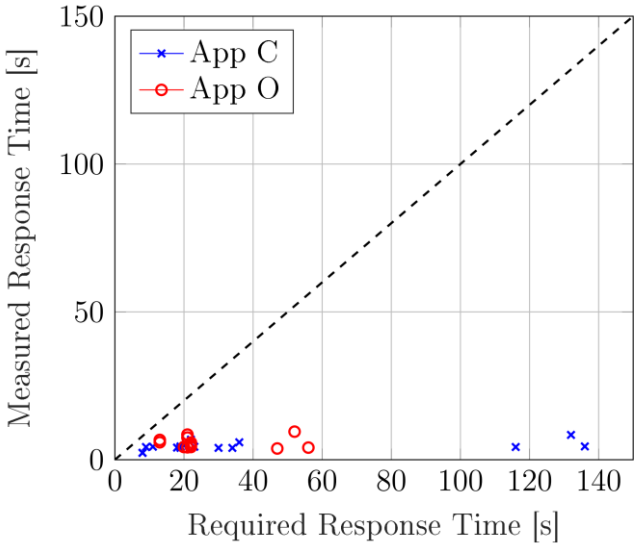

Figure 28 Graph showing measured vs required response time for all test points. All the points below the black dashed line indicate a response time that met the requirements.

3.3.4 Flight Test

For the flight test, a final update of the electronic sensor hardware was done to ensure continued functionality and the operability without the need of an operator besides activation and deactivation of the system. For redundancy and since the space was available in the 19” rack, which was used in the flight test, two individual sensor hardware units were installed. Figure 29 shows the final hardware and the sensor box.

Figure 29: Flight test sensor hardware.

The transducers for the actual ice testing have been installed on the right wing. There a pylon has been added which carries all atmospheric probes as shown in Figure 30 on the upper left. At this pylon, the transducers are placed on the inside of its leading edge. In the lower part of Figure 30 a photo of the transducers in comparison to one Euro coin is given as well as a photo of the inside of the leading edge. At the places with the red tape, the transducers have been mounted with a measurement distance of 30 cm.

Due to the small size of the transducers, the sensitive part of the sensor can be placed even in quite tight locations.

Figure 30: Transducer placement on test aircraft [aircraft image Safire].

During the flight test campaign, two clean air calibration flights and 15 actual test flights in icing conditions were performed. In the calibration tests it was observable, that an amplitude change was happening in clean air which triggered the ice detection. This was found to be a temperature effect of the mounting location of the transducers and could be compensated with the temperature sensors, that have been installed in parallel at the transducer locations.

In the icing test flights, a wide variety of different icing conditions could be encountered ranging from very light to heavy. To detect the presence of ice on the aircraft structure, a combination of pulse lag time and pulse amplitude thresholds were used. If one of the thresholds is exceeded, ice is detected on the aircraft. Furthermore, a linear relation was used to calculate the ice thickness on the basis of a lag time increase. With the current state of data analysis, the following conclusions can be drawn:

- The LILD sensor was able to detect an ice accretion in all cases when the aircraft entered the icing conditions with a previously clean airfoil.

- With the current state of the sensor, the main output is the “ice present” signal, which is reset when the ice is removed (e.g. in the flight tests by descending into warm air to melt the accreted ice).
- Reaction time of LILD is very short. The sensitivity to even thin layers of ice, which is already known from the wind tunnel tests, could be confirmed.
- The ice thickness estimation based on the additional lag time is imprecise with the current data since the temperature and shape of the ice layer also have an influence.

As an example, Figure 31 shows a diagram of one measurement with the LILD ice present flag together with the icing flag and the static air temperature<0 indication from DLR’s microphysics cloud probes. It can be seen, that LILD always indicates the presence of ice shortly after icing conditions are detected by the microphysics probes. Ice accretion from App. C and App. O conditions are both detected.

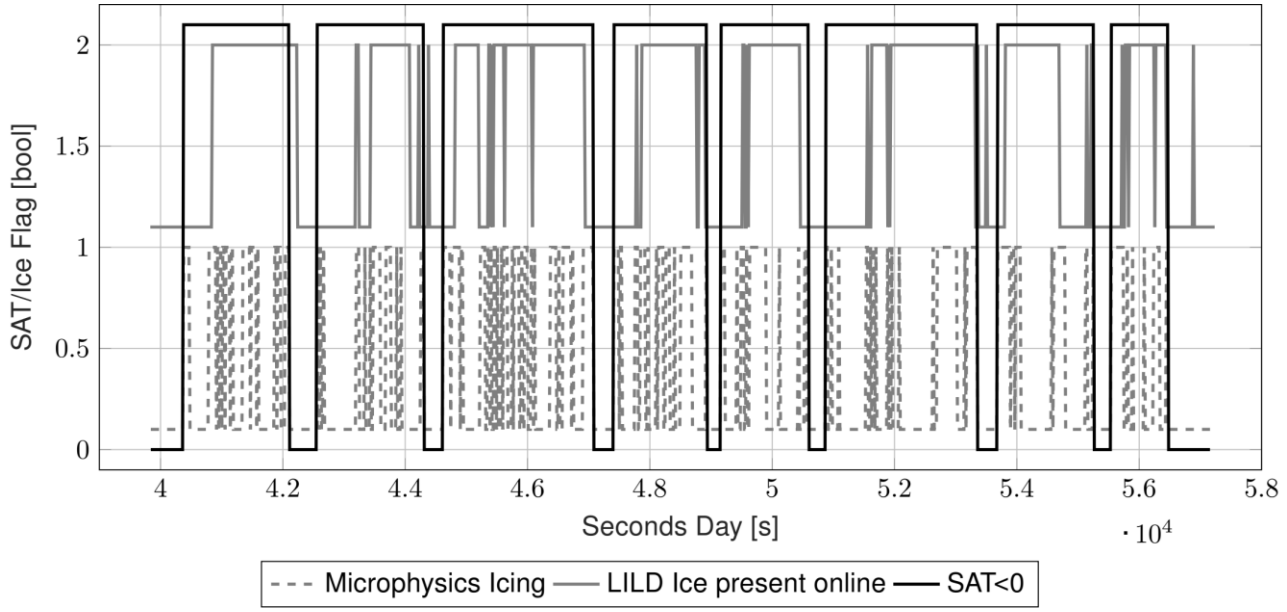

Figure 31: Ice flags of Microphysics (µP) and LILD with static air temperature.

3.4 DLR – CM2D

3.4.1 Technology Description

The CM2D is a combination of two scientific, flight-proven instruments. The CM2D is not developed for commercial aviation, but rather for scientific flights, development within SENS4ICE aims to enhance the possibilities of precisely measuring SLD conditions.

The two instruments which constitute the CM2D are:

- Nevzorov Hot-Wire LWC/TWC probe;
- Backscatter Cloud probe with Polarization Detection (BCPD).

The Nevzorov probe [10, 12] itself consists of four sensors, two TWC collector cones, an LWC collector hotwire and a reference sensor (see Figure 32). The reference sensor is aerodynamically protected from the impinging droplets and is used to correct the measurements of the other sensors for dry air losses. The Nevzorov probe derives liquid water content from the power that is needed to maintain its sensors at a constant temperature.

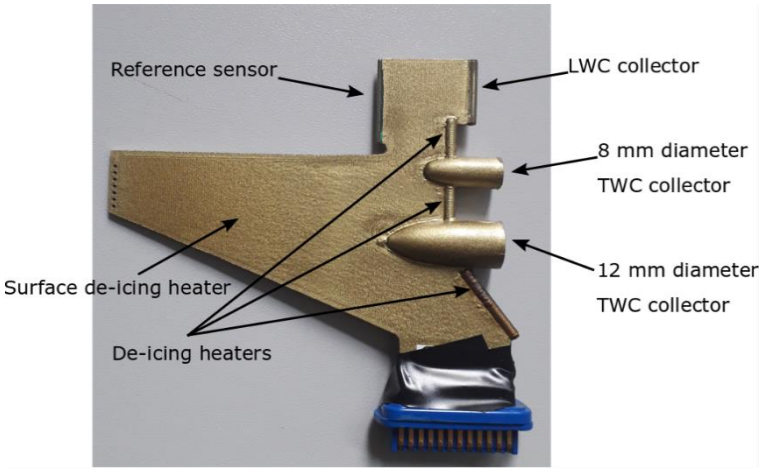

Figure 32: Sensor head of the Nevzorov probe.

The BCPD [11, 13] is a scattering instrument that measures droplet size from the intensity of backscattered light. It incorporates a polarization filter and is thus also able to determine the shape of the sampled particles. By doing so it is able to distinguish droplets from ice (spherical and non-spherical particles). The probe measures particles up to 42 µm.

3.4.2 Laboratory Tests

A special calibration fixture was constructed within SENS4ICE for the calibration of the BCPD.

3.4.3 Ice Wind Tunnel Tests

In total, four wind tunnel campaigns were conducted, which can be seen in Table 7.

Table 7: Wind tunnel testing of the CM2D components.

Time	Wind tunnel	Components tested
07.01.2020-10.01.2020	Braunschweig Icing Wind Tunnel	Nevzorov
20.07.2020-31.07.2020	Braunschweig Icing Wind Tunnel	Nevzorov + BCPD
September 2020	NRC	Nevzorov
09.11.2020-10.11.2020	Collins Aerospace	Nevzorov

During the wind tunnel testing, we found that the detection of icing is generally straightforward with the CM2D. In 100% of the cases ice was detected within one second of the start of the spray. Also, exit from icing is accurately detected within a second. The CM2D is able to differentiate liquid water from ice, so even when recirculation of ice was present it detected the exit from the icing conditions. Furthermore, we found, that the droplet size distribution that we measured with the BCPD compares well to that measured with established airborne instruments such as the CDP. The agreement of the MVDs of CDP and BCPD within their size range was within ±10% for the majority of the test points.

On the basis of the IWT tests, an algorithm was developed that establishes whether App. C or App. O conditions are present. This algorithm is based on the ratios of the different Nevzorov probe sensors, all of which collect droplets of different sizes differently well. The Hotwire sensor has the highest collection efficiency for droplets below 25 µm diameter, but at larger diameters droplets tend to splash on it and are not entirely collected. The 8 mm and 12 mm cone sensors have low collection efficiencies for small droplets, but collect droplets with large diameters without significant losses due to droplet splashing. The ratios between the sensor readings can therefore be used as an approximation for the MVD. However, this approximate MVD does not let us differentiate between App. C and O necessarily. App. O conditions with a small SLD mode are not detectable with this method. We therefore established a relationship between the ratios of the LWC measurements of the Nezvorov probe and the BCPD MVD for unimodal, App. C distributions. For App. O test

points, we observe a deviation from this relationship, as the sensor ratio increases but the BCPD is not able to detect any large droplets. We were able to reliably differentiate between App. C and O conditions using this approach (see Figure 33).

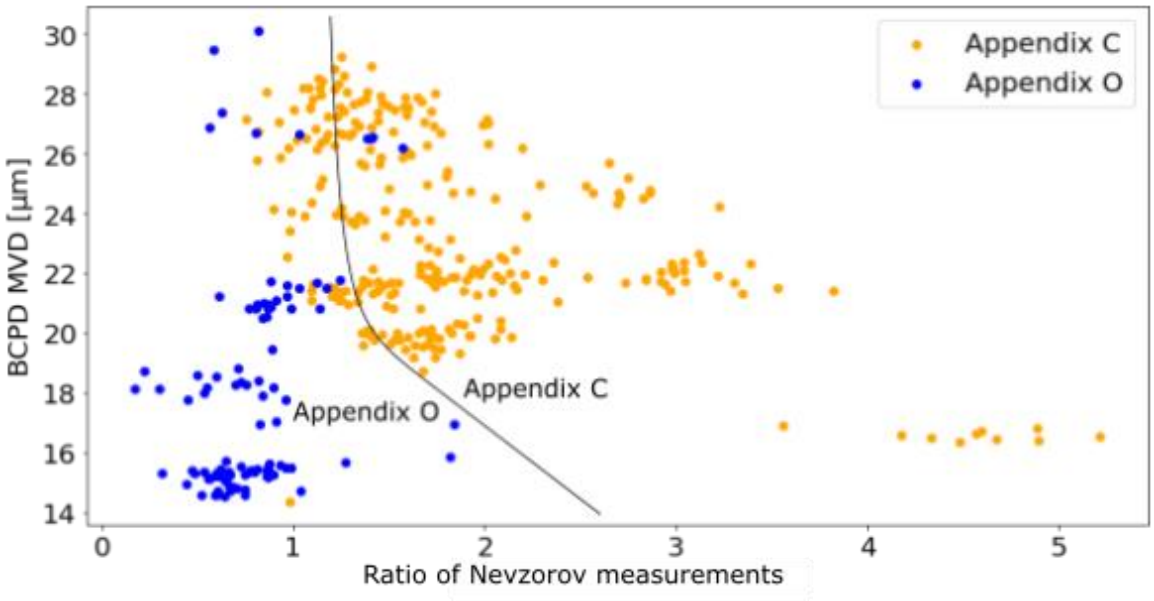

Figure 33: Illustration of the algorithm for the distinction between App. C and O.

3.4.4 Flight Test

DLR tested the CM2D and the individual components of the CM2D during several flight campaigns (seeTable 8). During the Cirrus-HL campaign, just the BCPD component was integrated into a side window on DLR's HALO Gulfstream 550 aircraft. The campaign focused on high-latitude cirrus clouds, but we were also able to obtain some data in low level and mixed-phase clouds. In the high cirrus clouds, the response of the CM2D to ice particles could be established. App. O conditions were not encountered during Cirrus-HL.

Both components of the CM2D were flown during the HALO-AC [11] campaign on the Polar-6 aircraft of Alfred-Wegener Institute. The campaign focused on Arctic mixed-phase clouds. Numerous icing conditions were encountered, but no App. O conditions. The data from the campaign allowed us to develop the algorithm for estimating the number of liquid and ice particles. On the basis of that algorithm, we are able to distinguish, pure ice, mixed-phase and supercooled clouds. The differentiation between the three types of clouds is however somewhat fluid and depends on the definition of mixed-phase clouds (e.g. what is the minimum number of ice crystals that need to be present in a given volume for a cloud to be considered mixed-phase). For the CM2D, the minimum ice particle concentration that can be detected is approximately 0.01 g/m³.

Table 8: Flight testing of CM2D components.

Time	Campaign name	Location	Components tested
24.06.2021-30.07.2021	Cirrus-HL	Oberpfaffenhofen, Germany	BCPD
14.03-2022-13.04.2022	$(AC)^3$	Longyearbyen, Spitzbergen	Nevzorov + BCPD
03.04.2023-27.04.2023	SENS4ICE	Toulouse	Nevzorov + BCPD

Finally, the CM2D was tested during the European SENS4ICE campaign, where a large number of App. O conditions were measured. The installation of the two instruments on the aircraft can be seen in Figure 34. Both instruments were mounted on the side of the fuselage, several meters behind the aircraft nose. The position of the instruments was mostly dictated by availability. The DLR team would have preferred a position further towards the nose of the aircraft for the BCPD, in order to reduce the influence of the fuselage on the measurement, but no such position was available.

Figure 34: Nevzorov probe and BCPD integrated on the SAFIRE ATR-42 aircraft during the European SENS4ICE campaign [image DLR/ SENS4ICE project].

We tested the analysis algorithm on the flight data. However, it was observed that the BCPD sample area lay in a region close to the fuselage where the airflow was strongly altered. The MVD measurements of the BCPD were thus deemed to be unreliable. A reduced version of the algorithm that relies solely on the ratio of the Nevzorov measurements was used to distinguish App. C and App. O conditions. App. C and O conditions can be distinguished with the CM2D, if a large number of large droplets is present and if the App. O conditions are relatively homogeneous. This can be seen from Figure 35. The three-minute long App. O encounter at approximately 14:33 is accurately detected by the CM2D. The shorter encounter at approximately 14:14 is missed, because the presence of ice crystals was detected. SLD and ice crystals both cause a decrease in the ratio between the LWC sensor and the TWC sensors of the Nevzorov probe. If ice crystals are present in the BCPD data, the decrease in the LWC sensor to TWC sensor ratio of the Nevzorov probe is assumed to be due to these ice crystals. Conditions where both SLD and ice crystals are present can therefore not be differentiated with the BCPD.

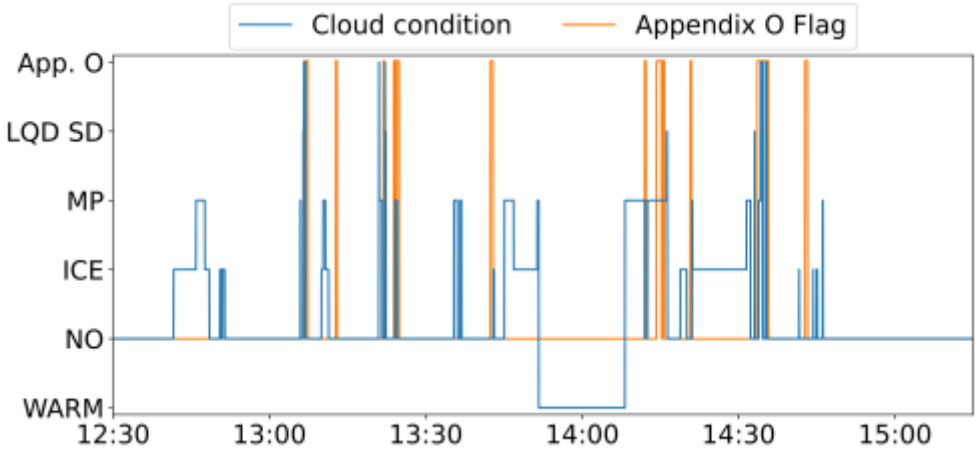

Figure 35: Cloud condition detected by the CM2D (blue) and App. O indication from the reference data (orange).

3.5 HON – SRP

3.5.1 Technology Description

The SRP (Short Range Particulate) sensor is an optical sensor based on collecting backscattered light from individual particles in the environment directly outside of the aircraft skin as shown in Figure 36. Using this particle-by-particle measurement, the sensor measures the overall particle size distribution, which are then used to derive the total number concentration, liquid water content (LWC), and median volume diameter (MVD). Using the size distributions, the sensor will discriminate between App. C and App. O. In the current SENS4ICE design, the sensor will not be able to detect the entire App. C envelope.

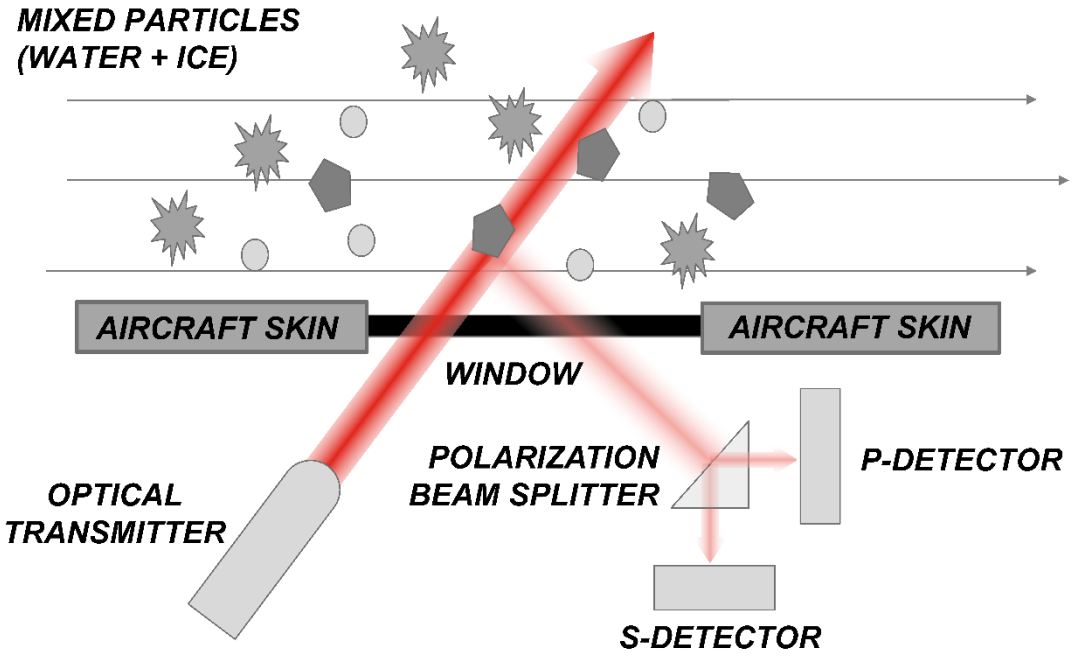

Figure 36: Flush mounted sensor optical design

3.5.2 Laboratory Tests

Prior the real life testing in Ice Wind Tunnel or Flight Testing, the updated SRP must have been calibrated and set up in laboratory. In Figure 36 is displayed optical head mounted in laboratory fixture for laser power setup and calibration. Calibration was done with use of water droplet generator which is designed to produce consistently sized water droplets.

In addition, prior to the Flight Test campaign the Safety Of Flight tests were required in order to be allowed to install SRP into aircraft. To fulfill SOF requirements compliance in following DO-160G areas was required to be shown:

1. Temperature
2. Temperature Variation
3. Humidity
4. Crash safety and Operational Shock
5. Vibrations
6. Power Input
7. Voltage Spike
8. Audio Frequency Conducted Susceptibility
9. RF Emissions
10. Lightning Direct Effects
11. ESD

Some of the test areas were identified as potentially harmful for the sensor lifespan and performance, analyses were done instead of real prototype testing (3,4,5,7,8,10,11).

Temperature testing was done in Honeywell Brno(CZ) Environmental Lab (Figure 37). Power testing was done in VTUPV Vyskov (CZ) (Figure 37) and RF Emissions tests were done in UNIS Brno (CZ) (Figure 37).

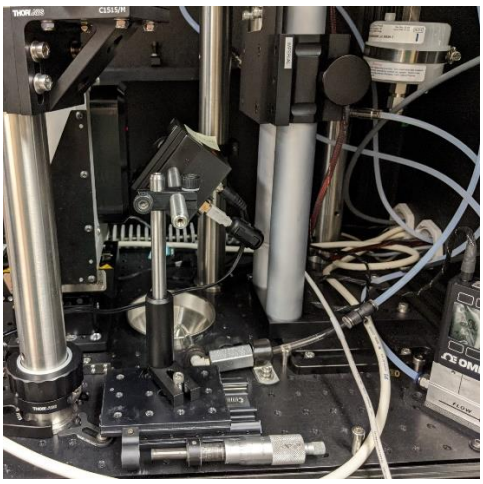

SRP calibration using droplet generator

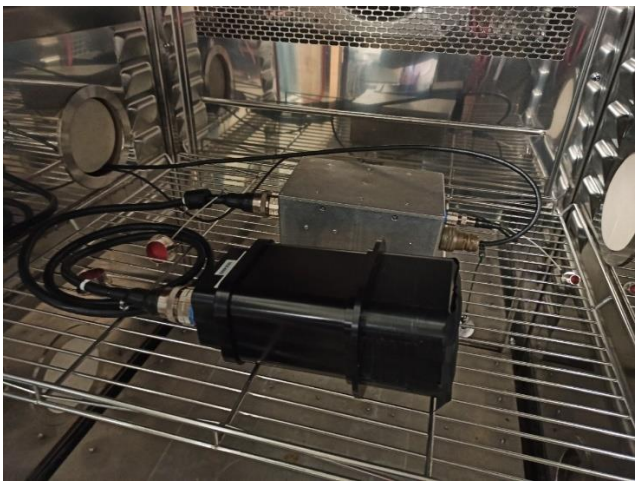

Temperature Testing – Honeywell Brno

Power Input Testing – VTUPV Vyskov

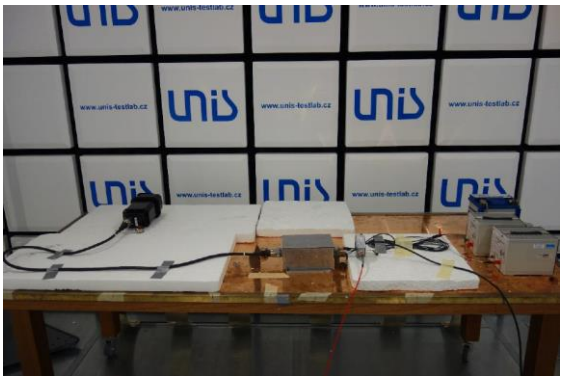

RF Emissions Testing – UNIS Brno

Figure 37: SRP sensor calibration and environmental testing.

3.5.3 Ice Wind Tunnel Tests

The SRP sensor was installed in a custom designed aerodynamical mount which positioned sensor sample area to the center of icing wind tunnel where the conditions are closest to the test point. The SRP sensor was tested in the Icing Wind Tunnel per agreed test matrix based on ED-103A (Minimum operational performance standard for inflight icing detection systems).

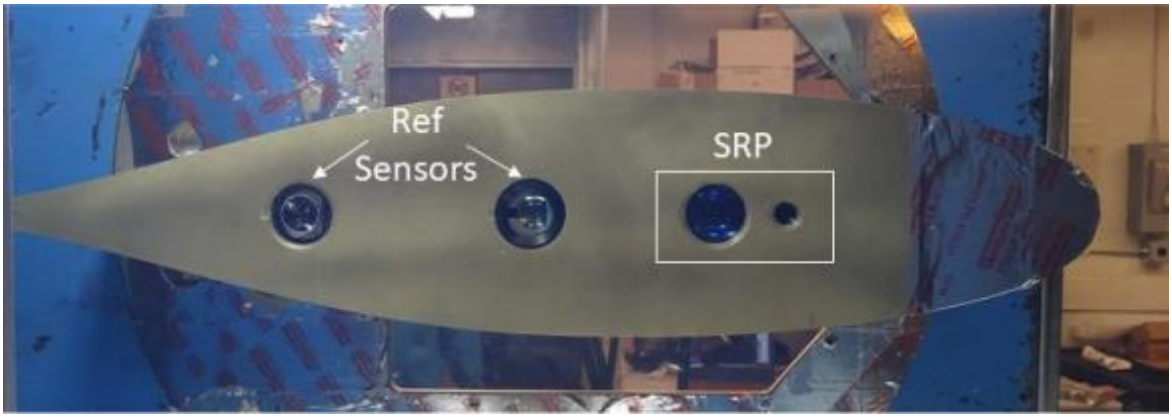

Figure 38: Custom designed aerodynamical mount [image Collins].

The ED-103A standard specifies requirements on measurement accuracy of ice accretion rate, particle size distribution, maximal droplet diameter, particulate content, response time. It specifies requirements on maximal response time of icing conditions detection and App. O detection.

The detailed description of Icing Wind Tunnel tests is provided within document SENS4ICE_T1.1_IWT_Sensor_Test_Report_SRP_HON_final. The summary of the wind tunnel test can be found in the Table 9. SRP sensor detected all the icing conditions within the required response time, with most of the response times being significantly faster than required by ED-103. App. O test conditions were correctly identified and detected within the required response time as well. The measurement error of LWC and MVD values for App. C test conditions was significantly lower compared to the App. O test conditions. The most probable explanation is presence of ice accretion from the outer side of sensor window and fogging from the internal side of sensor window, causing reduced optical transmissivity of the sensor window and resulting in underestimating of measured particle size.

Table 9: Icing Wind Tunnel test summary.

Test	Test Points Detected [%]	Test Points Detected within Response Time [%]	Test Points Detected within 1.5X Response Time [%]	Test Points with MVD Measurement [%]	Test Points with LWC Measurement [%]	Average MVD Error [%]	Average LWC Error [%]
Appendix C Test Points	100%	100%	100%	100%	100%	14%	28%
Appendix C Repeat Points	100%	100%	100%	100%	100%	15%	27%
Appendix O Test Points	100%	100%	100%	100%	100%	41%	67%
Appendix O Repeat Points	100%	100%	100%	100%	100%	24%	59%

Icing Wind Tunnel testing of SRP sensor confirmed measurement capabilities of the sensor and revealed minor issues which reduced sensor measurement accuracy. Those issues were addressed prior the icing flight test campaign.

3.5.4 Flight Test

The flight test campaign took place from 02/19/2023 to 03/10/2023, thirteen flights were performed and for eight flights icing conditions were encountered while SRP sensor data and reference instrumentation data

were successfully collected. The flights were performed in the airspace of the following states: Illinois, Indiana, Ohio, Michigan, Iowa and Wisconsin.

There were several App. C and App. O condition encounters during the icing campaign, which allowed us to evaluate performance of SRP sensor for various levels of LWC and various particle size distributions. After the icing campaing, DLR performed reference data analysis and applied corrections to increase reference data measurement accuracy. The comparison of SRP sensor measurements with the reference probe measurements is shown on Figure 39, Figure 40.

SRP sensor performance evaluation summary:

- The sensor successfully pefromed icing condition measurement over the whole flight campaign
  - Sensor optical parameters were not affected by the environmental conditions
- Sensor measurement accuracy
  - For events in which particulate MVD > 25 microns, there is very good correlation between SRP sensor LWC data and reference sensor LWC data
  - For events in which particulate MVD < 15-20 microns, the measurement accuracy is poor as the SRP sensor design developed under SENS4ICE does not cover the whole App. C

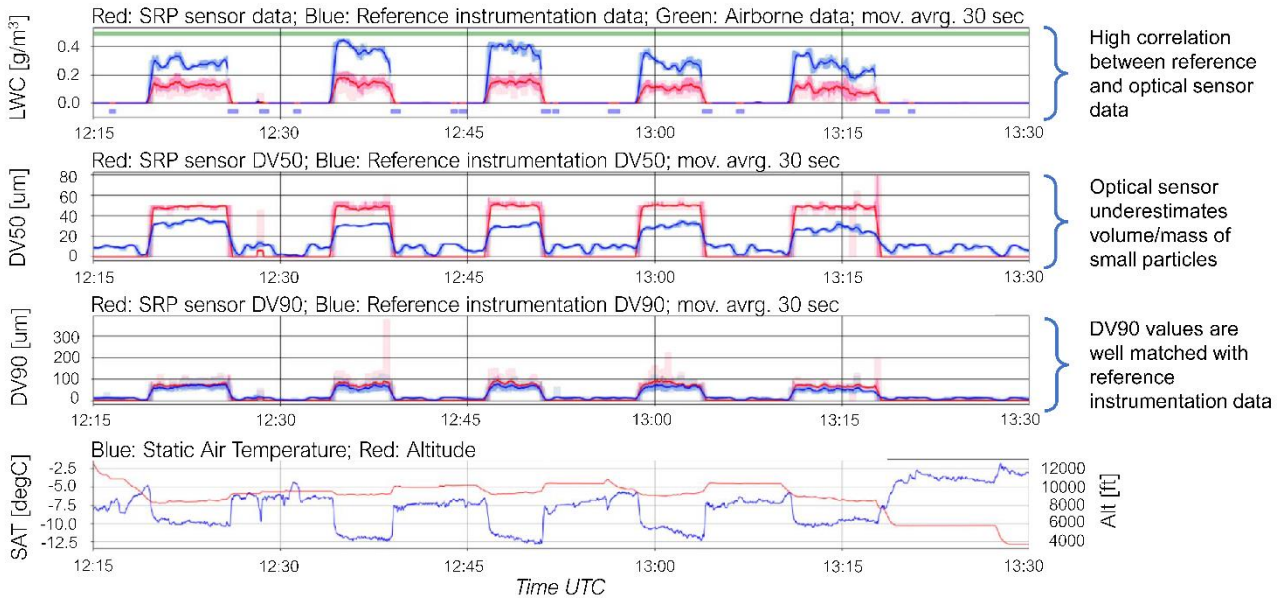

Figure 39: Optical sensor data analysis: Flight 1476.
(No collection efficiency corrections applied, sensor non-linearities corrections not applied, better results are expected)

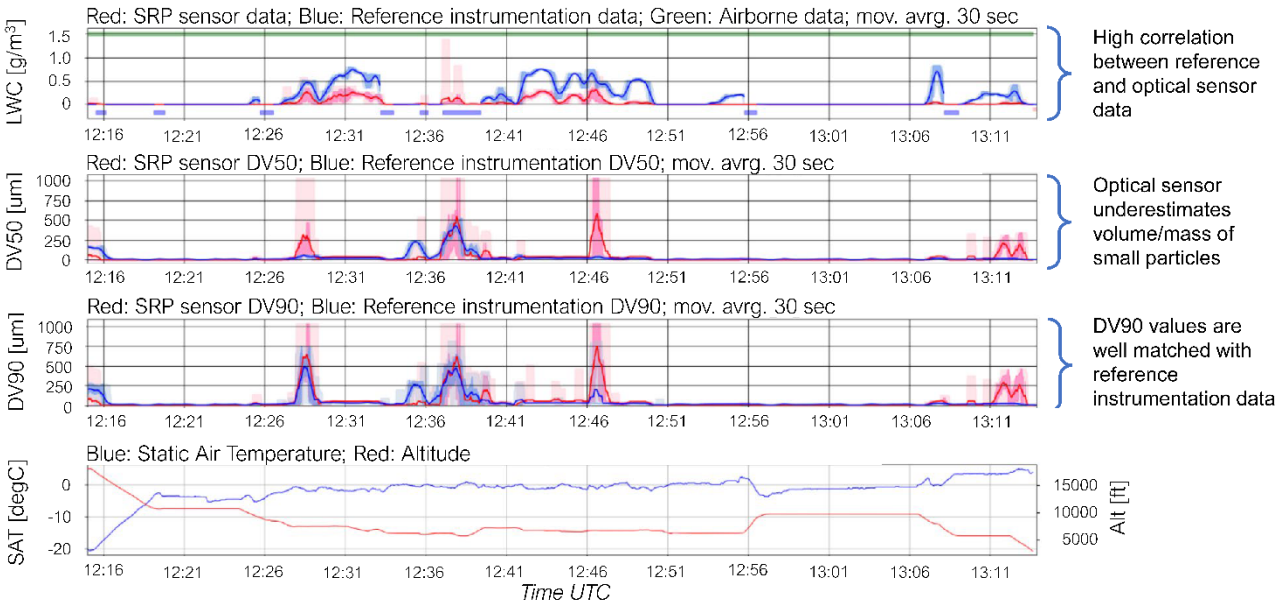

Figure 40: Optical sensor data analysis: Flight 1481.
(No collection efficiency corrections applied, sensor non-linearities corrections not applied, better results are expected)

3.6 INTA – FOD

3.6.1 Technology Description

The fiber Optic Detector is a Latent energy-based ice sensor. The latent energy released by the water during the phase change produces an abrupt temperature increase in the surface where ice is accreted. That temperature rising is a function of the icing cloud conditions, so the FOD can assess the ice severity in an approximate way.

The technology consists in an Optic Fiber embedded in a sensor surface. The fiber should be close to the sensor surface so the energy flux rate could be measured conveniently. The optic fiber has, all over its length, equispaced Bragg gratings with an eight millimetres separation, that back scatter the light in certain wavelengths. The wavelengths in which it backscatters the light are function of the temperature of the fiber. In a single fiber many temperature points could be measured. If the optic fiber is placed on the sensor surface, the temperature differences in several points on surface could be measured.

The sensor technology has two main capabilities:

a) Ice Detection: The ice detection is done measuring the temperature changing abruptness. The chosen temperature is the difference between a detection grating a reference grating that is not exposed to liquid water. The sensor first detects ice and then, using the temperature data asses if there are Appendix O conditions depending on the impingement limits.
b) Ice severity assessment: The ice severity assessment relates the temperature rising of the sensor line and icing cloud conditions. First of all, a sensor is used for calculating the ice accretion rate in a reference sensor (located on the probe stagnation point) and the rest are used for calculating the accretion all over the chord. With the relationship with the stagnation point sensor and the rest the droplet size could be calculated. In order to do that process, a standard airfoil NACA 0012 was used.

For more information see references (M. Gonzalez, 2022) (Miguel González del Val, 2021).

Temperature Calibration

The first important thing is to calibrate the sensor. That calibration should be accurate, feasible and durable. The calibration can be done with a cubic polynomial, relating the backscattered Bragg wavelength and the temperature measured in a calibrator. The optic fiber has to be isolated, using capillaries, in this case of polyimide, with an external diameter of 0.55 mm. The capillary is filled with silicone oil to enhance the thermal

heat transfer from the sensor surface to the sensor and, this way, its response time is improved (Miguel González del Val, 2021).

Thermal Model: Ice Assessment

In order to predict the external conditions a thermal model has been used. The model solves a heat transfer equation of this type:

$$q_{lat}^{node} - q_{evap}^{node} \pm q_{sens}^{node} + q_{k}^{node} - q_{nc}^{node} = 0$$

Being the first term qlat the latent flux energy flux, the second term qevap the evaporate heat flux, the third term qsens the sensible heat flux, the fourth term qk the kinetic energy heat flux and the last term qnc the net convective heat flux. In case of rime conditions and solving the last equation, the Ice Accretion dΔ/dt rate could be calculated with the following equation:

$$\frac{d\Delta}{d\tau} = \frac{h^0 \left(T_{sur}^0 - T_{rec}^0\right)}{\rho_{ice}\left(c_{p,is}^0 \left(T_{sur}^0 - T_{mp}\right) + \frac{V_\infty^2}{2} + L_f^0 - c_{pw}^0 \left(T_{mp} - T_\infty\right)\right)}$$

Where Tsur is the airfoil surface temperature, Trec the recovery temperature, Tmp the melting point temperature, cpi the ice specific heat, h the heat transfer coefficient, ρice the ice density, L the latent heat and v the airspeed. The App. O and App. C discrimination could be assessed with the differences between the icing accretion profiles as it can be seen in the following figure:

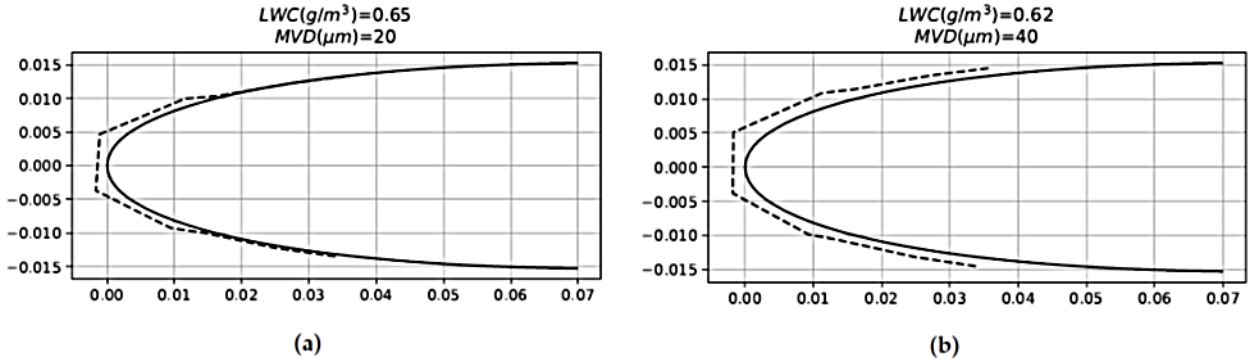

Figure 41: Sensor ice accretion profile predicted by the sensor.

Ice detection technology

In the beginning of the project, the icing detection technique used the temperature rinsing abruptness that was calculated from the first temporal derivative of the temperature difference between a reference sensor and the detection sensor. This method has been seen that requires a lot of computational time, because firstly a filter and then a finite difference method has to be used.

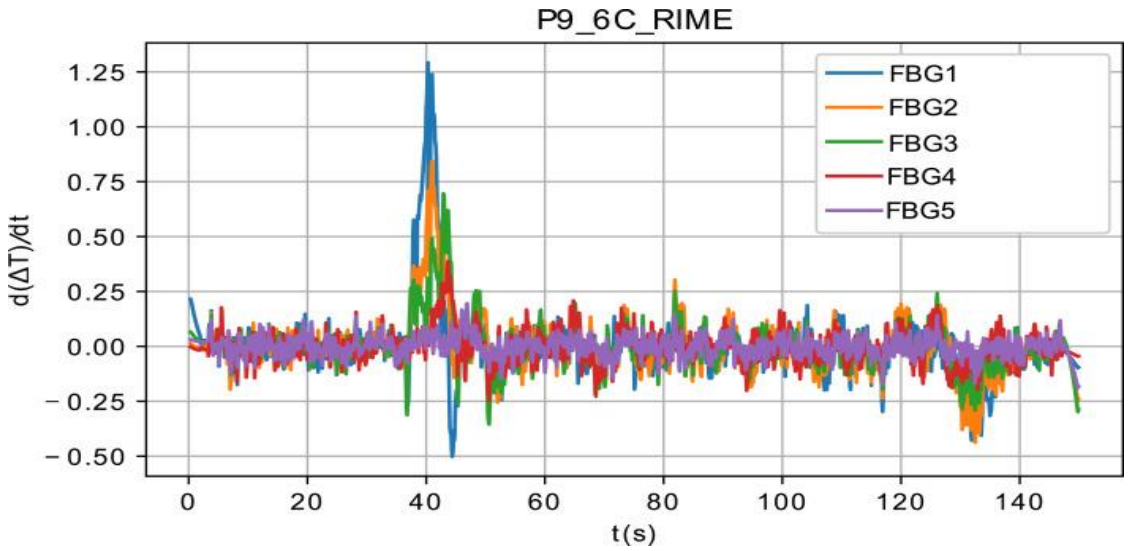

Figure 42: Sensor detection method in the beginning of the project.

Later, Discrete wavelet Transforms (DWT) were implemented in the detection algorithm. DWT do the filtering and the ice detection simultaneously. For more information about the algorithm, reference (M. Gonzalez, 2022) is recommended. Another advantage that presents the DWT is its capabilities to reduce the data size, so gives IAR and icing cloud parameters with logical sample rates (sampling time of 3 seconds).

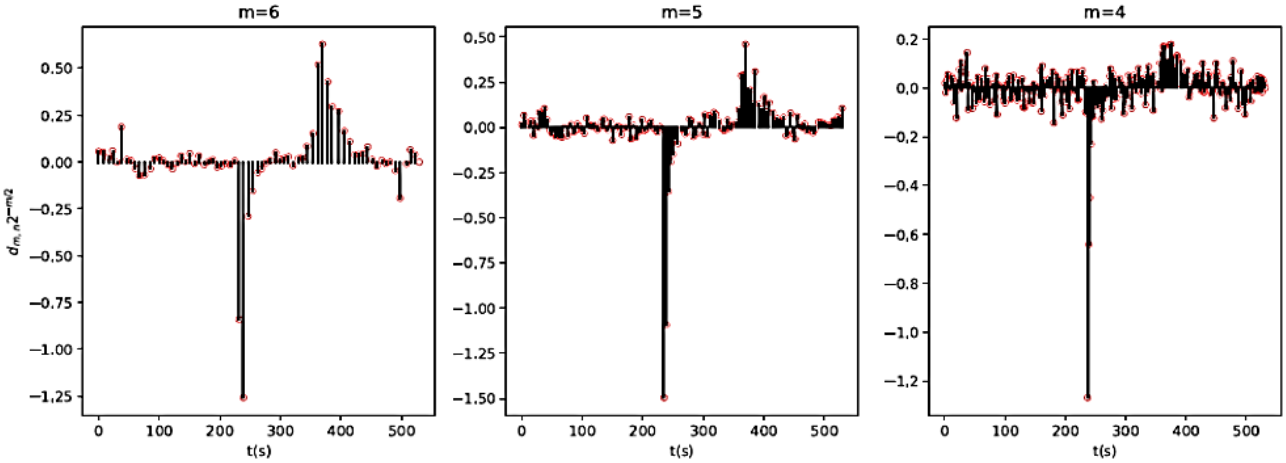

Figure 43: DWT coefficients of the sixth, fifth and fourth levels.

The discrete coefficients above a certain threshold that is calculated from test data are considered ice. The threshold has to be function of external parameters like airspeed or total temperature, so it maximizes the sensibility of the sensor and minimizes its specificity.

3.6.2 Laboratory Tests

Some laboratory tests were done in INTA IWT in order to simulate some App. C and App. O FZDZ conditions. The conditions were used in order to evaluate the predictions of the performance of a thermal model and to see the different performance of the sensor in different environments and with different detection parameters.

The laboratory tests results were published in reference (Miguel González del Val, 2021). The testing conditions were done with different temperatures, LWC, MVD and probe angles of attack. The testing matrix was the following:

Table 10: Test carried out in INTA IWT.

Test	MVD	LWC	Test	MVD	LWC
	(μm)	(g/m3)		(μm)	(g/m3)
1	20	0.39	10	20	0.39
2	40	0.35	11	40	0.35
3	70	0.33	12	70	0.33
4	20	0.65	13	20	0.65
5	40	0.63	14	40	0.63
6	70	0.64	15	70	0.64
7	20	0.95	16	20	0.95
8	40	0.92	17	40	0.92
9	70	0.93	18	70	0.93
Tt=-5ºC			Tt=-13.5ºC		

3.6.3 Ice Wind Tunnel Tests

Several icing conditions were tested in NRC IWT in order to see detection, App. C/ O discrimination and LWC or IAR assessment. The results of those tests were published in reference (M. Gonzalez, 2022). The results showed a good detection ratio in general. The sensor only had problems detecting glaze conditions and in the cases when the total temperature is close to zero degrees. The sensor was generally faster than the maximum response time detailed in ED-103. The sensor response is faster with higher LWC, so it adapts well with the requirements of the standard.

Table 11: Detection results in tests carried out in NRC IWT.

Case	Detection	Case	Detection	Case	Detection	Case	Detection
1	Y	10	Y	19	N	28	Y
2	Y	11	Y	20	Y	29	Y
3	Y	12	Y	21	Y	30	Y
4	N	13	Y	22	Y	31	Y
5	Y	14	Y	23	Y	32	Y
6	Y	15	Y	24	Y	33	Y
7	Y	16	Y	25	Y	34	Y
8	Y	17	Y	26	Y	35	Y
9	N	18	N	27	Y	36	Y

On the other hand it had an average error value in the LWC of a 40 % caused by some specific tests that probably detected different values due to icing cloud homogeneity. The endurance tests showed a good performance for the detector durability but the sensor did not detect the icing cloud stop.

3.6.4 Flight Test

For flight tests a new icing probe was designed, according to the DO-160G and with a different material and design than the previous one. The probe has a larger span than the previous one, so the bigger droplets can impact the probe surface. The used material was ULTEM® that is a very high resistance polymer and was fabricated with additive manufacturing, because it was considered the easiest solution for the proposed design. The used airfoil was the same than before, a shorten NACA 0012 with a better aerodynamic design in the tip. After placing two Fibers in the sensing probe, it was painted with a polyurethane painting. The sensing probe was previously tested in INTA IWT so it could be seen if all the system worked well, including detection algorithm, communication, and data acquisition.

Figure 44: INTA-FOD Flight Test direct sensing probe installed in the left side fuselage of the aircraft [images INTA/ SENS4ICE project].

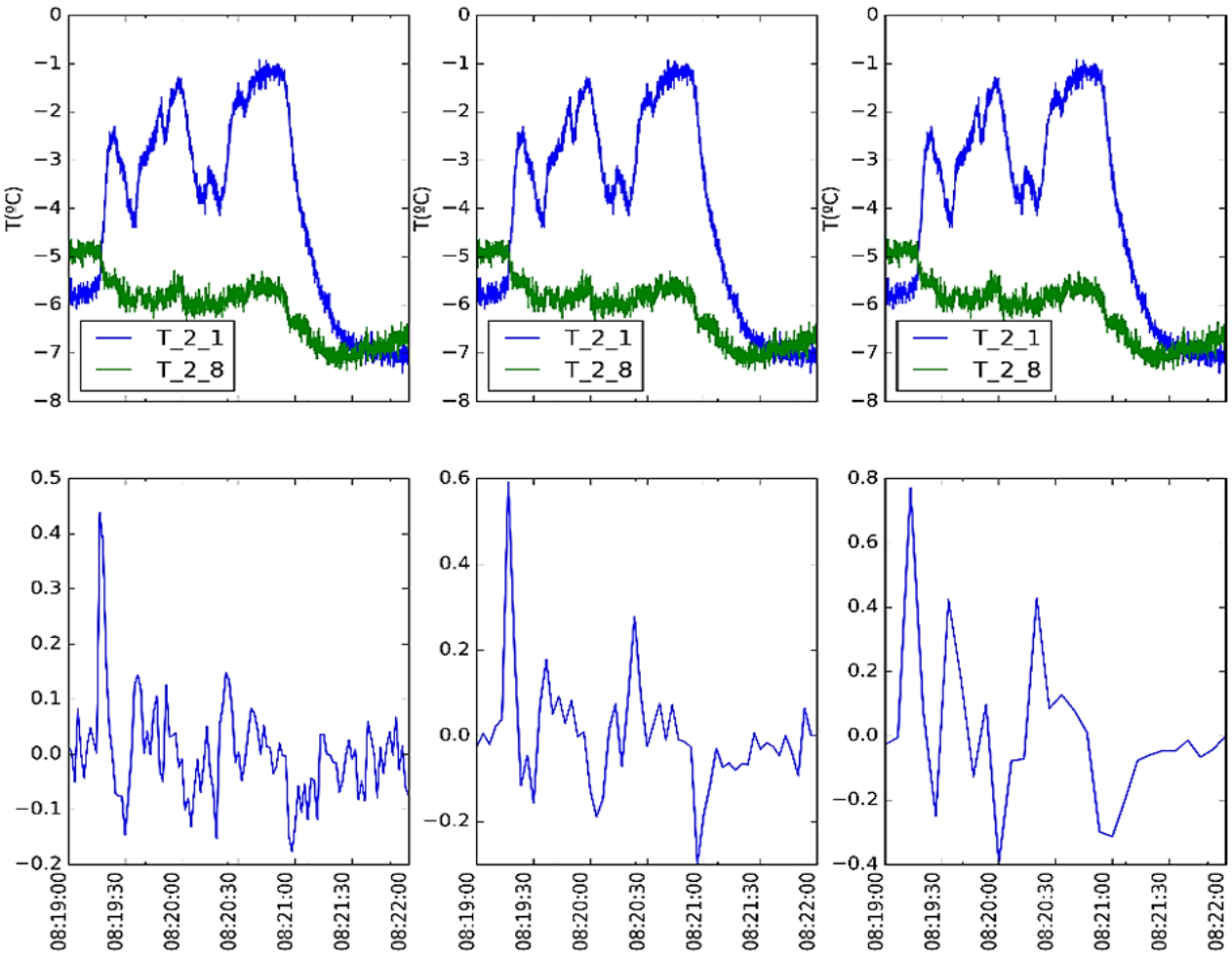

Figure 45: DWT during an icing cloud in a Flight test.

In the case of flight tests, a different behavior of the icing cloud was seen compared with IWT tests. In the IWT tests the icing cloud had a very good temporal stability, so it was easy to detect when the sensor entered the cloud and when it left it because inside the icing cloud there was only two temperature abrupt changes. In the case of inflight clouds, the LWC is quite instable, so the previous assumptions cannot be made, due to the amount of temperature changes recorded in the FBGS when the aircraft goes in an icing cloud. This makes a noisier behavior in the Discrete Wavelet Transform and in the FBGS signal. Other detection alternatives have

been considered. The first one is considering the standard deviation of the discrete detail coefficients during an interval of time (during fogging the amplitude of the DWT signal is higher but it has not a very big peak). Other solution is establishing a low threshold and just considering the ice presence when there is a peak.

In the case of IAR or LWC detection it was different. IAR values were postprocessed after the flights, but it is difficult to compare those values and check if they are right because ice thicknesses were not measured during the flight. Even though there are inaccuracies in the case of LWC measurement because the freezing fraction is unknown a priori, Liquid Water Content could be compared with other sensors data Nevzorov for example. The majority of the flights were done close to the 0ºC isotherm, so glaze conditions, with freezing fraction different than one, were present, making more inaccurate the LWC results. In Figure 46 can be seen the LWC measured by the FOD and Nevzorov. It can be seen that even when there is LWC present if the total temperature is higher than 0ºC FOD does not detect ice so, sometimes Nevzorov measures LWC while FOD LWC output is zero. Many times, there was LWC that was not supercooled, so the probe only detected a cooling effect without a latent energy release.

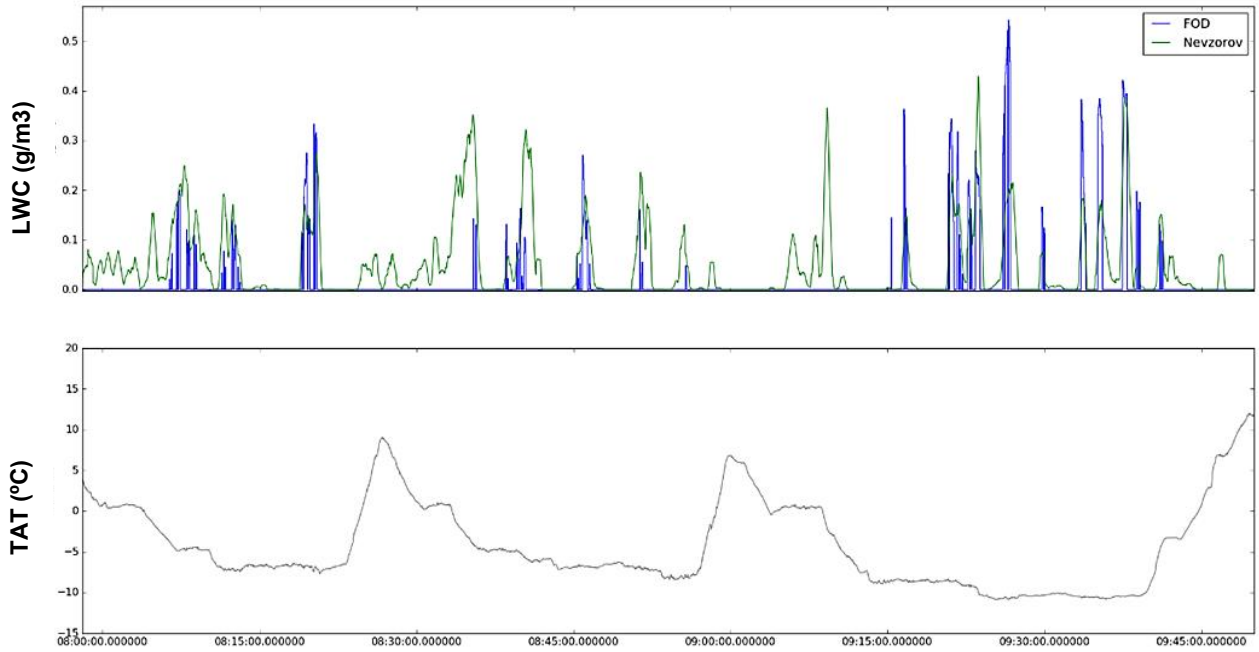

Figure 46: LWC and Total temperature (flight 27 APR 2023).

The App. O and App. C discrimination is being studied comparing the microPhysics data and the temperature data along the chord. It has been seen that, according to microPhysics data, depending on the MVD, there are more or less sensors that accreted ice. There are other factors that affect to the number of sensors that experience a temperature rising in the sensors located downstream the leading edge, like angle of attack or true airspeed so a more detailed study must be made.

Finally, it has been seen that during the deicing of the probe, there is an effect that can help to know if there is an ice layer accreted, and where the ice was formed. The ice is a good thermal insulator, so the temperatures in the sensors where the ice was not accreted change faster than the others. When the aircraft descents under the zero isotherm, the sensors without ice measure more than 0ºC but the other ones measure temperatures much lower. In the moment when the ice layer is removed, the temperature rises drastically because the temperature of air is much higher than the surface temperature. That abrupt temperature rise is due to the convection heat that is proportional to the temperature difference between the surface and air. Previously that abrupt temperature rise, the temperature was stable in a value lower than 0ºC that is the fusion temperature. That makes sense because when the ice is changing of state the temperature is constant. This physical effect could be used in systems that want to integrate a deicing and sensing system in order to know when the ice layer is removed and stop the heating power.

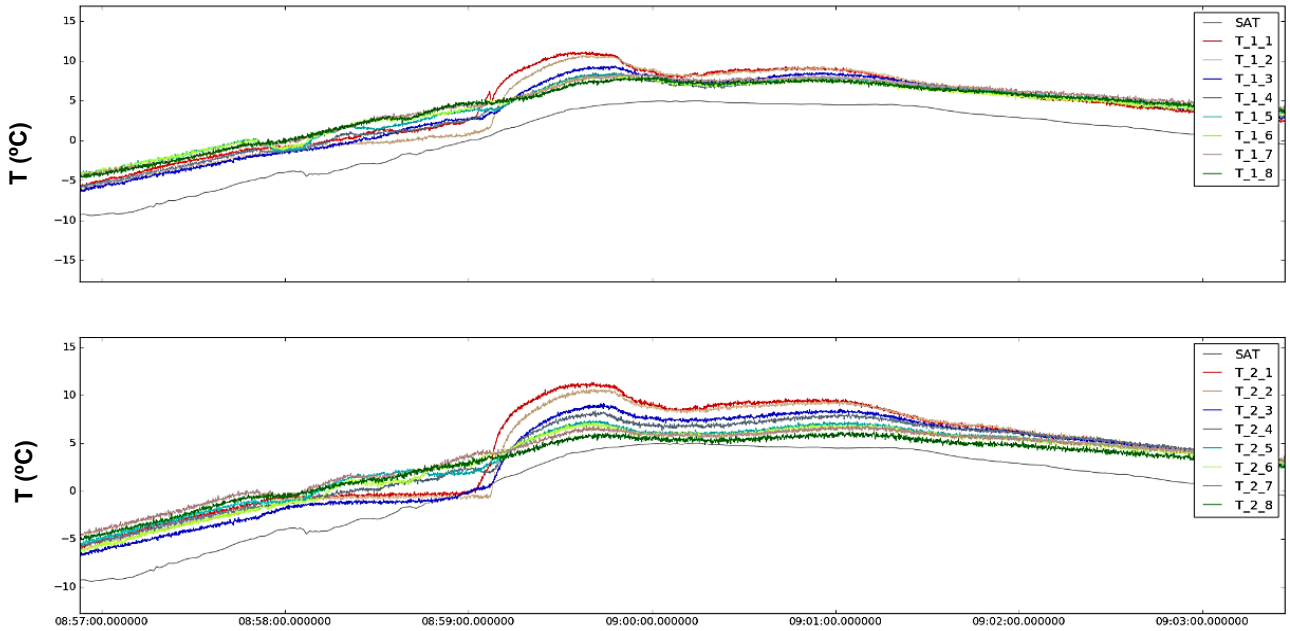

Figure 47: Probe Deicing (flight 27 APR 2023).

3.7 ONERA – AHDEL

3.7.1 Technology Description

The AHDEL sensor is based on the charging of the droplets by a corona discharge, followed by the detection and measurement of their electric charge, allowing the inference of the particle diameter. The sensor is composed of three main sub-systems: a droplet size discriminator, a droplet charging system and a droplet electric charge detector. Figure 48 illustrates the charging and the detection principles.

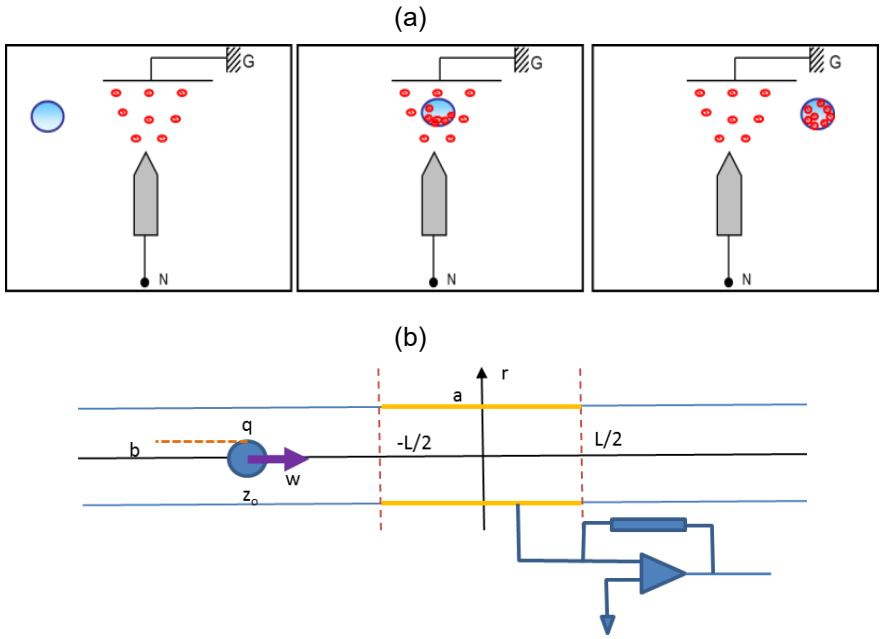

Figure 48: (a) Diagram of the electrical charging of a particle when crossing electric charges created between two electrodes (N and G). (b) Measurement of particle's electric charge (*q*) by an inductive ring of radius *a* and length *L*. This ring is connected to an electronic circuit that amplifies the inductive current.

The purpose of the charging system is to produce enough electric charges to charge the droplet to its saturation value, which is a direct function of the droplet surface (and consequently the droplet diameter squared). It consists of one high voltage electrode designated N and a grounded electrode G integrated in the sensor body. This subsystem generates a corona discharge between N and G, creating a cloud of electrical charges in the medium. When the droplets enter the region of corona discharge, they collect the electric charges drifting between N and G.

The detection system measures the droplet electric charge using one or several capacitive rings integrated in the sensor body. This subsystem generates electric signals that are function of the electric charge carried by the droplets. The shape of this signal is a function of the ring geometry and the particle speed, but its integral should be only function of the particle charge.

For the droplet size discriminator, two filters are evaluated, one based on inertial principle and other based on electrostatic principle. The inertial discriminator is located upstream of the charging chamber. Using the internal sensor geometry, it filters the small particles that are driven by the flow and keeps only large droplets. The latter reach the charging-detection zone. The electrostatic filtering takes place along the charging zone. In an axisymmetric corona discharge, charged droplets experience an outward radial force which increases near the corona wire. Heavier (larger) droplets will be less deflected than lighter (smaller) droplets. As a consequence a collection electrode located near the detector axis only collects droplets which have not been significantly deflected. By changing either the intensity of the electrostatic force or the location of the detector, different classes of droplets can be detected and quantified.

3.7.2 Laboratory Tests

First, an experimental setup has been developed to investigate the charging process and the charge detector performance. The water droplet is produced with a calibrated size droplet generator (less than 1 % of standard deviation). In this setup, the droplet falls by gravity and enters the charging region (corona generator) and finally crosses the charge detector, where the induced current is measured. In these tests the detector had a ratio length/diameter near to one. The measurements are highly repeatable, with relative error lower than 1% on the charge estimation. Then, to work with high particle velocities, which have an impact on the measured current amplitude (but not on the electrical charge) an improved setup was developed, where a droplet generator releases particles inside an air flow of 80 m/s (an acrylic tube of 20 mm diameter), at room temperature. The droplets are accelerated along 1 m long before crossing the charging system. Two high speed cameras (Phantom V711 from Vision Research) are used to visualize droplet sizes and their motion before and after the detector system. Figure 49(a) illustrates the setup. As the large droplets fragment during the acceleration, we are able to create particles ranging from 60 to 600 µm. The particle velocity at the detector level is function of the droplet size and ranges from 30 to 60 m/s. Figure 49(b) shows an example of a few images (20 µm/pixel, 10 kfps and 4 µs of exposure time) of a droplet with 320 µm diameter and at 40 m/s, approximately. Figure 49(c) presents the results of current measurement for three droplets. For very low concentration, where we have only one particle inside the detector volume (20 mm^3 in these tests) the measurements are very accurate and the current signal and the droplet charge are well determined. In the case of many particles inside the detector at the same time, the standard bipolar peak current waveforms of each droplet overlap and the result is barely exploitable. Figure 49(d) shows an example of this situation, where a first 200 µm droplet is detected (at 21.4 ms), and then, 3 ms later, 12 particles in order of 80 to 200 µm, cross the detector in a time interval inferior to 2 ms, producing a signal that cannot be exploitable.

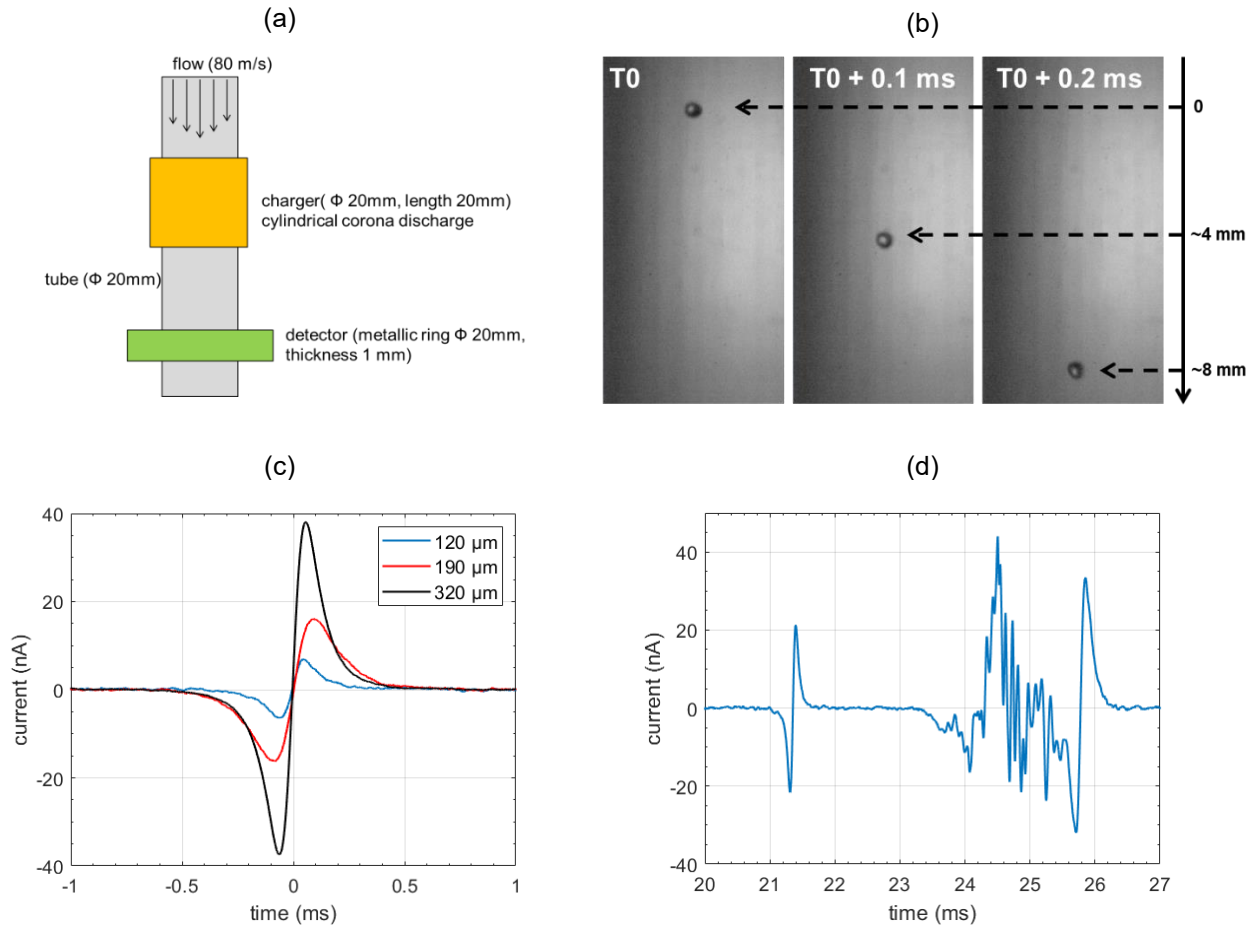

Figure 49: (a) Setup to droplet charging and detection in a flow. (b) Pictures of a 320 µm droplet at 40 m/s. (c) Typical current signal for different isolated particles. (d) Example of current signal for multiple droplets at the detector simultaneous.

The results presented in Figure 49 indicate that the sensor has an excellent potential to assess the droplet size when the concentration inside the detector is low. For that reason, the droplet size discriminator before that droplets reach the detection zone is crucial.

Two prototypes based on theoretical and numerical studies are designed and fabricated to be evaluated in IWT. Figure 50 shows the pictures of each hardware version. The current version of the inertial prototype was designed to have a flexible and easily adaptable internal shape allowing setting the threshold of the droplet size filtering by modifying the flow control plates. For lab testing and calibration purposes, transparent acrylic side walls are used for flow visualization and droplet characterization (concentration, motion and size) by fast cameras. A simplified spray nozzle is used to create droplets with diameters up to 600 µm at room temperature. The imaging resolution being 20 µm per pixel, we were not able to verify the presence of particles less than 40 µm in the generated spray. For the entrance size of the prototypes (40 x 40 mm^2 for inertial version and Φ 30 mm for electrostatic one) and using the available facilities, we were able to accelerate the droplets up to 25 m/s at the sensor level. The nozzle is used in a pulsed mode, generating a droplet concentration varying from 5 to 100 droplets per cm^3.

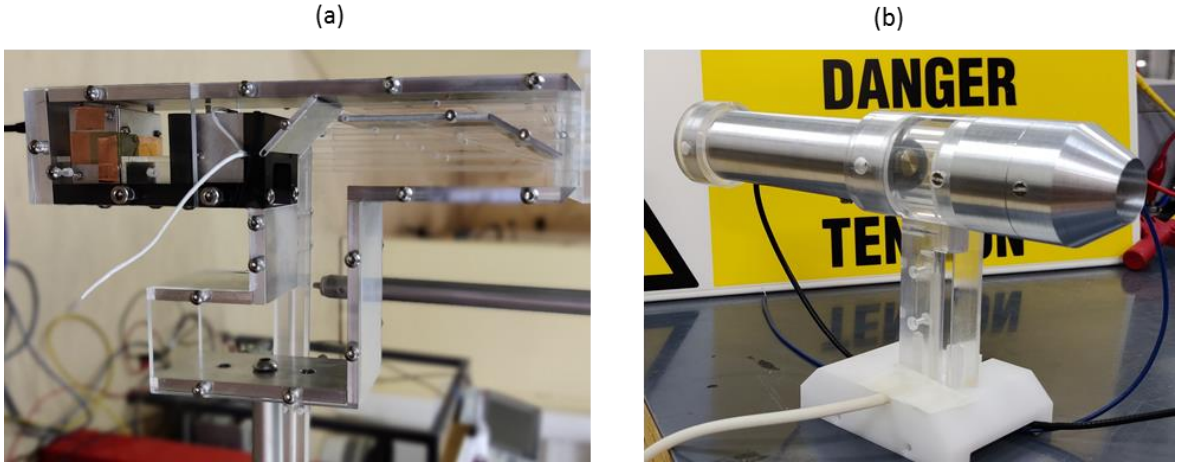

Figure 50: Pictures of the assembled hardware with transparent acrylic side walls for the two versions. (a) Inertial. (b) Electrostatic.

Using the inertial discriminator prototype, we were able to reduce the droplet concentration inside the detector volume, which is inferior to 0.01 cm^3. For the experimental setup described above, the concentration is decreased, in average, to approximately one droplet per 20 ms inside the detector.

3.7.3 Ice Wind Tunnel Tests

The IWT testing for AHDEL sensor was performed in the first week of June 2021. The two AHDEL versions, one based on electrostatic and other on inertial principle were tested in IWT at TUBS. We started the test campaign with the points of the SENS4ICE test matrix, both in App. C and App. O conditions, for points with low water density, respecting the SENS4ICE test procedure for IWT. We were able to test 4 points of App. C and 4 points of App. O. Once the water concentration increased (LWC >0.6 g/m^3) we had unexpected problems with water accumulation in the charging system that led to a short circuits. This rendered the charging system inoperative. In addition, in these higher density conditions, we noticed ice accretion in some internal parts of the model. After a few minutes (3 to 5 minutes), the icing was enough to block the detector zone entrance, making this subsystem also inoperative. These were conditions (low temperature and a large water concentration) that we were not able to reproduce in our lab during the preliminary testing of the sensor.

Nevertheless, we decided to perform academic tests to get a better understanding of the sensor performances and limits. For this purpose, we explored additional test points outside of the SENS4ICE test matrix. We did a sweeping in different parameters, having runs of around 5 to 10 minutes. During these runs, several 30-second ON-spray cycles were repeated. For each cycle, a single parameter was changed (LWC, MVD, temperature and flow speed). With this parametric study, around twenty additional points were tested. In the Figure 51 and Figure 52, we present a summary of the IWTT results. Table 12 summarises the results considering the tested points.

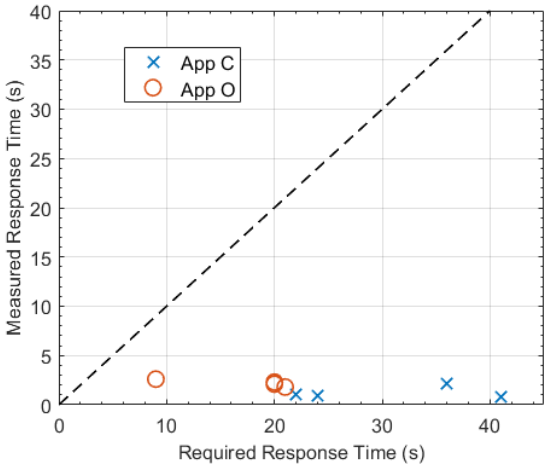

Figure 51: Graph showing measured vs required response time for all test in the SENS4ICE matrix (8 points). All the points below the black dashed line indicate a response time that met the requirements.

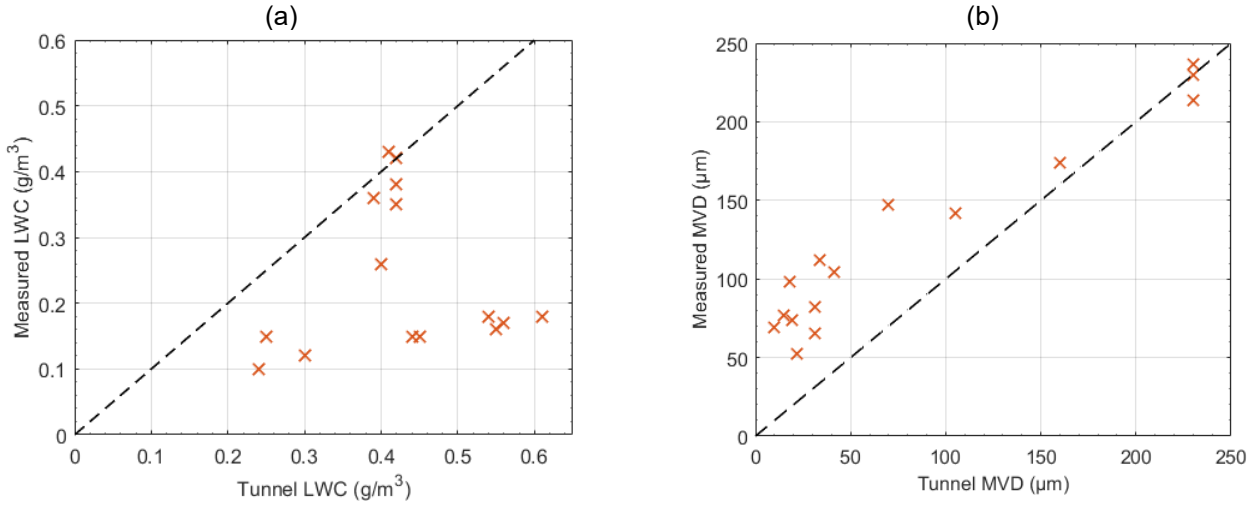

Figure 52: Graph showing measured vs tunnel LWC (a) and MVD (b) for the tested points concerning SENS4ICE matrix and academic runs. All the points below (above) the black dashed line indicate a measured LWC/MVD underestimating (overestimating) the calibrated tunnel values.

Table 12: Results summary table, including the standard and academic test points (AHDEL Sensor).

Test	Percentage of Test Points Detected	Percentage of Test Points Within Required Response Time	Percentage of Test Points with MVD Measurement	Percentage of Test Points with LWC Measurement	Average MVD Error	Average LWC Error
App. C Test Points	100%[1]	100%	100%	100%	185%	59%
App. O Test Points	100%[2]	100%	100%	100%	170%	70%
Academic runs	100%[3]	100%	100%	100%	17%[4]	27%[5]

3.7.4 Flight Test

As the necessary modifications and improvements to perform a successful aircraft flight test were not compatible with the remaining time and resources in the SENS4ICE project, the ONERA team decided, by end of June 2021, to withdrawn AHDEL sensor from the SENS4ICE flight tests.

3.8 ONERA – AMPERA

3.8.1 Technology Description

When an aircraft flies inside a cloud, atmospheric particles (droplets, ice crystals …) run into the fuselage. The particle impacts lead to electric charge exchanges through a triboelectric process as illustrated inFigure 53. These electric charges on the aircraft fuselage produce an electrostatic field on the metallic part of the airframe.

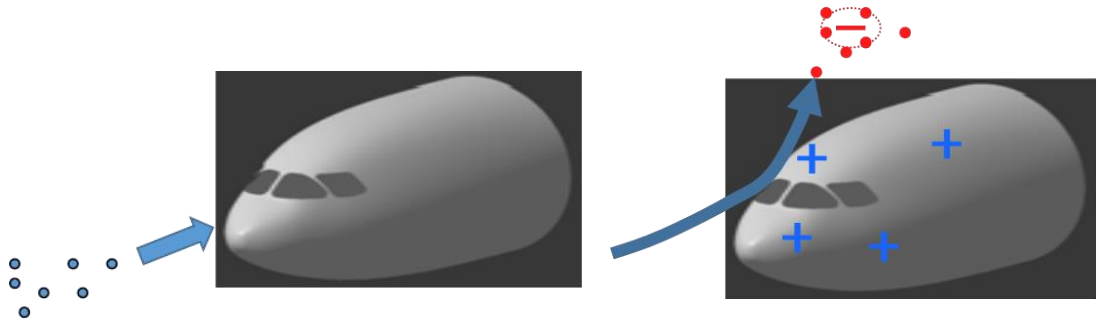

Figure 53: Illustration of the aircraft charging process due to particle impacts. (a) Before impacts and (b) after impacts.

AMPERA system is an electric field mill network that locally measures the electrostatic field at the surface of the aircraft fuselage. The distribution and amplitude of the electrostatic field on the aircraft skin depends on

[1] Only 4 out of 19 App. C test conditions were tested from the SENS4ICE test matrix. This is due to unexpected problems with water accumulation in the high-voltage when LWC >0.6 g/m^3.
[2] Only 4 out of 18 App. O test conditions were tested from the SENS4ICE test matrix. This is due to unexpected problems with water accumulation in the high-voltage when LWC >0.6 g/m^3.
[3] Seven academic runs with calibrated tunnel conditions were realized.
[4] Only points with MVD > 25 µm are considered in this average error.
[5] Only points with MVD > 25 µm are considered in this average error.

the atmospheric electrostatic field around the aircraft and the net electric charge of the aircraft. This latter parameter depends on the balance between the triboelectric current due to the impact of the cloud particles on the aircraft fuselage, the current due to the charged particles emitted by the engines, and the corona current emitted by the aircraft through the static dischargers. In contrast to conventional TWC probes, which sample a local area of the atmosphere, the AMPERA system uses the entire aircraft as the sensitive part, providing an overall estimation of the net TWC exposure. Therefore, the sensor in its current version is not relevant for IWT tests.

Figure 54 shows a strong correlation between the time evolution of the aircraft electrostatic potential (net electric charge of the aircraft divided by the electric capacitance of the aircraft) and the time evolution of the TWC measured by the IKP2 probe during a flight of the HAIC campaign [14]. The results of this campaign showed that the sensor could not discriminate the size of particles. All the particles of ice crystal or water droplets that impinge the aircraft generate triboelectric effects on the aircraft skin. One of the main advantages of this sensor is that it does not need to be located in an icing impingement area on the aircraft, but can be located everywhere in the airframe.

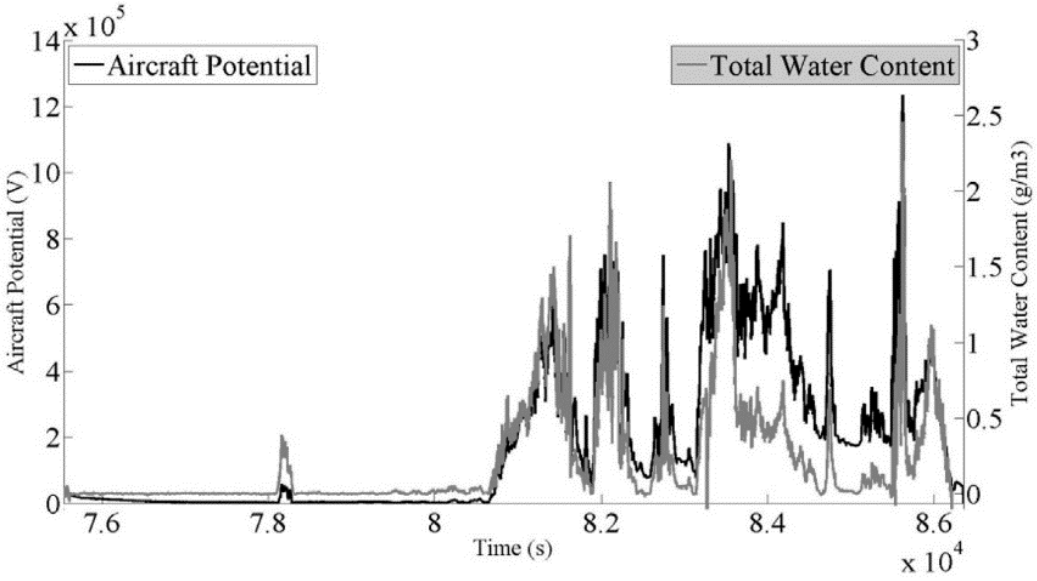

Figure 54: Time history of aircraft potential (black curve- units: V) deduced from AMPERA, and TWC (grey curve – units: g.m^{-3}) from the IKP2 probe. Figure taken from reference [14].

3.8.2 Flight Test

In April 2023, the European flight test campaign was conducted, consisting of 15 flights and more than 50 flight hours carried out under various icing conditions. Throughout the campaign, the AMPERA system demonstrated exceptional robustness, as no technical issues were observed with either the hardware or software components. The real-time communication with the HIDS interface, to receive the aircraft data input (temperatures, velocities, altitude, etc.) and to send the AMPERA outputs (status, icing flag, TWC and trust level) worked well during all flights.

The first calibration flights in clear air were very useful to set the baseline for the aircraft electrostatic potential in different flight phases, including the take-off, landing, and during manoeuvres and engine power variation. At constant level and speed, V_A is around 300 V, and during high power engine phases, it can reach up to 3 kV. During the flight tests conducted under icing conditions, this measurement exhibited excellent sensitivity when encountering particles. The response time for entering and exiting a cloud with particles was approximately 1 second, and the electric potential inside the cloud exceeded 100 kV. This significant increase in potential clearly distinguishes it from a phase of clear air. Figure 55 shows the measurement during a flight with multiple cloud encounters.

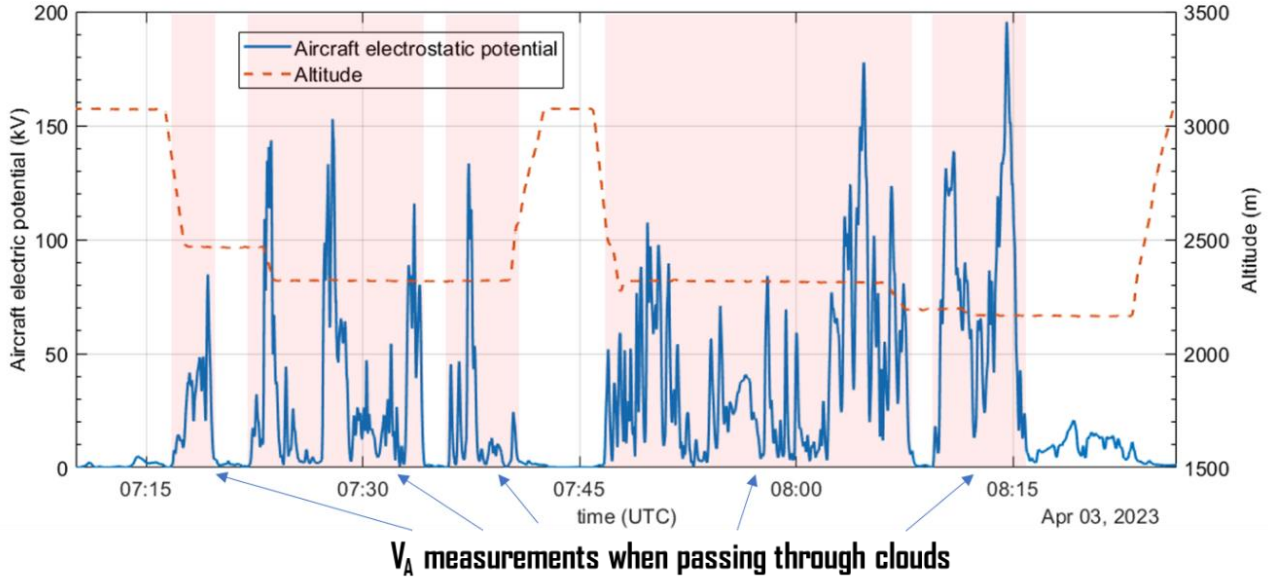

Figure 55: Aircraft electrostatic potential and altitude for the flight of April 3rd 2023, showing the excellent sensitivity of this measurement when passing through clouds.

The preliminary analysis and comparisons conducted with the reference probe have shown a strong correlation between the shape and variations of the measured LWC and the electrostatic potential. Figure 56 depicts the comparison between the AMPERA output and the Robust reference probe from SAFIRE, highlighting a significant agreement between the two signals.

In order to calculate a real-time atmospheric icing detection flag, we have proposed, during this campaign, a flag derived from three parameters: the aircraft potential (V_A) the static temperature (*SAT*), and dew point temperature (*DEW*). When comparing this flag with the airframe ice accretion flag obtained from the Rosemount Ice detector, we observe that the AMPERA flag demonstrates higher sensitivity. This is because the AMPERA flag takes into account the specific atmospheric conditions encountered by the aircraft during flight, while the Rosemount flag primarily accounts for ice accretion.

Further analysis with the reference microphysics measurements is necessary to extend our understanding of the physics behind the triboelectric process. Additionally, these measurements will help evaluate the AMPERA sensor's capability to differentiate between aircraft charging caused by water droplets and ice crystals.

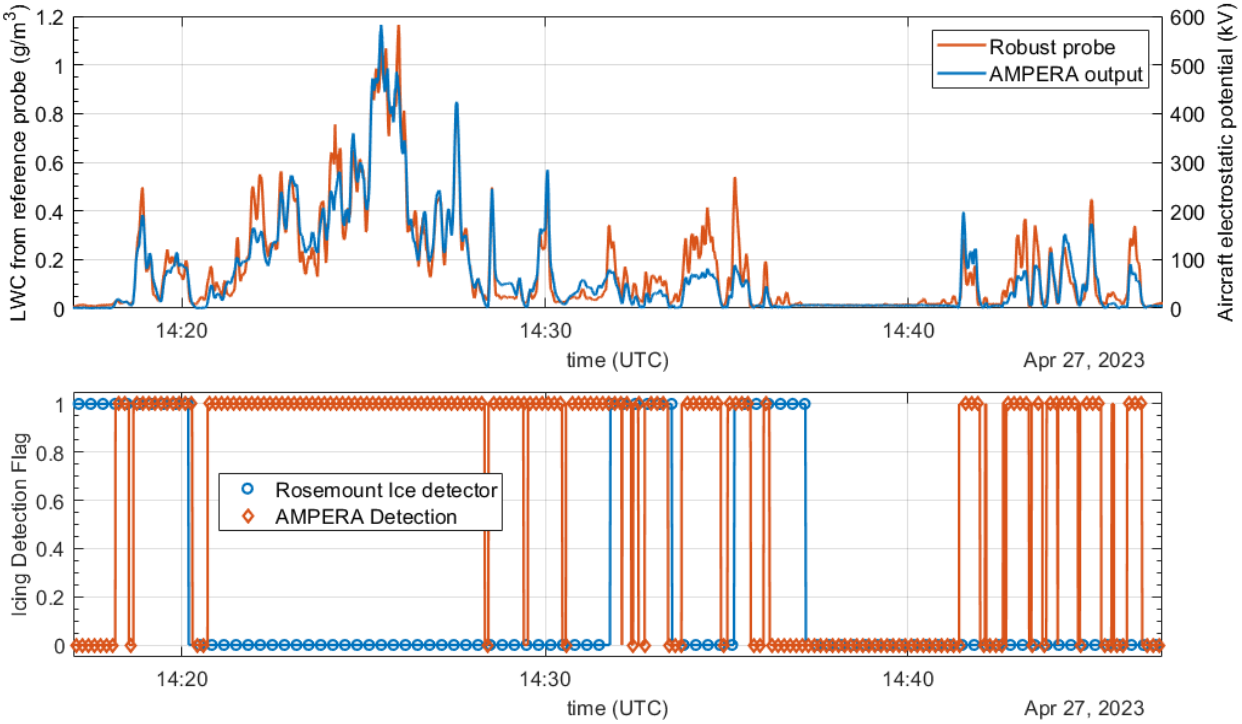

Figure 56: LWC and Aircraft electrostatic potential comparison (upper) and AMPERA atmospheric icing flag and Rosemount Ice accretion flag (lower).

3.9 SAFRAN – AOD

3.9.1 Technology Description

The App. O Discriminator (AOD) aims to specifically detect icing conditions originating from the presence of Supercooled Large Droplets (SLD) of diameter larger than 100 µm in the atmosphere. It is an optical sensor based on imaging. It relies on shadowgraphy. This technique had been developed to obtain images of objects made of transparent material, such as droplets.

Short duration light pulses are emitted at high frequency. As they propagate in the atmosphere, they impinges the droplets and are deviated by refraction. A high resolution camera equipped with an objective located in front of the light source grabs the images of the droplets. This configuration enables one to get very high contrast images.

Each frame is then processed for detecting the objects and counting them. The AOD can detect objects as small as 10 µm and can size them from 30 µm to 10 mm. Parameters of the droplet size distribution are derived to determine the nature and the severity of the icing conditions.

3.9.1 Laboratory Tests

The sensor design was mainly tested in laboratory. An AOD mock-up was set-up for lab testing. The tests consisted in using calibrated bead suspended in water in a cuvette. Indeed, the polystyrene beads behave similarly to water droplet for our sensor, are easy to handle, dilute and mix. Calibrated beads of 10, 30, 75, 90, 100 and 200µm were used for testing our system. A picture obtained with our sensor can be seen inFigure 57.

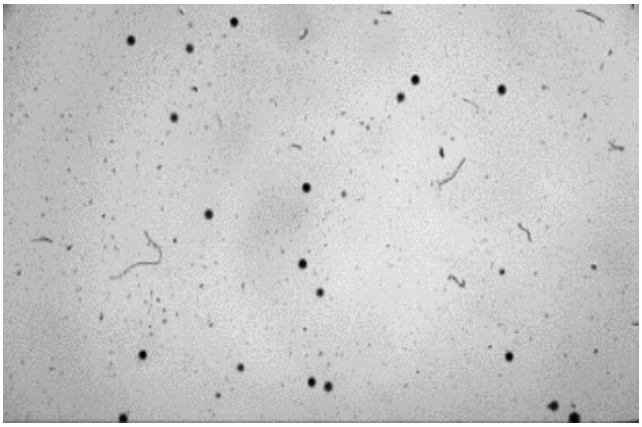

Figure 57: Picture of a cuvette filled with 200 µm diameter beads grabbed with the lab AOD.

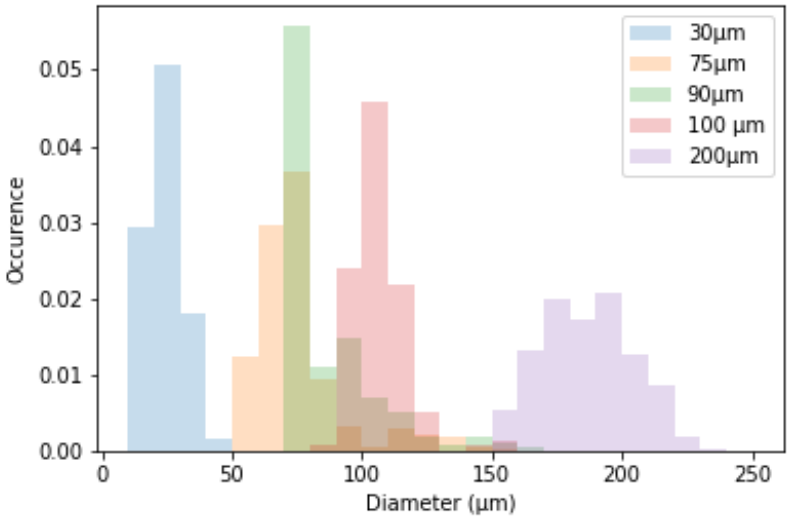

Figure 58: Diameter measured by the AOD.

The beads size and number were measured from image acquisition followed by processing on an FPGA board. The results can be seen on the histogram in Figure 58. The diameter of the beads could be measured with a relatively high accuracy. Indeed, as it can be seen of Figure 59, the error on the MVD was less than 10% for all the diameters tested but the 30 µm. In this case, the error was slightly larger than the 20% recommended by the ED-103. However, it is out of the App. O droplets diameter.

The error on the maximum measured diameter noted D_{max} hereafter was much larger and reached up to 120% for 75 µm beads. This was mainly due to out-of-focus beads. However, it did not affect too significantly the App. O discrimination capabilities as Figure 60 shows. Indeed, this graph represents the proportion of beads detected as a bead, whose diameter is larger than 100 µm. In other words, it corresponds to the beads that could be counted as an App. O icing condition SLD. It varied from 9% for 75 µm to 21% for 90 µm and reaches almost 100% for 100 µm diameter beads. It can then be concluded that, by setting the appropriate threshold diameter to rise App. O alarm, only few false alarms could be triggered and almost all the App. O conditions would be detected.

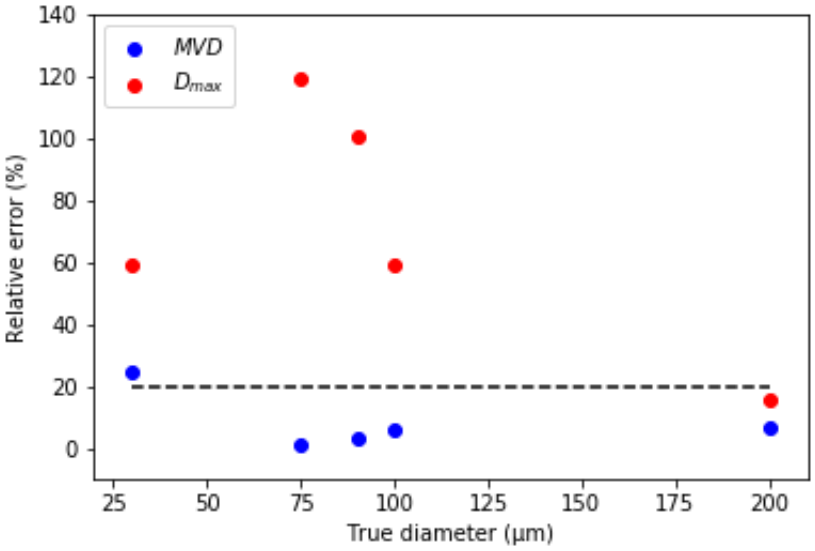

Figure 59: Relative error on the MVD and Dmax measured with the AOD.

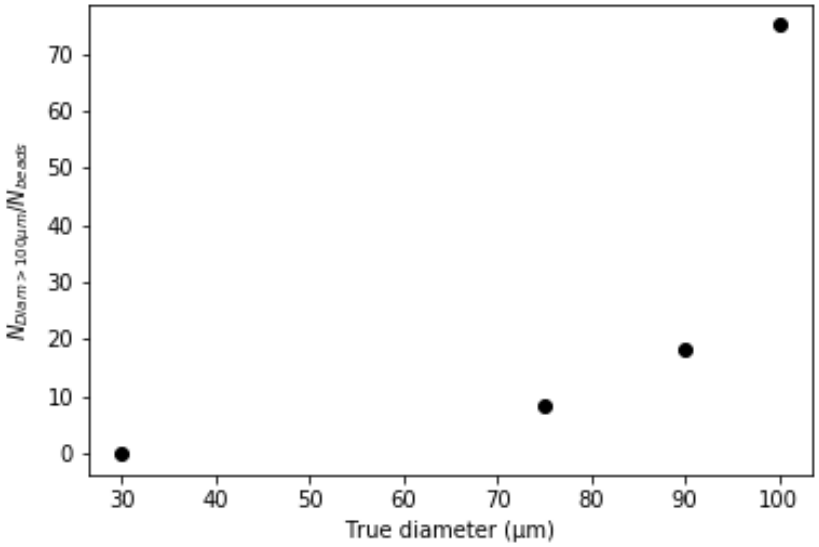

Figure 60: Number of beads detected as an SLD larger than 100 µm with regard to the bead diameter.

3.9.2 Ice Wind Tunnel Tests

Several issues related to the COVID crisis and the Safran healthcare policy led us to postpone the IWT tests. In addition, successive issues with our mechanical subcontractor increased our delay and planning deviation.

A careful analysis of the AOD sensors design revealed some strong drawback of this technology, which convinced us that it did not fit the market. It was then decided that this development would not be conducted any further. It was decided to cancel the IWT test campaign for the AOD, in order to save time and also budget, that would be allocated to top priority activities: the sensors that prepared for flight test.

3.10 SAFRAN – PFIDS

3.10.1 Technology Description

PFIDS is an optical ice accretion sensor able to measure Ice Accretion Rate. The PFIDS ice catch area, highlighted by a white circle inFigure 61, is illuminated by two wavelengths, λ_1 and λ_2, and then a contrast is calculated by measuring the reflected light for both wavelengths. In order to determine the presence or not of ice, this contrast value is compared to a threshold, the “ice detection threshold”.

The contrast evolution, being proportional to the ice thickness accreted on the ice catch area, is used to evaluate the local Ice Accretion Rate, see Figure 62 where a classic example of PFIDS contrast signal is reported.

PFIDS can detect App. C, App. O and App. D/P mixed phases, but cannot discriminate between them.

To avoid the Ludlam limit at temperature close to 0°C, PFIDS ice catch area is cooled down in order to increase the local freezing fraction, which tends to 1, and to force ice accretion.

After any ice detection, the PFIDS probe is heated thanks to a deicing system in order to be ready to start a new detection cycle.

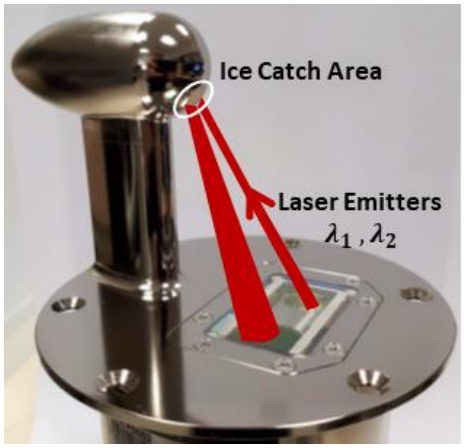

Figure 61: PFIDS working principle.

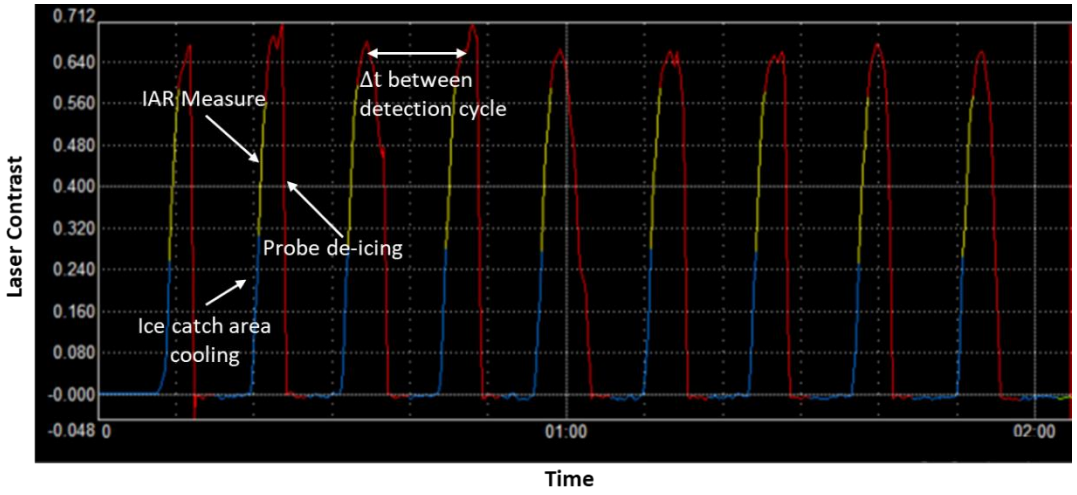

Figure 62: Typical PFIDS detection cycle.

3.10.2 Ice Wind Tunnel Tests

Due to travel restriction cause by COVID-19 pandemic, the SENS4ICE icing wind tunnel tests were performed at TUBS in May 2022.

PFIDS passed the evaluation gate thanks to the results of IWT test campaign performed at NRC in July 2019. This test campaign was part of CleanSky2 ICASSIO project.

In order to show the PFIDS capabilities in icing condition “similar’ to SENS4ICE IWT test matrix ones, different NRC tests have been selected and presented in deliverable 15.

TUBS Ice Wind Tunnel Test campaign

SENS4ICE Ice Wind Tunnel Tests were performed by SAFRAN team at TUBS facility from the 9th to the 13th May 2023.

The main goals of such test campaign were to:

- Evaluate PFIDS capability to detect App. O conditions;
- Evaluate PFIDS performance at low aircraft speed (note that the max speed provided by TUBS IWT is 40 m/s);
- Test the new IAR algorithm mentioned in §3.10.1.

During the week spent at TUBS, the following tests were performed:

- 24 App. C conditions (both CM and IM)
- 23 App. O conditions (mainly FZDZ)

A detailed list of all the tested conditions is reported in Table 13.

In Figure 63 are illustrated the IAR measures provided by PFIDS as function of a theoretical IAR. The chosen reference has been calculated by the following formula:

$$IAR_{theo_{MAX}} = \frac{TAS \cdot (LWC_1 + LWC_2) \cdot \beta_{CFD}}{\rho_i}$$

where β_{CFD} is the collection efficiency on the PFIDS target, computed via 3D CFD simulations, and $\rho_i = 917\ Kg/m^3$ is the ice density. Very good results were obtained for App. O conditions.

Note that, thanks to discussions with the TUBS team, it has been noted that for all the conditions where PFIDS measured an $IAR > IAR_{theo_{MAX}} + 30\%$ (all the points above the gray dotted line), the LWC provided by the tunnel was greater than the requested one. TUBS operator, indeed, used PFIDS results to check the tunnel calibration.

Table 13: Icing conditions tested at TUBS IWT

Case	TUBS Filename	Condition	Measured-MVD	Measured - LWC	TAS	SAT	TAT	LWC1	MVD1	LWC2	MVD2	Altitude
			µm	g/m3	m/s	°C	°C	g/m3	µm	g/m3	µm	ft
Run1	401_R1	CM	14.8	0.334	40	-20	-19.20	0.300	14.8	0	0	0
Run2	402_R2	CM	19.5	0.488	40	-10	-9.20	0.540	19.5	0	0	0
Run3	403_R3	CM	14.8	0.532	40	-10	-9.20	0.600	14.8	0	0	0
Run4	404_R4	CM	23.7	0.346	40	-20	-19.20	0.216	23.7	0	0	0
Run5	405_R5	CM	30.9	0.260	40	-10	-9.20	0.247	30.9	0	0	0
Run6	406_R6	CM	22.7	0.331	40	-10	-9.20	0.319	22.7	0	0	0
Run7check	407_R7a	CM	22.7	0.475	40	-1	-0.20	0.580	22.7	0	0	0
Run7A	407_R7c	CM	22.7	0.514	40	-1	-0.20	0.580	22.7	0	0	0
Run8	408_R8	CM	14.2	1.029	40	-1	-0.20	0.910	14.2	0	0	0
Run9	409_R9	CM	19	0.457	40	-5	-4.20	0.440	19	0	0	0
Run10	410_R10	CM	31	0.291	40	-5	-4.20	0.240	31	0	0	0
Run11	411_R11	IM	20.8	1.126	40	-20	-19.20	1.190	20.8	0	0	0
Run12	412_R12	IM	28.5	1.151	40	-10	-9.20	1.020	28.5	0	0	0
Run13	413_R13a	IM	23.6	1.788	40	-10	-9.20	1.310	23.6	0	0	0
Run14	414_R14	IM	38.7	0.423	40	-20	-19.20	0.360	38.7	0	0	0
Run15	415_R15	IM	45.2	0.437	40	-10	-9.20	0.420	45.2	0	0	0
Run16	416_R16	IM	31	0.889	40	-10	-9.20	0.760	31	0	0	0
Run17	417_R17	IM	39.8	0.939	40	-1	-0.20	0.770	39.8	0	0	0
Run18	418_R18	IM	29.6	1.279	40	-5	-4.20	0.990	29.6	0	0	0
Run19	419_R19	IM	28.5	1.136	40	-5	-4.20	1.020	28.5	0	0	0
Run20	410_rb_R20	CM	26.5	0.680	40	-5	-4.20	0.570	26.5	0	0	0
Run21	412_rb_R21	IM	21.6	1.257	40	-10	-9.20	0.814	21.6	0	0	0
Run22	413_rb_R22	IM	21.1	1.419	40	-10	-9.20	0.980	21.1	0	0	0
Run23	415_rb_R23	IM	45	0.647	40	-10	-9.20	0.850	72	0	0	0
Run24	417_b_R24	IM	39	0.687	40	-1	-0.20	0.780	33.9	0	0	0
Run25	521_R25	SLD	15.85	0.550	40	-2	-1.20	0.290	14	0.13	87.5	0
Run26	522_R26	SLD	23.5	0.630	40	-2	-1.20	0.530	12.5	0.14	95.5	0
Run27	523_R27	SLD	18.38	0.610	40	-2	-1.20	0.290	13.5	0.2	109.5	0
Run29	525_R29	SLD	41.6	0.450	40	-2	-1.20	0.290	25.5	0.15	94.5	0
Run30	537_R30	SLD	70.1	0.556	40	-2	-1.20	0.290	14	0.24	113.5	0
Run37	521_R37	SLD	15.85	0.550	40	-10	-9.20	0.290	14	0.13	87.5	0
Run38	522_R38	SLD	23.5	0.630	40	-10	-9.20	0.530	12.5	0.14	95.5	0
Run39	523_R39	SLD	18.38	0.610	40	-10	-9.20	0.290	13.5	0.2	109.5	0
Run40	524_R40	SLD	23.8	0.420	40	-10	-9.20	0.330	19.5	0.15	111.5	0
Run41	525_R41	SLD	41.6	0.450	40	-10	-9.20	0.290	25.5	0.15	94.5	0
Run42	537_R42	SLD	70.1	0.556	40	-10	-9.20	0.290	14	0.24	113.5	0
Run43	521_R43	SLD	15.85	0.550	40	-15	-14.20	0.290	14	0.13	87.5	0
Run44	522_R44	SLD	23.5	0.630	40	-15	-14.20	0.530	12.5	0.14	95.5	0
Run45	523_R45	SLD	18.38	0.610	40	-15	-14.20	0.290	13.5	0.2	109.5	0
Run46	524_R46	SLD	23.8	0.420	40	-15	-14.20	0.330	19.5	0.15	111.5	0
Run47	525_R47	SLD	41.6	0.450	40	-15	-14.20	0.290	25.5	0.15	94.5	0
Run48A	537_R48a	SLD	70.1	0.556	40	-15	-14.20	0.290	14	0.24	113.5	0
Run49	521_R49a	SLD	15.85	0.550	40	-20	-19.20	0.290	14	0.13	87.5	0
Run55	531_R55	SLD - Mono	128.5	0.316	40	-10	-9.20	0.316	128.5	0	0	0
Run56	533_R56	SLD - Mono	143.5	1.110	40	-10	-9.20	1.110	143.5	0	0	0
Run57	535_R57	SLD - Mono	74.5	0.270	40	-10	-9.20	0.270	74.5	0	0	0
Run59	531_R59	SLD - Mono	128.5	0.316	40	-5	-4.20	0.316	128.5	0	0	0
Run60	533_R60	SLD - Mono	143.5	1.110	40	-5	-4.20	1.110	143.5	0	0	0

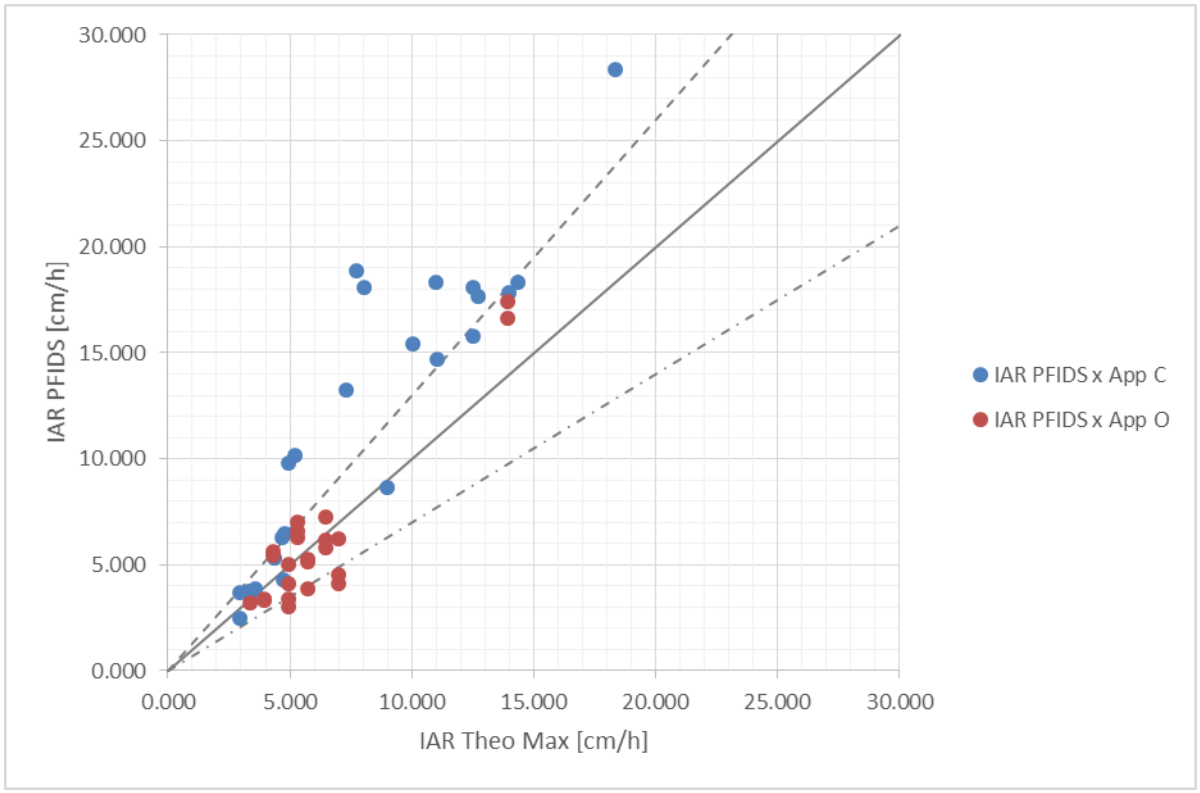

Figure 63: IAR measures provided by PFIDS as function of theoretical IAR.

3.10.3 Flight Test

PFIDS participated to the North America Flight Test campaign with Embraer. The detector was installed on the door of the right luggage rack of Phenom 300, seeFigure 64.

Figure 64: Installation of PFIDS on Phenom 300 [images Embraer/ SENS4ICE project].

This position was suggested by Embraer, who realized collection efficiency analyses showing that, in this location, PFIDS could have been able to detect both App. C and App. O conditions, seeFigure 65.

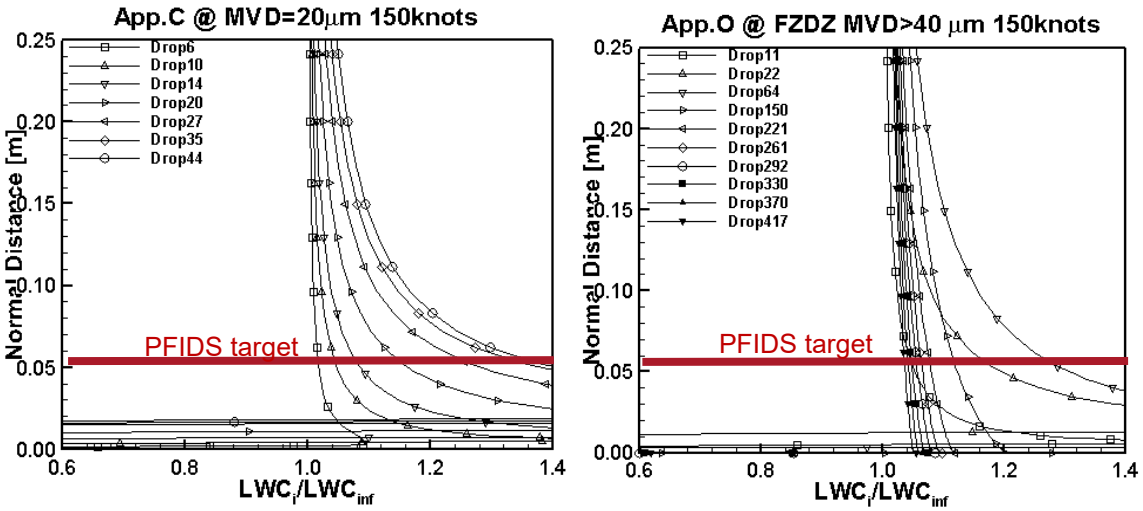

Figure 65: Example of water catch simulations results.

During the Flight Test campaign performed from the 23rd of February to the 10th of March in the West and South regions of the Great Lakes, the Phenom 300 realised a total of 25 flight hours. 4.3 flight hours were realised in icing conditions, among them 1.2 hours in SLD conditions, see Table 14.

Table 14: North America campaign flights.

No	EMB internal No	Date	Duration	Comment
1	1474-1	22 FEB 2023	0:39	Check flight
2	1475-1	23 FEB 2023	2:45	App. O
3	1475-2	23 FEB 2023	1:12	App. C
4	1476-1	25 FEB 2023	2:03	App. O
5	1476-2	25 FEB 2023	1:37	App. C
6	1477-1	01 MAR 2023	2:45	App. O
7	1477-2	01 MAR 2023	2:12	App. O
8	1478-1	06 MAR 2023	1:07	App. C
9	1478-2	06 MAR 2023	-	Dry Air
10	1479-1	08 MAR 2023	2:21	App. O
11	1479-2	08 MAR 2023	0:40	Return to base
12	1480-1	08 MAR 2023	-	Check flight
13	1481-1	09 MAR 2023	1:23	App. C
14	1482-1	10 MAR 2023	2:15	App. O
15	1482-2	10 MAR 2023	1:08	App. C

All the icing conditions encountered were detected by PFIDS.

The following figures show preliminary results of PFIDS for both App. C and App. O conditions.

In Figure 66, results of PFIDS detection for the flight 1475-leg 2 of the 23rd of February are illustrated. During this flight several App. C conditions were encountered, as demonstrated by both the MVD and LWC signals reported in the first two subplots of the figure. PFIDS was able to detect very fast (in about 10s) all the conditions but the second one, since the SENS4ICE network was disconnected for about 20 minutes.

The IAR measured by PFIDS, the black curve in the last subplot, is well correlated to LWC. Actually, accurate comparisons are ongoing in order to properly take into account PFIDS installation factor.

Figure 67 displays PFIDS results for the flight 1476-leg 1 of the 25th of February. During this flight 5 App. O conditions were encountered, as shown by the blue curve of the first subplot representing the MVD of the

droplets with a diameter greater than 100 μm. Even in SLD conditions, PFIDS was able to detect very fast (its response time is again of the order of 10s) and the IAR measures are always well correlated to the LWC ones.

Please note that at the time of writing of this deliverable report, the analyses of flight test data are still ongoing in order to verify the response time compliance with ED-103revB and to evaluate the PFIDS installation factor (IF). Once this factor is defined, it will be possible to obtain an LWC measure from PFIDS IAR since the aircraft speed is known:

$$LWC = IAR_{PFIDS} \cdot \frac{\rho_i}{TAS \cdot IF}$$

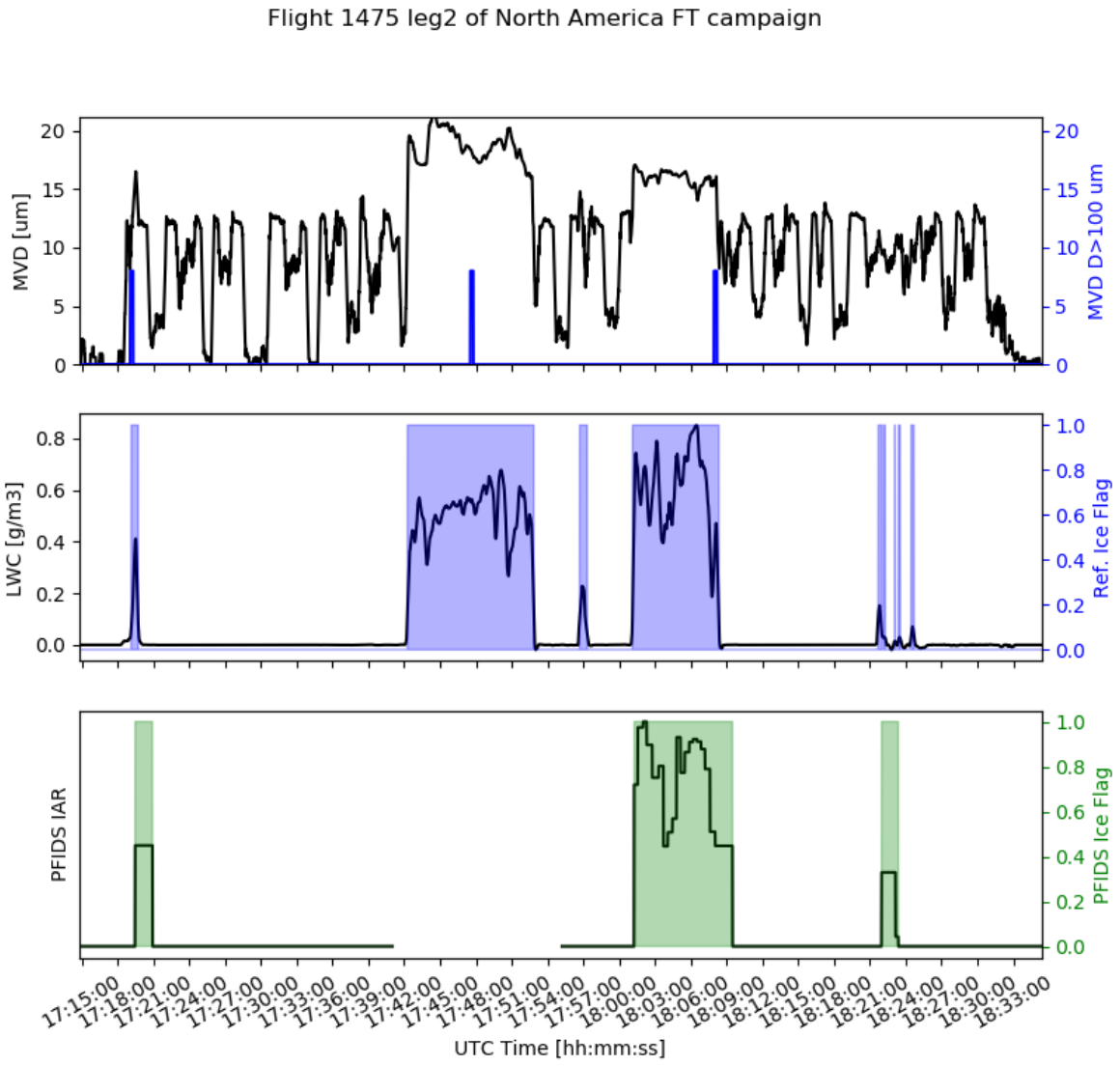

Figure 66: PFIDS detection results for the flight 1475-leg 2 of North America FT campaign. In the first subplot is reported the MVD signal; in the second subplot is reported the LWC signal, in black, and the reference Ice Flag represented by the areas filled in blue; the third subplot displays PFIDS IAR measure, in black, and the PFIDS Ice Flag represented by the areas filled in green.

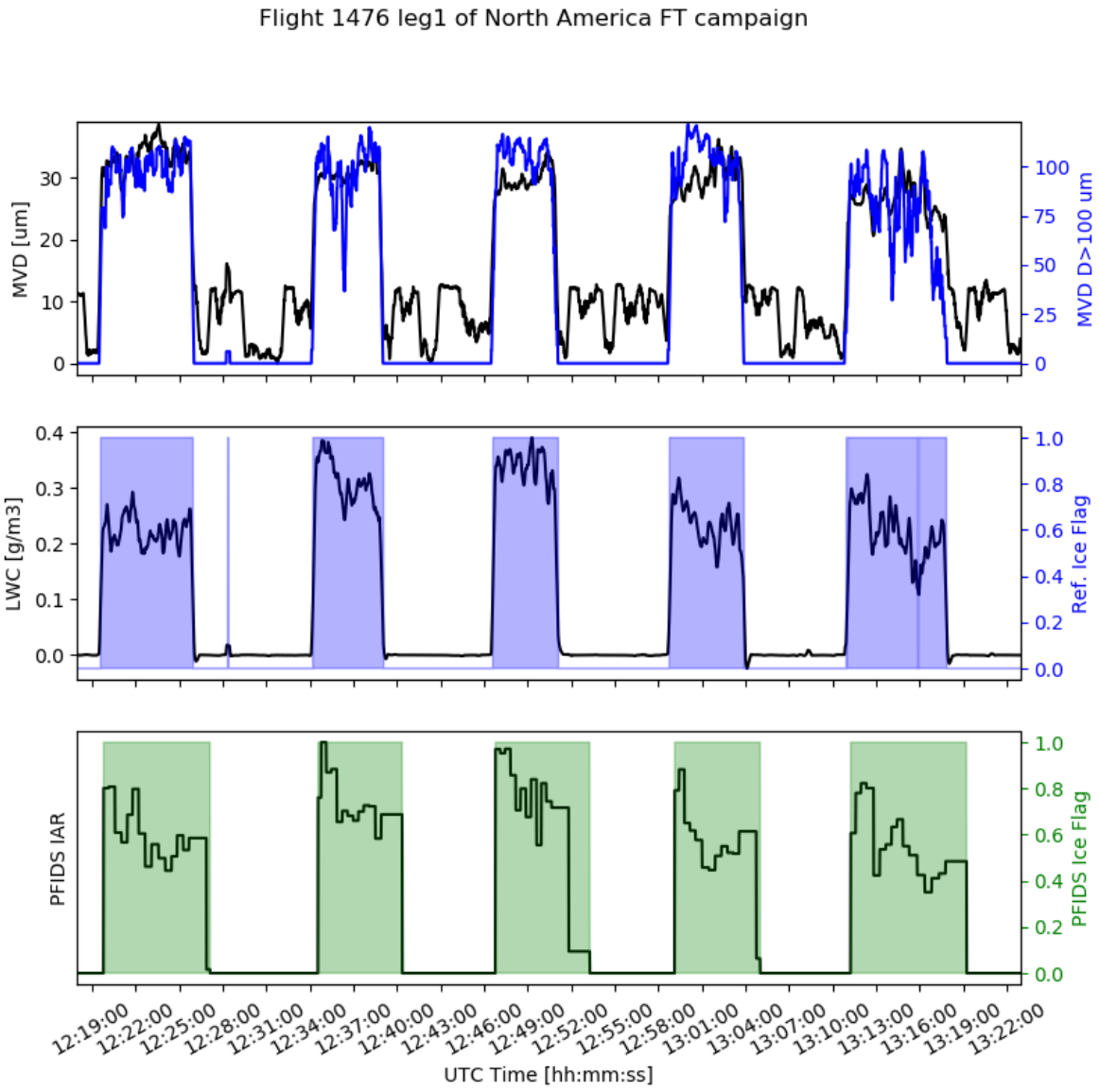

Figure 67: PFIDS detection results for the flight 1476-leg 1 of North America FT campaign. In the first subplot is reported the MVD signal; in the second subplot is reported the LWC signal, in black, and the reference Ice Flag represented by the areas filled in blue; the third subplot displays PFIDS IAR measure, in black, and the PFIDS Ice Flag represented by the areas filled in green.

4. TRL Progression during SENS4ICE

Significant progress was made on technology maturation during SENS4ICE project. A summary of the TRL progression is illustrated in Table 15. Most technologies started at low TRL and made significant progression to higher TRLs, which is a major achievement of SENS4ICE project.

Table 15: SENS4ICE technology maturation progression in terms of TRLs

Technology	TRL at project start (January 2019)	TRL at project mid-term (Dec 2020)	TRL objective at project end	TRL App C detection at project end	TRL App O detection at project end	TRL App O discrimination at project end
Atmospheric Hydrometeor Detection based on Electric measurement (AHDEL)	TRL2-3	TRL3-4	TRL5	TRL4	TRL4	TRL4
Atmospheric Icing Patches (AIP)	TRL2	TRL3	TRL5	TRL5-6	TRL5-6	TRL5-6
AMPERA	TRL4-5	TRL4-5	TRL5	TRL5-6	TRL5-6	-
Appendix O Discriminator (AOD)	TRL2	TRL2	originally TRL5, stopped at TRL3	-	-	TRL3
Aircraft Flight Performance Monitoring (AFPM)	TRL3-4	TRL3-4	TRL5	TRL5	TRL5	-
Cloud Multi Detection Device (CM2D)	TRL5	TRL5	TRL6	TRL6	TRL6	TRL6
Fibre Optic Ice Detector (FOD)	TRL3-4	TRL5	TRL6	TRL6	TRL6	TRL4
Local Ice Layer Detector (LILD)	TRL3-4	TRL3-4	TRL5-6	TRL6	TRL6	TRL3
Primary in-Flight Icing Detection System (PFIDS)	TRL6	TRL6 (TRL4 for XTAL and IAR functions)	TRL6	TRL6	TRL6	TRL3
Nowcasting	TRL2	TRL3-4	TRL5		TRL5	TRL5
Collins Ice Differentiator System (IDS)	TRL2	TRL4	TRL6	TRL6	TRL6	TRL6
Short Range Particulate Sensor (SRP)	TRL3	TRL6	TRL6	TRL6	TRL6	TRL6

5. Technology Roadmaps

This section documents the technology roadmaps for the different technologies in terms of further development and exploitation beyond the SENS4ICE project. Most of these technologies are currently at TRL 5/6 maturity level and this section outlines future plans to further mature and exploit the technologies towards future products.

5.1 AeroTex – AIP

5.1.1 Further development and maturation

The AIP technology is being further developed under a programme called Robust Atmospheric Ice Detection System (RAIDS) that has been funded under the National Aerospace Technology Exploitation Programme (NATEP) by the UK government's Innovate UK. The aim of this programme is to develop a suite of capabilities that are concentrated around the core sensor function demonstrated in SENS4ICE (Figure 68). The goals of the specific 18-month programme are:

- Improved icing severity measurement through novel heater technology;
- Small/flexible detection technology that can be integrated into small components for local ice detection or as part of a Smart Ice protection System (SIPS); and;
- Ice Crystal Icing (ICI) detector.

To deliver this programme we have partnered with Printed Electronics Limited, who are experts in the development of bespoke printed circuit technologies and Cranfield University where the developed sensor will be tested.

Figure 68: RAID technology vision.

5.1.2 Technology exploitation

AeroTex has initiated discussions with a number of interested parties, both airframers and Tier 1 suppliers, to investigate how the technology can be rapidly matured. Initial interest has focused on implementing the system on aircraft that currently use visual cues for both ice detection and SLD differentiation. The concept is that the system will reduce pilot workload by acting as an indicator that it would be advisable for the pilot to check their visual cue location. Adopting this approach significantly reduces the software Design Assurance Level (DAL) required allowing the system to come to market more rapidly and also allows AeroTex to gather data that will be useful for maturation of the technology.

5.2 Collins – IDS

5.2.1 Further development and maturation

Collins-IDS capability to detect and differentiate App. C and App. O icing conditions was successfully demonstrated in icing tunnel, dry air and natural icing. The major areas of development and maturation is the control hardware, software level implementation and qualification as well as IDS sensoring method. It will require additional resources and investment to bring the technology to the level of maturation required for a plurality of applications.

5.2.2 Technology exploitation

Collins-IDS is a lower cost option suitable for any category of airplane. It suites very well helicopter, UAM and commercial airplanes, where icing is desired to be detected at the surface. It can be used exclusively for App. C icing conditions or as differentiator for App. C and App. O.

5.3 DLR - LILD

5.3.1 Further development and maturation

With the successful wind tunnel and flight tests, the potential of the LILD sensor as a small and lightweight system to detect ice accretion was shown. For a better understanding of the intent and severity of the icing conditions a better estimation of the ice accretion rate and by this the liquid water content would be very helpful. The main step to achieve this consists in a deeper understanding of the interaction of an ice layer and the lamb wave behavior, which is not yet provided with the available data. Therefore additional wind tunnel test campaigns are required, where the sensor data are obtained for a variety of icing conditions with different temperatures and repeated measurements of the same test point. These data will then be used to train neuronal networks, which may be effective to solve the inverse problem of determining the icing conditions based on the lamb wave data.

A second path is the discrimination of SLD conditions. This was unfortunately not possible with the LILD test setup in SENS4ICE, since the impingement on the used airfoil was too similar between SLD and non-SLD conditions. With additional sensor locations on the aircraft, where only SLD lead to an ice accretion, a discrimination is possible. This should be implemented in a following flight test.

To ease the use especially in smaller airplanes the sensor electronics should be miniaturized. There is still potential if the hardware is fully reduced to the sensor functions. Furthermore the detection time can be reduced by an increased sampling frequency. Transferring more functions to the FPGA can significantly increase the signal processing. Additionally an increase in excitation voltage allows a detection of thicker ice layers.

As a last step the LILD sensor should be combined with a deicing capability at least along one sensing channel to detect continued icing conditions and the end of icing conditions, which is currently not possible when a certain ice thickness is exceeded.

5.3.2 Technology exploitation

Based on the work in SENS4ICE some industry contacts have already been made where follow-up projects are possible and in discussion. Furthermore, two internal projects have already been granted at DLR dealing with the LILD technology.

In parallel the project results have been published in a variety of scientific conferences.

5.4 DLR – CM2D

5.4.1 Further development and maturation

The CM2D is a powerful instrument combination, that can be regarded as a minimal set up for measurements of LWC, TWC and droplet size distribution, especially for research aircraft where classical underwing probes

cannot be deployed. The measurements of the droplet size distribution by the BCPD can serve to correct the Nevzorov LWC and TWC measurements, hence improving the accuracy of the data.

For a commercial application, it is however necessary to extend the sample area of the BCPD outwards, to reduce the influence of the fuselage on the measurement position. Also, this avoids measurement artefacts from the shattering of ice crystals.

Furthermore, discrepancies remain between the measurements of number concentration of the BCPD and the CDP (reference instrument), where a difference of a factor of two was commonly observed. This difference might be due to the sampling position of the BCPD, but interestingly it was also observed for the IWT testing, where the airflow at the sampling position is assumed to be relatively unaffected. The difference in number concentration could also be due to errors in the sample area calibration of the manufacturer. Several discussions with the manufacturer of the BCPD yielded no conclusive answer, therefore further research into the topic is necessary.

As for the Nevzorov probe, only improvements to the algorithm that combines its data with that of the BCPD are planned. Since the 12 mm cone has been characterized, we regard this part of the CM2D as mature.

5.4.2 Technology exploitation

Key findings on the components of the CM2D technology from SENS4ICE have been already made public to the wider community in [10,11]. Future research efforts can also profit from facilitated computations of scattering cross sections for backscatter probes, which are possible with the adaptations made to pyScatmech, which are available under [16].

5.5 HON - SRP

5.5.1 Further development and maturation

The primary development work towards a commercial sensor will involve merging the existing sensor design, which covers droplets less than 50 µm, with the SENS4ICE design, which covers larger droplets, into a single consolidated sensor. It is expected that each standalone sensor will have sufficient performance to accurately measure the droplets within its designed size range. In addition, sensor updates and calibration measurement will need to be done in the ice crystal icing regime.

As Honeywell transitions to a productized version of the device, we believe there is substantial room for miniaturization. The electronics can be easily shrunk to half their current size, perhaps farther. Trade studies will be conducted on the optical design to find what room for miniaturization exists, but we believe it will be substantial. The planned system being developed for SENS4ICE already has many features which could be used to develop built-in test for an eventual product, such as logging of voltage levels, laser current, several temperatures, and photodetector properties.

The main challenges in developing a commercial product will involve balancing the many design trades of the separate designs into a single sensor at a reasonable cost which can be commercially sold. Honeywell has foreseen that the use of lasers in an aviation application may be a potential issue and we are working to address this issue through conversations with the relevant authorities and by adjusting the wavelength/ power into a more eye safe regime.

5.5.2 Technology exploitation

The technology development beyond SENS4ICE project will be focused on the following items:

- Design of single sensor covering all icing App.es.
- Improvement of volcanic ash/ sand/ dust detection capabilities.
- Size, weight, power, and cost optimization.

5.6 INTA - FOD

5.6.1 Further development and maturation

Future development of FOD include:

- Maturation and development of optimized probe design, such us the used material for 3D- impression, the design parameters of the sensor allocations and the aerodynamic design in the tip.
- Optimization of fiber optic sensor distribution along the chord of the probe.
- Maturation of the robustness of the egressing optic cables.
- Maturation of the detection algorithms.
- Development and maturation of the de-icing system of the probe.
- Aerodynamic design of a sensor probe that maximizes the performance in App. C/ O discrimination.
- Maturation in the possibility of using the optic fiber as a direct sensor in an aircraft aerodynamic surface. A certification process is required.
- Maturation in the possibility of using other optical interrogators with less cost.
- Development of a geometry that delays the flux turbulence. The turbulence changes dramatically the convective heat transfer coefficient, and the LWC and IAR predictions could not be done.
- Development of a detection system integrated with a deicing system that activates automatically the deicing system when detects ice and stops the power supply when ice is removed.

5.6.2 Technology exploitation

The FOD has been patented already before the SENS4ICE project start. Now the patent has been granted. The department for technology transfer of INTA is including the FOD in its portfolio of technologies for exploitation and proposes the technology on their website and on meeting for technology transfer and congresses. The FOD will be offered to different companies in the aeronautic field and in the field of energy distribution, wind energy systems or in the railway sector. The FOD is going to be probably incorporated in the INTA next Flight Test platform. The sensor will be operative in all flights. Several companies were contacted of different sectors (aeronautic, military…) and of different countries (USA, Europe or India).

5.7 ONERA - AHDEL

5.7.1 Further development and maturation

Based on the feedback and the results obtained in IWT testing, two major modifications have to be done. This includes the improvements on the insulation of high-voltage parts and on the anti-icing of internal parts. A modification of the internal geometry, involving a combination of electrostatic and inertial versions seems to be an interesting approach to solve the two main problems observed in IWT tests.

An internal ONERA project concerning the development of ice protection system in an aeronautical context was launched in 2020. Among different purposes and subjects of study and development, this project also includes the continuation of development and maturation of AHDEL technology, as well as the development of an ONERA IWT facility. This new internal facility will be very useful for new testing with AHDEL sensor and the maturation of its technology.

The main goal for the ONERA team is to achieve a reliable and robust on-board direct detector of icing conditions that will be able to perform scientific flight campaigns in future projects.

5.7.2 Technology exploitation

The ONERA objectives beyond SENS4ICE are to continue the development and improvement of the sensor and employ it in scientific flight tests. A roadmap is dedicated to the increase the TRL of this sensor in order that its industrialization could be done through the technology transfer to an industrial. In this roadmap, other detection functions should be added to the sensor (dust and ashes characterisation, aircraft flight parameters, etc.). Also, we expect to improve the sensitivity and the LWC and MVD measurements of the sensor to use it for scientific in-flight atmospheric characterisation.

One of the main challenges to the industrialisation of this sensor should be the control of the aging of the charging system in order to be compliant with aircraft maintenance.

5.8 ONERA - AMPERA

5.8.1 Further development and maturation

ONERA's plan beyond SENS4ICE entails ongoing improvements and utilization of the AMPERA system for scientific in-flight campaigns. The aim is to enhance its capability to detect various atmospheric hazards, including lightning, volcanic ashes, and dust. Additionally, the system will be utilized for monitoring certain aspects of aircraft health by processing the signal from the field mill.

Moreover, the AMPERA system holds potential for deployment in other applications such as atmospheric electrification and contrails characterization.

The work plan for industrialization focuses on the challenge of reducing the size of the field mill. This will be achieved through the execution of two roadmaps. The first roadmap, based on MEMS (Microelectromechanical systems) technology, is currently underway at ONERA, starting at TRL2 (Technology Readiness Level 2). The objective is to miniaturize the sensor to the size of a rivet, which will serve as a significant technological breakthrough. This size reduction will help minimize the cost of the field mill sensor and enable seamless integration on aircraft and UAV platforms.

The second roadmap, which carries lower risk, involves reducing the size and weight of the field mill through classical mechanical design. The goal is to achieve a three-fold decrease in size and weight, making the field mill compatible with installation on UAVs.

5.8.2 Technology exploitation

In both roadmaps, one of the primary challenges is to ensure a high mean time between failures (MTBF) that aligns with aircraft maintenance requirements. It is crucial for the field mill sensor to demonstrate reliability and durability in order to meet industry standards.

Ultimately, ONERA aims to transfer the technology to an industrial partner for the commercialization of the sensor. This technology transfer will facilitate the availability of the AMPERA sensor in the market, allowing for broader utilization and integration into various aircraft systems.

5.9 SAFRAN- AOD

A careful analysis of the AOD sensors design revealed some strong drawback of this technology: a poor compactness, a large volume in the atmosphere leading to a high power consumption for de-icing, a large drag coefficient and a cumbersome image processing need. This technology then, did not appear as the best candidate for App. O discriminator, which was confirmed by the technology assessment during the evaluation stage. It was then decided that this development would not be conducted any further.

5.10 SAFRAN- PFIDS

5.10.1 Further development and maturation

SAFRAN wants to develop and commercialize a hybrid solution (PFIDS with indirect sensor) on all platforms.

This solution will be capable to detect App. C, O and D/P mixed phase and it will be used as a Primary mean for ice detection.

At the end of the SENS4ICE project, all needed activities, especially related to certification, will be continued by external or internal projects with the aim of proposing the new hybrid sensor by 2024-2025.

5.10.2 Technology exploitation

SAFRAN wants to develop and commercialize a hybrid solution (PFIDS with indirect sensor) on all platforms.

This solution will be capable to detect all the icing conditions and discriminate between App. C, and it could be used as a Primary mean for ice detection.

6. Conclusions

The objectives of the EU-funded project SENS4ICE are to increase flight safety in icing conditions and especially for SLD conditions and to enhance the knowledge base on the formation, occurrence and effects of Appendix O conditions. Ten different technologies with diverse physical principles for directly detecting icing conditions have been developed and/or advanced with EU funding. SENS4ICE approach is to investigate the potential to combine direct sensor technologies (atmospheric conditions/ ice accretion) with an indirect technique based on changing aircraft characteristics in a novel hybrid approach to ice detection. Details on the hybrid and indirect flight test results are available in the SENS4ICE deliverable D4.2 “Final report on hybrid ice detection development”.

At the project start, the sensor technologies had different levels of technology readiness, some at very low levels (TRL2) and others having had already passed steps of technology testing (TRL5/6).

In the first part of the project, icing detection technologies have been developed specifically aiming at Appendix O icing conditions with the goal to perform icing wind tunnel tests and complete a first technology evaluation. The SENS4ICE IWT test campaign was successfully completed for all the technologies, apart from AMPERA for which IWT testing is not feasible, and provided data in App. C and O conditions.

The second part of the project was devoted to flight test in order to test ice detection technologies under natural icing conditions, with a focus on Appendix O. Two flight campaigns with a total flight test time of about 75 hours have been conducted in 2023 to test and demonstrate eight of the direct ice detection technologies under development in particular in App. O/ SLD icing conditions. Data analysis from both the North America and Europe flight test campaigns provides a very good amount of measurements of liquid water icing conditions and SLD conditions in particular. Assessment of ice detection technologies shows that successful detections have been achieved advancing the technology maturation at the end of SENS4ICE to higher readiness levels (TRL5/6) for most technologies. For more details on flight campaigns please refer to the SENS4ICE deliverable D4.3 “Final report on airborne demonstration and atmospheric characterisation”.

The technology advancements within SENS4ICE are key to prove the detection and differentiation capabilities of the different detection concepts through IWT and flight test. The project also identified gaps and areas for further development to bring the sensors closer to production ready technologies. Such gaps are translated into roadmaps for further development and exploitation by the technology owners in future collaboration opportunities targeting additional testing in IWT and flight tests. This is very important despite the very good progress made, as the relevant icing conditions particularly for App. O/ SLD are very complex and the envelopes for the relevant parameters are large, multi-dimensional and have not been fully covered with the test data obtained in this project. However, it is very clear based on the flight test results that the matured and demonstrated technologies allow for a broad and promising application for various different purposes and types of vehicles, as many of the novel technologies are of low size/ low weight/ low power. This is considered to be particularly beneficial also beyond usual aircraft configurations, namely for future novel air vehicle concepts like greener aviation, more/all electric aircraft and UAV/UAM.

7. References

1. Schwarz, C., “The SENS4ICE EU project – SENSors and certifiable hybrid architectures for safer aviation in Icing Environment – A project midterm overview” 6th International Conference “Prospects of Civil Avionics Development”, online / Moscow, Russia, GosNIIAS, July 22, 2021.
2. Schwarz, C., “SENS4ICE EU Project Preliminary Results”, SAE International Conference on Icing of Aircraft, Engines, and Structures 2023, Vienna, Austria, 20-22 June 2023, 2023-01-1496.
3. Bansmer, S. E., Baumert, A., Sattler, S., Knop, I., Leroy, D., Schwarzenboeck, A., Jurkat-Witschas, T., Voigt, C., Pervier, H., and Esposito, B., “Design, construction and commissioning of the Braunschweig Icing Wind Tunnel”, Atmos. Meas. Tech., 11, 3221–3249, DOI: 10.5194/amt-11-3221-2018, 2018.
4. Orchard, D. M., Clark, C., Chevrette, G., “Measurement of Liquid Water Content for Supercooled Large Drop conditions in the NRC’s Altitude Icing Wind Tunnel”, SAE Icing Conference on Icing of Aircraft, Engines, and Structures 2019, Minneapolis, MN, USA, 17 – 21 JUN 2019.

5. EUROCAE, ED-103A/B Minimum operational performance standard for inflight icing detection systems. November 2017. http://www.eurocae.net
6. Bouchard, A. et al., “Relationship between airborne electrical and total water content measurements in ice clouds”, Atmospheric Research, Vol 237, 103836, 2020, DOI: 10.1016/j.atmosres.2019.104836
7. Roberts, I., “Development of the Atmospheric Icing Patch (AIP) under the SENS4ICE programme”, SAE International Conference on Icing of Aircraft, Engines, and Structures 2023, Vienna, Austria, 20 – 22 June 2023, 2023-01-1488.
8. Hamman, M., Gelao, G., Ridouane, El H., Chabukswar, R., Botura, G., “Development and Validation Testing of the Collins Ice Differentiator System in App C and App O Icing Conditions”, SAE International Conference on Icing of Aircraft, Engines, and Structures 2023, Vienna, Austria, 20 – 22 June 2023, 2023-01-1490.
9. Orazzo, A., Thillays, B., “Hybrid Ice Detection System development and validation”, SAE International Conference on Icing of Aircraft, Engines, and Structures 2023, Vienna, Austria, 20 – 22 June 2023, 23ICE-0049.
10. J. Lucke, T. Jurkat-Witschas, R. Heller, V. Hahn, M. Hamman, W. Breitfuss, V. R. Bora, M. Moser und C. Voigt, „Icing wind tunnel measurements of supercooled large droplets using the 12 mm total water content cone of the Nevzorov probe,“ Atmospheric Measurement Techniques, Bd. 15, p. 7375–7394, December 2022.
11. J. Lucke, T. Jurkat-Witschas, D. Baumgardener, F. Kalinka, M. Moser, E. de la Torre Castro und C. Voigt, „Characterization of atmospheric icing conditions during the HALO-AC3 campaign with the Nevzorov probe and the Backscatter Cloud Probe with Polarization Detection,“ in International Conference on Icing of Aircraft, Engines, and Structures, Vienna, 2023.
12. A. Korolev, J. W. Strapp, G. A. Isaac and E. Emery, "Improved Airborne Hot-Wire Measurements of Ice Water Content in Clouds," Journal of Atmospheric and Oceanic Technology, vol. 30, p. 2121–2131, September 2013.
13. K. Beswick, D. Baumgardner, M. Gallagher, A. Volz-Thomas, P. Nedelec, K.-Y. Wang und S. Lance, „The backscatter cloud probe - a compact low-profile autonomous optical spectrometer,“ Atmospheric Measurement Techniques, Bd. 7, p. 1443–1457, May 2014.
14. A. Bouchard et al. 2020, Relationship between airborne electrical and total water content measurements in ice clouds, Atmospheric Research, Vol 237, 104836 (https://doi.org/10.1016/j.atmosres.2019.104836)
15. SENS4ICE WP1 report: IWT Sensor Test Report - PFIDS Primary in-Flight Ice Detection Sensor
16. National Institute of Standards and Technology, pySCATMECH, 2023. https://github.com/johanneslucke/pySCATMECH/tree/jluckehttps://github.com/johanneslucke/pySCATMECH/tree/jlucke
17. González del Val, M.; Mora Nogués, J.; García Gallego, P.; Frövel, M. Icing Condition Predictions Using FBGS. Sensors 2021, 21, 6053. https:// doi.org/10.3390/s21186053
18. M. Gonzalez, M. Frövel, “Fiber Bragg Grating Sensors ice detection: Methodologies and performance”, Sensors and Actuators A: Physical, Volume 346, 2022, 113778, ISSN 0924-4247, Q1, https://doi.org/10.1016/j.sna.2022.113778. https://www.sciencedirect.com/science/article/pii/S0924424722004149
19. Hamman, M., Gelao, G., Ridouane, El H., Chabukswar, R., Botura, G., “Development and Validation Testing of the Collins Ice Differentiator System in App C and App O Icing Conditions”, SAE International Conference on Icing of Aircraft, Engines, and Structures 2023, Vienna, Austria, 20 – 22 June 2023, 2023-01-1490.

ACKNOWLEDGEMENTS

North America flight campaign data was obtained with the Embraer Phenom 300 operated by Embraer.

Airborne data for the European flight campaign was obtained using the aircraft managed by Safire, the French facility for airborne research, an infrastructure of the French National Center for Scientific Research (CNRS), Météo-France and the French National Center for Space Studies (CNES). Distributed data are processed by SAFIRE.